AD-A144 224 A BOUNDARY LAYER PARAMETERIZATION FOR A GENERAL MODEL (U) OREGON STATE UNIV CORVALLIS DEPT OF ATMOSPHERIC SCIENCES L MAHRT ET AL. MAR 84 AFGL-TR-84-0063 1/2

UNCLASSIFIED F19628-81-K-0046 F/G 8/13 NL

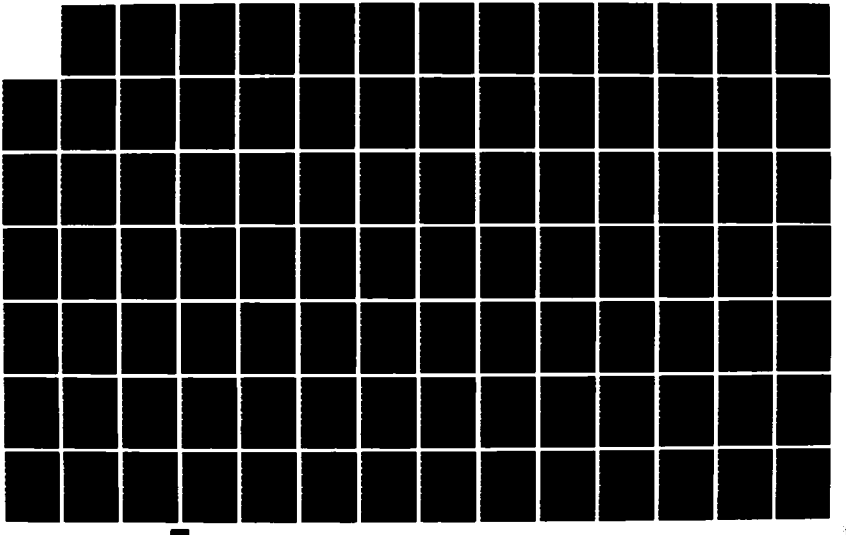

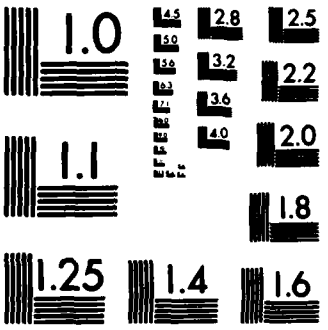

MICROCOPY RESOLUTION TEST CHART
NATIONAL BUREAU OF STANDARDS-1963-A

AFGL-TR-84-0063

A BOUNDARY LAYER PARAMETERIZATION FOR A GENERAL CIRCULATION MODEL

L. Mahrt
H. Pan
J. Paumier
Ib Troen

Oregon State University
Department of Atmospheric Sciences
Corvallis, Oregon 97331

Final Report
1 July 1981-31 December 1983

March, 1984

Approved for public release; distribution unlimited

AIR FORCE GEOPHYSICS LABORATORY
AIR FORCE SYSTEMS COMMAND
UNITED STATES AIR FORCE
HANSCOM AFB, MASSACHUSETTS 01731

This report has been reviewed by the ESD Public Affairs Office (PA) and is releasable to the National Technical Information Service (NTIS).

This technical report has been reviewed and is approved for publication.

Kenneth E. Mitchell
KENNETH E. MITCHELL
Contract Monitor

Donald A. Chisholm
DONALD A. CHISHOLM, Chief
Atmospheric Prediction Branch

FOR THE COMMANDER

Robert A. McClatchey
ROBERT A. McCLATCHEY, Director
Atmospheric Sciences Division

Qualified requestors may obtain additional copies from the Defense Technical Information Center. All others should apply to the National Technical Information Service.

If your address has changed, or if you wish to be removed from the mailing list, or if the addressee is no longer employed by your organization, please notify AFGL/DAA, Hanscom AFB, MA 01731. This will assist us in maintaining a current mailing list.

Do not return copies of this report unless contractual obligations or notices on a specific document requires that it be returned.

Unclassified

SECURITY CLASSIFICATION OF THIS PAGE

AD-A144224

REPORT DOCUMENTATION PAGE

1a. REPORT SECURITY CLASSIFICATION Unclassified	1b. RESTRICTIVE MARKINGS
2a. SECURITY CLASSIFICATION AUTHORITY	3. DISTRIBUTION/AVAILABILITY OF REPORT Approved for public release; distribution unlimited
2b. DECLASSIFICATION/DOWNGRADING SCHEDULE	
4. PERFORMING ORGANIZATION REPORT NUMBER(S)	5. MONITORING ORGANIZATION REPORT NUMBER(S) AFGL-TR 84-0063
6a. NAME OF PERFORMING ORGANIZATION Oregon State University Dept. of Atmospheric Sciences 6b. OFFICE SYMBOL (If applicable) AtS OSU	7a. NAME OF MONITORING ORGANIZATION Air Force Geophysics Laboratory
6c. ADDRESS (City, State and ZIP Code) Corvallis, Oregon 97331	7b. ADDRESS (City, State and ZIP Code) Hanscom AFB Massachusetts 01731 Monitor/Kenneth Mitchell/LYP
8a. NAME OF FUNDING/SPONSORING ORGANIZATION 8b. OFFICE SYMBOL (If applicable)	9. PROCUREMENT INSTRUMENT IDENTIFICATION NUMBER F19628-81-K-0046
8c. ADDRESS (City, State and ZIP Code)	10. SOURCE OF FUNDING NOS. PROGRAM ELEMENT NO. 61102F; PROJECT NO. 2310; TASK NO. G7; WORK UNIT NO. AB
11. TITLE (Include Security Classification) A Boundary Layer Parameterization for a General Circulation Model	
12. PERSONAL AUTHOR(S) Mahrt, Larry J.; Pan, Hua-Lu; Paumier, James O.; Troen, Ib	
13a. TYPE OF REPORT Final	13b. TIME COVERED FROM 81Jul01 TO 83Dec31
14. DATE OF REPORT (Yr., Mo., Day) 1984 March 31	15. PAGE COUNT 172
16. SUPPLEMENTARY NOTATION NA	

17. COSATI CODES		
FIELD	GROUP	SUB. GR.
04	02	

18. SUBJECT TERMS (Continue on reverse if necessary and identify by block number)

Soil hydrology, evapotranspiration, atmospheric boundary layer, turbulent transport, surface energy balance.

19. ABSTRACT (Continue on reverse if necessary and identify by block number)

A two-layer model of soil hydrology is developed from the basic soil moisture transport equations. The thin upper layer responds to short term evaporation. A thick lower layer includes the root zone and longer term water storage. The model is tested against a high-resolution soil hydrology model. Simple transpiration and canopy interception models are also included in the surface water budget. A surface energy balance is employed. Fluxes from the surface to the atmosphere are formulated with a stability-dependent bulk aerodynamic relationship and a stability dependent Penman relationship. The latter is evaluated with the Wangara data set.

The model of the atmospheric boundary layer uses a stability-dependent, height dependent eddy diffusivity which provides for countergradient convective transport. Boundary layer growth is modelled with a bulk Richardson number which is generalized to include purely convective boundary layer growth. The model development emphasizes self-consistency and reduction of the number of velocity scales compared to previous models of this type.

20. DISTRIBUTION/AVAILABILITY OF ABSTRACT UNCLASSIFIED/UNLIMITED ☐ SAME AS RPT. ☒ DTIC USERS ☐	21. ABSTRACT SECURITY CLASSIFICATION Unclassified
22a. NAME OF RESPONSIBLE INDIVIDUAL Kenneth E. Mitchell	22b. TELEPHONE NUMBER (Include Area Code) (617)861-2954 22c. OFFICE SYMBOL AFGL/LYP

DD FORM 1473, 83 APR EDITION OF 1 JAN 73 IS OBSOLETE.

SECURITY CLASSIFICATION OF THIS PAGE

Foreword

This report summarizes work done on AFGL Contract No. F19628-81-K-0046. While specific goals of the research are discussed in Chapter I, it is worthwhile to briefly discuss this work from a philosophical and strategical point of view.

Firstly, one must recognize that when considering an entire hemisphere on a routine basis, a wide variety of boundary layer situations are encountered. In contrast, boundary layer models have been developed for special situations such as the convective well-mixed layer or the fully turbulent stable boundary layer. In the real world, these models represent asymptotic limits or special cases.

Secondly, a given grid box contains a variety of surface types and associated boundary layer responses. Advection from one part of the grid box to the other is important in the corresponding real world. In the model, this advection can appear only as subgrid scale flux. Since the flux parameterization is necessarily based on turbulence theory, such advection is in effect omitted in present formulations.

As a result of these complications, and others, only a simple boundary layer model is appropriate; additional sophistication is wasted no matter how appealing from a physical point of view. In addition to simplicity, the model must be robust. It cannot breakdown or lead to instability in special situations even if rare. Thus we are willing to tolerate substantial errors or physical shortcomings in order to achieve versatility. This is not the usual initial goal of modelling, but in effect becomes the goal as the model is tested or runs operationally.

In the development of our model, we have tried to keep this perspective at the forefront. However, our model contains many unique features which we consider to be important improvements, but have not been tested under a variety of conditions nor tested on a routine basis. With complete certainty, troubleshooting and model modification will be necessary after use with the entire atmospheric model under a variety of conditions.

Acknowledgements

This work was primarily carried out by the four principle scientists, Larry Mahrt, Hua-Lu Pan, James Paumier and Ib Troen. The evaluation of the formulation for potential evaporation was carried out by Michael Ek who wrote a Master's degree thesis on this subject. Jean-Francois Louis of the European Centre for Medium-Range Weather Forecasting provided help with formulation and testing of the surface exchange relationships. Stuart Childs and Larry Boersma of the Soils Department, Oregon State University, offered useful suggestions on formulation of the soil model. Manuscript comments by Kenneth Mitchell, AFGL, and James Deardorff, Oregon State University, were also helpful.

This research was sponsored by the Air Force Geophysics Laboratory, Hanscom Air Force Base, Massachusetts, under Contract No. F19628-81-K-0046.

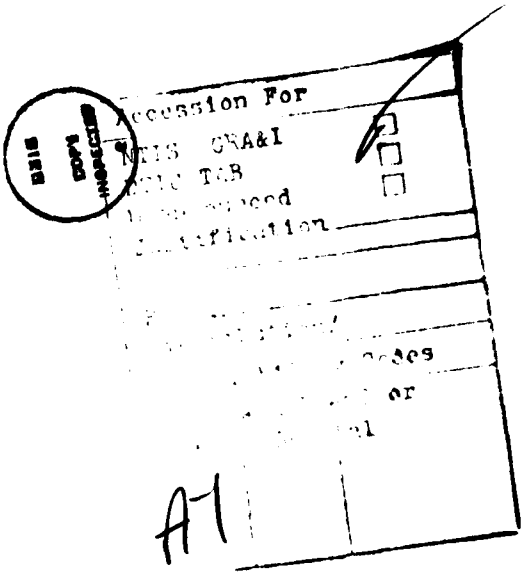

TABLE OF CONTENTS

TABLE OF CONTENTS (Continued)

LIST OF FIGURES

LIST OF FIGURES (Continued)

LIST OF FIGURES (Continued)

LIST OF FIGURES (Continued)

LIST OF TABLES

I. Introduction

This report presents the physical motivation for the components of the one dimensional model and discusses the advantages and disadvantages of each component.

The main components of the model are the evaporation routine (Chapter II), the soil hydrology model (Chapter III), the canopy-transpiration model (Chapter IV) and the atmospheric boundary layer model (Chapter V). The need for simplicity is imposed on all facets of the model development.

The organization of this report is conveniently illustrated by considering the expression for total evapotranspiration of water from the soil-vegetation complex to the atmosphere

$$E = E_{dir} + E_T + E_c = F \cdot E_p$$

where E_{dir} is the direct evaporation from the soil, E_T is the transpiration, E_c is the direct evaporation of precipitation intercepted by the canopy and E_p is the potential evaporation. The three contributions can be linearly related to the potential evaporation and functions of the soil water distribution, plant density, stomatal resistance and canopy water content. F is the sum of such functions.

Chapter II discusses the representation of potential evaporation and devotes considerable attention to the inclusion of the influence of atmospheric stability in the Penman relationship for potential evaporation. The stability influence has not been previously included at the level of simplicity sought in this development. The use of 24-hour averaged variables is examined in some detail since transpiration parameters are typically defined in terms of 24-hour averaged variables. Over water surfaces, we are recommending the usual bulk aerodynamic relationship (Chapter V).

Chapter III develops the two-layer soil hydrology model with special emphasis on the representation of transport of water near the air-soil interface and on the behavior of truncation errors which become important in a two-layer representation. The behavior of truncation errors is studied by comparing results with a high resolution model.

The soil heat flux is not modelled here. Instead a surface energy balance is employed (Chapter V). The heat flux from the soil to the atmosphere is small, particularly when accumulated over a day or more. Heat transport from the soil is most unimportant with organic debris or litter such as dead grass, leaves or needles. The conductivity of such a layer is small, especially when dry. From a global point of view, land surfaces are typically covered with such debris. The commonly-studied bare soil case occupies only a small percentage of the land surface. However, even with organic debris, the evapotranspiration to the atmosphere may still be large. As a result, water flux from the soil to the atmosphere is often important even when the corresponding heat flux is not important.

Chapter IV develops the transpiration and canopy water budget relationships. Section IV.1 motivates the need for a canopy water budget and surveys various approaches. Section IV.2 discusses the representation of transpiration. Section IV.3 presents the model of transpiration and canopy water budget used here. Chapter V develops the model for the atmospheric boundary layer. A new depth formulation is based on a bulk Richardson number which is generalized to include the free convection case. This generalization is developed concurrently with the countergradient heat flux modification to the eddy exchange coefficient.

The values of transpiration coefficients and soil properties appearing in the model have been chosen in an attempt to represent typical or average condi-

tions in a global sense. This selection is tenuous and there undoubtedly exists a prejudice toward mid-latitude situations where most of the observational evidence has been collected. Specification of the global distribution of such values would be useful future work.

We emphasize that much of the material presented in this report motivates, develops, and tests various model components. For purposes of quickly identifying the main equations, one need only to read Sections II.2-3, III.2, III.4, IV.3 and V. The components of the model are discussed independently so that it is not necessary to study the chapters in order. The software and users guide for operation of the model have been provided to the Atmospheric Prediction Branch of the Air Force Geophysics Laboratory.

II. The Influence of Atmospheric Stability on Potential Evaporation

Abstract

The Penman relationship for potential evaporation is modified to simply include the influence of atmospheric stability on turbulent transport of water vapor. Explicit expressions for the stability-dependent, surface exchange coefficient developed by Louis are used. The diurnal variation of potential evaporation is computed for the stability-dependent and original Penman relationships using Wangara data.

The influence of afternoon instability increases the aerodynamic term of the modified Penman relationship by 50% or more on days with moderate instability. However, the unmodified Penman relationship predicts values of daily potential evaporation close to that of the stability-dependent relationship. This agreement is partly due to compensating overestimation during nighttime hours. Errors due to use of daily-averaged variables are examined in detail by evaluating the nonlinear interactions between the diurnal variation of the variables in the Penman relationship.

A simpler method for estimating the exchange coefficient is constructed from an empirical relationship between the radiation-Richardson number and the Obukhov length. This method is less accurate but allows estimation of the stability-dependent exchange coefficient using only parameters already required for evaluation of the Penman relationship. Finally, the diurnal variation of the atmospheric resistance coefficient appearing in the Penman-Monteith relationship is presented.

1. Introduction

The surface moisture flux is often parameterized in terms of potential evaporation and associated coefficient representing soil moisture deficit, resistance of the vegetation, and radiative properties of the surface. The potential evaporation is defined as that evaporation occurring over a free water surface. In theory, the potential evaporation is independent of the state of the water surface and depends only on atmospheric conditions. In practice the value of the potential evaporation depends on the methodology of measurement.

In most atmospheric models, the potential evaporation is parameterized in terms of bulk aerodynamic relationship while in other disciplines the potential evaporation is more often equated to a Penman (1948) or combination formulation. The Penman formulation can be derived by combining the aerodynamic relationship with the surface energy balance. The Penman approach has the following advantages:

a) Surface temperature or surface saturation vapor pressure is eliminated. In practice surface temperature is difficult to define over land where the difference between vegetation and soil temperatures can exceed 5°C. Associated errors in the bulk aerodynamic relationship have been shown to be large (Yu, 1977).

b) The Penman relationship includes an explicit dependence on net radiation which, when calibrated to actual evapotranspiration, may indirectly include biological dependencies on solar radiation such as photosynthesis. In fact, the frequently used Priestley-Taylor model (1972) expresses evapotranspiration exclusively in terms of net radiation.

c) The Penman relationship has been compared to actual evaporation or evapotranspiration in a large number of studies, although many studies are hard to compare due to use of different versions of the Penman

equation, use of different observational levels, and influences of horizontal inhomogeneity.

In comparison with more empirical approaches, the Penman relationship is usually found to perform as well or better (e.g., Seguin, 1975). The Penman relationship has not been tested explicitly for downward moisture flux associated with negative net radiation and dew formation.

Evaluation of any model of potential evaporation from atmospheric variables, which are in equilibrium with a surface evaporating at less than potential, can be considered to be inconsistent (Bouchet, 1963; Morton, 1975 and others). Here we require the potential evaporation to be a function of only atmospheric variables and independent of reduction of actual moisture flux due to soil moisture deficit and plant resistance. However, the results of the present development can be transformed to modified expressions of potential evaporation.

The most serious disadvantage of the usual Penman relationship, and many other models of potential evaporation, is failure to explicitly include the influence of atmospheric stability on atmospheric transport of water vapor. Such an influence can significantly contribute to diurnal variation of the potential evaporation. The influence of stability can be reduced by using atmospheric variables measured closer to the ground. However, observations close to or within the canopy are difficult to interpret and the usual similarity theory no longer applies. As a result, studies of turbulent fluxes over land almost always include the influence of atmospheric stability.

However, only a few of the many applications of the Penman or combination formulations have included the influence of atmospheric stability. Such

formulations are usually based upon similarity modification of the log law and thus also include a dependence on surface roughness in contrast to the original Penman relationship. Businger (1956) modified the Penman relationship to include a stability correction which was expressed in monogram form. Fuchs et al. (1969) included the influence of stability in a version of the combination equation which did not eliminate surface temperature. Federer (1970) included a stability adjustment in the Penman relationship which required knowledge of the Obukhov length or an additional unspecified relationship between stability parameters.

The Penman-Monteith (Monteith, 1965) relationship has been modified to include certain aspects of the stability influence using Obukhov similarity theory (Stewart and Thom, 1973; Thom and Oliver, 1977; Verma et al., 1976; DeHeer-Amissah et al., 1981; Berkowicz and Prahm, 1982). Such inclusion of the stability influence generally requires iterative procedures. Stricker and Brutsaert (1978) apply an iterative technique to estimate the stability parameter and its influence on the actual surface moisture flux as computed from the surface energy budget, while Brutsaert (1982) suggests an iterative procedure based on the Penman relationship. They conclude that the influence of atmospheric stability cannot be neglected although they found little difference between the various stability formulations examined.

The first goal of this study is to present a method for estimating potential evaporation from the Penman relationship which includes the influence of atmospheric stability yet is simpler than the procedures above. In particular, we wish to avoid the need for iteration in order to construct a method suitable for use in those atmospheric models or routine applications where computer time

is restricted. This will be done by using the dependence of surface exchange coefficients on the bulk Richardson number presented in Louis (1979) and Louis et al. (1982) for both the stable and unstable cases (Section 2).

A second goal of this study is to estimate the importance of the influence of atmospheric stability since most applications of the Penman relationship still neglect such an influence. Toward this goal, we will systematically evaluate the Penman relationship with and without the stability influence using data from the Wangara experiment (Clarke et al., 1971). The inclusion of the stability influence in this study is expected to substantially improve the Penman relationships since the Louis (1979) formulation approximates similarity theory which has been calibrated and tested against classical data sets. However, the modelled stability influence will incur some error so that the evaluation of the original Penman relationship will be only approximate.

Also of interest is the influence of the diurnal variation of stability on the 24-hour evaporation since evaporation values are often reported for 24-hour periods. While afternoon instability can significantly enhance the surface moisture flux, nocturnal stability can significantly reduce such fluxes leading to some cancellation between stability influences. The third goal of this study is to assess the magnitude of errors resulting from use of 24-hour averaged variables since the Penman relationship is frequently evaluated with such averaged data.

Note that this study is concerned only with potential evaporation dictated by atmospheric variables; no attempts are made to estimate the actual evaporation or relate it to the potential evaporation. The daily potential evaporation during the Wangara observational period averaged a little more than 2mm per day

reaching near 4mm on some days. These modest values would be more than enough to evaporate the 2 1/2 cm of precipitation which fell during the 43-day period. Therefore, the actual evaporation rate was probably well below the potential rate for much of the observational period.

The study of the behavior of potential evaporation under conditions where the actual evaporation is less than potential is of considerable interest. Plant-soil models, which are forced by expressions for potential evaporation, are typically applied to situations of moisture stress.

It should be noted that models or expressions which relate actual evaporation to potential evaporation depend largely on observational calibration. Consequently, improved physical basis sought in this study will not necessarily lead to improved prediction of evapotranspiration in field situations. The relationship between actual and potential evaporation are addressed in Chapters III and IV. However, the procedures presented here will allow future construction of simple, physically more consistent, models of interaction between evaporation and the atmosphere.

2. Basic development

We begin with the bulk aerodynamic relationships for surface moisture and temperature flux:

$$\overline{(w'q')}_{sfc} = C_q \, u(q_{sfc} - q) \qquad (1)$$

$$\overline{(w'T')}_{sfc} = C_h \, u(T_{sfc} - T) \qquad (2)$$

where u, q, and T are the atmospheric wind speed, specific humidity and temperature, respectively, measured at a standard level such as 2m. C_q and C_h are non-dimensional exchange coefficients, the subscript "sfc" refers to surface values, w is the vertical motion and primes indicate turbulent fluctuations. Relationships (1) and (2), in principle, assume that the mean flow is sufficiently horizontally homogeneous so that the turbulence is uniquely in equilibrium with the mean flow.

The exchange coefficient appearing in the bulk aerodynamic relationship can vary by several factors with only modest diurnal variations of atmospheric stability. The same can be said of the coefficient appearing in Dalton's law used to derive the original Penman formula. In fact, the bulk aerodynamic relationship and Dalton's law are essentially equivalent (Appendix).

The potential evaporation can be defined by replacing q_{sfc} in (1) with the saturation surface value q^*_{sfc} corresponding to the temperature of the surface, in which case

$$\overline{(w'q')}_{sfc} = C_q \, u(q^*_{sfc} - q). \qquad (3)$$

In analogy with the usual Penman derivation, we expand (3) so that

$$\overline{(w'q')}_{sfc} = C_q \, u[(q^*_{sfc} - q^*) + (q^* - q)] \qquad (4)$$

where q^* is the saturation value of the atmospheric specific humidity at the standard observational level.

To continue the analogy, we express the saturation specific humidity as a function of temperature. Using the relationship

$$q^* \approx .622e^*/p$$

we obtain the approximation

$$q^*_{sfc} - q^* = \frac{.622}{p} \frac{de^*(T)}{dT} (T_{sfc} - T) \qquad (5)$$

where e^* is the saturation vapor pressure and p is atmospheric pressure. Substituting (5) into (4), we obtain

$$(\overline{w'q'})_{sfc} = C_q u\left[\frac{.622}{p} \frac{de^*(T)}{dT} (T_{sfc} - T) + q^* - q\right]. \qquad (6)$$

Using (2), the surface energy balance can be written as

$$-\rho L_v \overline{w'q'} + R_n - S - \rho c_p C_h u(T_{sfc} - T) = 0 \qquad (7)$$

where ρ is the surface density, L_v the specific latent heat, c_p the specific heat capacity, R_n the net radiative energy gained by the surface and S the flux of heat to the soil or vegetation. R_n and S are expressed in watts/m^2.

To eliminate surface temperature we combine (6) and (7) and obtain

$$E = \frac{\Delta(R_n - S)}{C_h/C_q + \Delta} + \frac{\rho L_v C_q u(q^* - q)}{(1 + (C_q/C_h)\Delta)} \qquad (8)$$

where

$$E \equiv \rho L_v (\overline{w'q'})_{sfc}$$

$$\Delta \equiv \frac{.622}{p} \frac{L_v}{c_p} \frac{de^*(T)}{dT}$$

and E is the potential latent heat flux at the surface in watts/m^2. Equivalently, the evaporation of water in mm/day is 3.46×10^{-2} E. The surface moisture flux $\overline{w'q'}$ in ms^{-1} g/kg is $\frac{10^3 E}{\rho L_v} = 3.1 \times 10^{-4}$ E.

With no other information, we assume that the turbulent exchange coefficients for heat and moisture are equal. Then (8) becomes

$$E = \frac{\Delta(R_n - S)}{1 + \Delta} + \frac{\rho L_v C_q u(q^* - q)}{1 + \Delta} . \qquad (9)$$

Relationship (9) is similar to other Penman formulations except that the usual wind function f(u) is replaced by $C_q u$.

The second term is normally referred to as the advection term since with no mean wind speed and no evaporation the specific humidity may approach saturation. However, even in the theoretical limit of vanishing wind speed, turbulence generated by any surface heating will mix drier air downward, keeping air near the surface unsaturated. As in the original Penman relationship, the second term in (9) does not vanish with vanishing wind speed if the air is not saturated and if the dependence of C_q on stability is appropriately chosen. The same can be said of the second term when it is identified with the evaporation measured by a Piche atmometer (Brochet and Gerbier, 1972). Even as the wind speed vanishes, convectively driven turbulence can ventilate the atmometer leading to evaporation. For lack of a better term, we will refer to the second term as the "aerodynamic" term although it must be remembered that both terms in (9) originate from the bulk aerodynamic relationship.

The original Penman relationship is derived in the same manner as (9) except Dalton's law (Appendix) is used as a starting point in place of (1). This relationship is typically expressed in the form (e.g., Brutsaert, 1982)

$$E = \frac{\tilde{\Delta}}{\tilde{\Delta}+\gamma} \frac{Q}{L_v} + \frac{\gamma}{\tilde{\Delta}+\gamma} f(u)\ (e^*-e) \qquad (10)$$

$$f(u) = .26(1+.54u)$$

$$\tilde{\Delta} \equiv \frac{de^*(T)}{dT}$$

$$\gamma = \frac{c_p P}{.622 L_v}$$

where E here is expressed in mm/day, Q is the net radiation flux density less soil heat flux, and e* and e are, respectively, the saturation and actual values of vapor pressure at 2m. The wind function f(u) was determined from evaporation pan measurements (Penman, 1948). Many modifications of the Penman wind function have been suggested although the original form still enjoys widespread usage. Comparison of (10) and (9) indicates that the wind function is proportional to the exchange coefficient

$$f(u) \propto C_q u$$

where the coefficient of proportionality depends on the units employed in (1) and (10) (Brutsaert, 1982).

3. Dependence of exchange coefficient on stability

The dependence of the exchange coefficient C_q on atmospheric stability can be expressed in terms of a Richardson number of the form

$$Ri = g/\theta \frac{(\theta-\theta_{sfc})z}{u^2}$$

where g is the acceleration of gravity, z is the height of the atmospheric observations, θ is the atmospheric potential temperature at z and θ_{sfc} is the potential temperature of the air at the lower reference level. The application of Monin-Obukhov similarity theory to the bulk aerodynamic relationship requires integration between two reference levels. The lower reference level is typically chosen to be the roughness height which simplifies the bulk aerodynamic relationship. The derivation of the Penman relationship demands integration from the surface where saturation is assumed in order that the vapor pressure can be determined from the temperature. The appropriate integration constant is then the roughness length for moisture (Brutsaert, 1982). Because of the approximate nature of this development and most applications to actual data, we will not distinguish between the roughness lengths for momentum and scalar quantities. For the present data analysis, the influence of water vapor on buoyancy is generally small and therefore also neglected.

Based on previous observations and certain asymptotic constraints, the development in Louis (1979) along with modifications in Louis et al. (1982) lead to the following dependence for the unstable case (Ri<0)

$$C_q = \left(k/\ell n\left(\frac{z + z_o}{z_o}\right)\right)^2 \left(1 - \frac{15\ Ri}{1 + C[-Ri]^{1/2}}\right) \qquad (11a)$$

where

$$C = \frac{75\ k^2\left(\frac{z + z_o}{z_o}\right)^{1/2}}{\left[\ell n\left(\frac{z + z_o}{z_o}\right)\right]^2}$$

$$k = .4$$

and stable case (Ri>0)

$$C_q = \left(\frac{k}{\ln\left(\frac{z + z_o}{z_o}\right)} \right)^2 \frac{1}{(1 + 15Ri)(1 + 5Ri)^{1/2}} \quad . \qquad (11b)$$

Both formulations reduce to the usual log law as Ri→0. Note that the exchange coefficient increases with increasing instability (increasing negative Richardson number). In the limit of extreme instability (Ri→-∞), after substituting for the Richardson number into (11), the wind function becomes

$$C_q\, u \rightarrow \frac{2}{15} \left(\frac{z_o}{z + z_o}\right)^{1/2} \left[\frac{g}{\theta} (\theta_{sfc} - \theta) z\right]^{1/2} \quad . \qquad (12)$$

Thus, the evaporation rate becomes independent of wind speed and depends on surface heating through a square root dependence on the surface temperature excess.

In the free convection limit, the roughness length becomes a somewhat arbitrary lower limit to the integration, which allows smooth matching to the usual Monin-Obukhov similarity theory. Ideally the expected rapid increase of $\theta_{sfc}-\theta$ with increasing z/z_o is such that the free convection limit (12) becomes independent of the roughness length. However, the actual sensitivity of (12) to the roughness length cannot be determined in practice since the air temperature becomes extremely inhomogeneous at the surface.

Other attempts to include the free convection limit involve additional criteria and separate formulation of the free convection case. These criteria could be added to the above development. However, the free convection limit is not usually of practical importance. For example, in the Wangara experiment,

-Ri rarely exceeded one. As is evident from Fig. 1 of Louis (1979) for such stability limits, the modelled influence of roughness length on the stability correction to the exchange coefficient (11) is well-behaved in that it closely approximates the original fit to data by Businger et al. (1971). Consequently, for simplicity, we proceed with (11) without further modification.

The stability corrections in the above exchange coefficient for heat and water vapor is different than that for momentum. However, the differences between the neutral values of the exchange coefficients for momentum and heat or moisture have been neglected in the above formulation based on Louis et al. (1982). This is in contrast to the neutral limits in Louis (1979) and others where the exchange coefficient for heat was larger than momentum and also contrasts with Stewart and Thom (1973) where the relationship between the exchange coefficients was more complicated.

4. Asymptotic cases

We now identify various special or limiting cases where the wind speed, exchange coefficient, humidity deficit and/or net radiation less soil heat flux vanish (Table 1). Combinations which do not satisfy the surface energy balance have been eliminated. As before, molecular diffusion of vapor is not considered. The type of evaporation has been classified as free convection if the wind speed vanishes and the implied turbulence and vapor transport are driven only by buoyancy. Conversely, the evaporation is classified as mechanical if the sensible heat flux is zero or downward in which case vapor is transported only by shear-generated turbulence.

Table 1a. Limiting cases of potential evaporation for the original Penman relationship.

Case	Surface Energy Balance							Type of Evaporation
	Latent Heat Flux E						Sensible Heat Flux	
	Rad. term	aerodynamic term				E		
	R -S	u	C	q*-q	aero. contrib.			
1a	0	0	>0	0	0	0	0	none
2a	<0	0	>0	0	0	<0	<0	dewfall
3a	>0	0	>0	0	0	>0	>0	free conv.
4a	0	>0	>0	0	0	0	0	none
5a	<0	>0	>0	0	0	<0	<0	dewfall
6a	>0	>0	>0	0	0	>0	>0	
7a	0	0	>0	>0	>0	>0	<0	(see text)
8a	<0	0	>0	>0	>0	(1)	<0	(see text)(1)
9a	>0	0	>0	>0	>0	>0	>0	free conv.
10a	0	>0	>0	>0	>0	>0	<0	mech. turb.
11a	<0	>0	>0	>0	>0	(1)	<0	(1)
12a	>0	>0	>0	>0	>0	>0	<0	(2)
13a	>0	>0	>0	>0	>0	>0	0	(2)
14a	>0	>0	>0	>0	>0	>0	>0	(2)

Table 1b. Limiting cases for the modified Penman relationship.

1b	0	0	0	0	0	0	0	none
2b	<0	0	0	0	0	<0	<0	dewfall
3b	>0	0	>0	0	0	>0	>0	free conv.
4b	0	>0	>0	0	0	0	0	none
5b	<0	>0	>0	0	0	<0	<0	dewfall
6b	>0	>0	>0	0	0	>0	>0	
7b	0	0	0	>0	0	0	0	none
8b	<0	0	0	>0	0	<0	<0	dewfall
9b	>0	0	>0	>0	>0	>0	>0	free conv.
10b	0	>0	>0	>0	>0	>0	<0	mech. turb.
11b	<0	>0	>0	>0	>0	(1)	<0	(1)
12b	>0	>0	>0	>0	>0	>0	<0	mech. turb.
13b	>0	>0	>0	>0	>0	>0	0	mech. turb.
14b	>0	>0	>0	>0	>0	>0	>0	

(1) depends on magnitude of each contribution.
(2) 12a=13a=14a because the original relationship is independent of stability.

Both the original and modified expressions agree on the existence of evaporation or dewfall for the various cases, except for cases 7 and 8. Since the original Penman wind function contains no dependence on stability, its aerodynamic term incorrectly predicts free convection of water vapor away from the surface for vanishing wind speed under stable conditions (7a and 8a) when there should be no turbulence. The same problem would theoretically occur with vanishing wind speed and exactly neutral conditions. With the stability-dependent exchange coefficient, free convection of water vapor correctly occurs only for unstable conditions (upward heat flux).

5. Diurnal variations in Wangara

We now compute the diurnal variations of potential evaporation from micrometeorological data collected during the Wangara experiment near Hay, Australia in the winter of 1967 (Clarke et al., 1971). The diurnal variation of stability during the Wangara experiment was, on the average, less than most would expect. Except for day 33, the magnitude of the afternoon Obukhov length was generally greater than 10m and on many afternoons greater than 100m. This only modest instability is due to relatively low winter sun angles and generally significant airflow.

Potential evaporation is calculated from Wangara data using both the original Penman equation and the Penman equation modified to include the stability-dependent exchange coefficient. The 40 days of data provided by the Wangara program allow nearly 900 hourly calculations of potential evaporation. Unfortunately, the temperature and specific humidity at the reference height of two meters needed for the Penman calculation were not measured. These variables were approximated by temperature and humidity data available at a height of approximately 1.2m. In the daytime, use of the 1.2m temperatures would

overestimate the saturation vapor pressure at 2m while the 1.2m specific humidity would underestimate the 2m specific humidity. Therefore, the net error in the estimated 2m humidity deficit is smaller than the errors in the estimated 2m temperature and specific humidity.

Since the surface temperature was not measured and cannot be simply defined over land surfaces, the surface-based bulk Richardson number could not be computed. Instead, the layer Richardson number is computed using observations at the one and four meter levels. Because the exchange coefficient is a slowly varying function of the Richardson number, except near neutral stability, the error in the estimation of the surface-based bulk Richardson number will normally cause much smaller errors in the exchange coefficient. Note that we cannot reintegrate the similarity theory between 1m and 4m to obtain a new exchange coefficient relationship because the Penman relationship demands integration from the surface; that is, the bulk aerodynamic relationship for moisture must be defined with respect to surface properties so that saturation can be assumed allowing surface vapor pressure to be related to surface temperature. We assess the importance of these potential errors in Section 8 where the exchange coefficients are also computed using an iterative procedure.

To compute the typical diurnal variations, parameters for each hour are averaged over all of the Wangara days including both sunny and cloudy days. Since ρ and L_v vary by only a small percentage during the day, they are considered constant and set equal to 1.275 kg/m^3 and 2.5x10^6 J/kg, respectively. The roughness length is assigned to be 1.2mm (Clarke et al., 1971). Figs. 1-2 show the diurnal variation of the remaining variables averaged over 40 days. Occasional missing observations contribute to some of the hour-to-hour noise. For most hours, less than 10% of the observations of a given variable were missing. As expected, the stability-dependent exchange coefficient

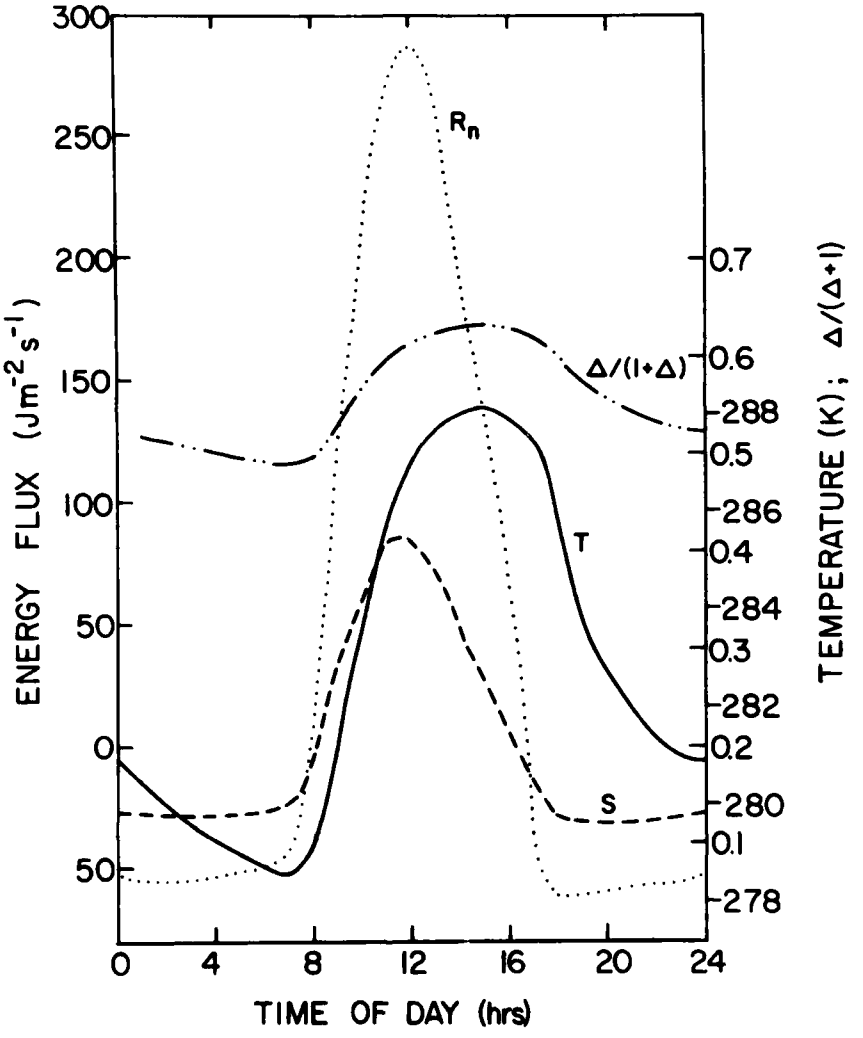

Fig. 1. (a) The mean diurnal variation of net radiation (dotted), heat flux to the soil (broken), temperature (solid) and coefficient of the radiation term Δ/(Δ+1) (dot-dash).

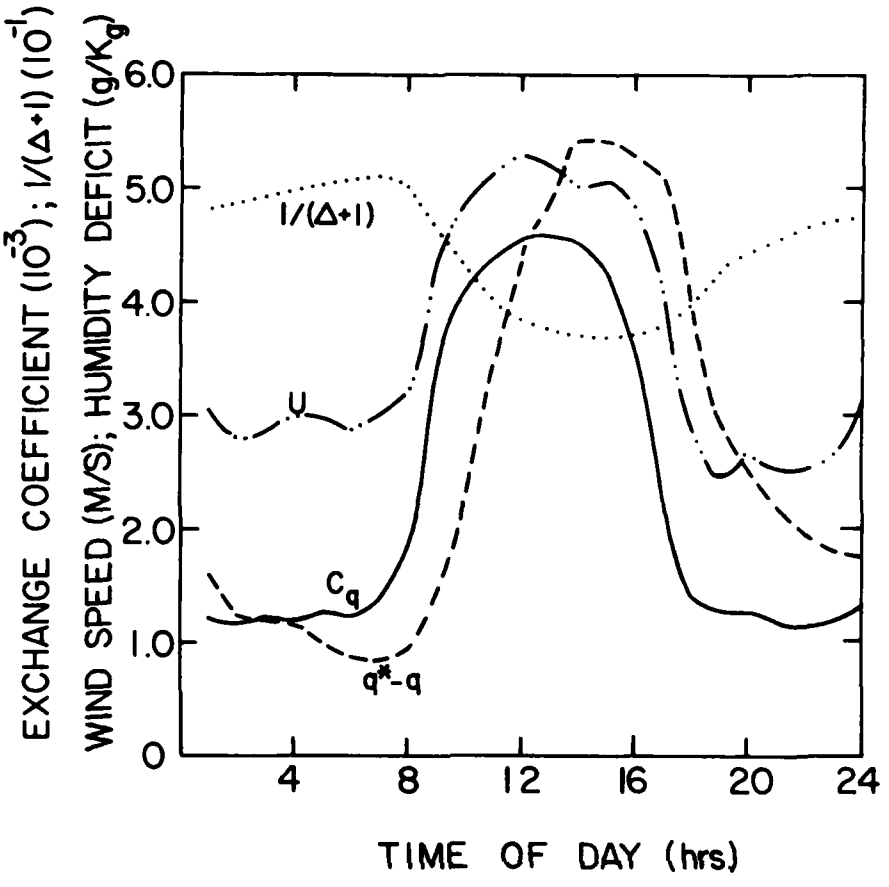

Fig. 1. (b) Mean diurnal variation of wind speed (dot-dash), specific humidity deficit (broken), Louis stability-dependent exchange coefficient C_q (solid), and temperature-dependent coefficient $1/(1+\Delta)$ (dotted).

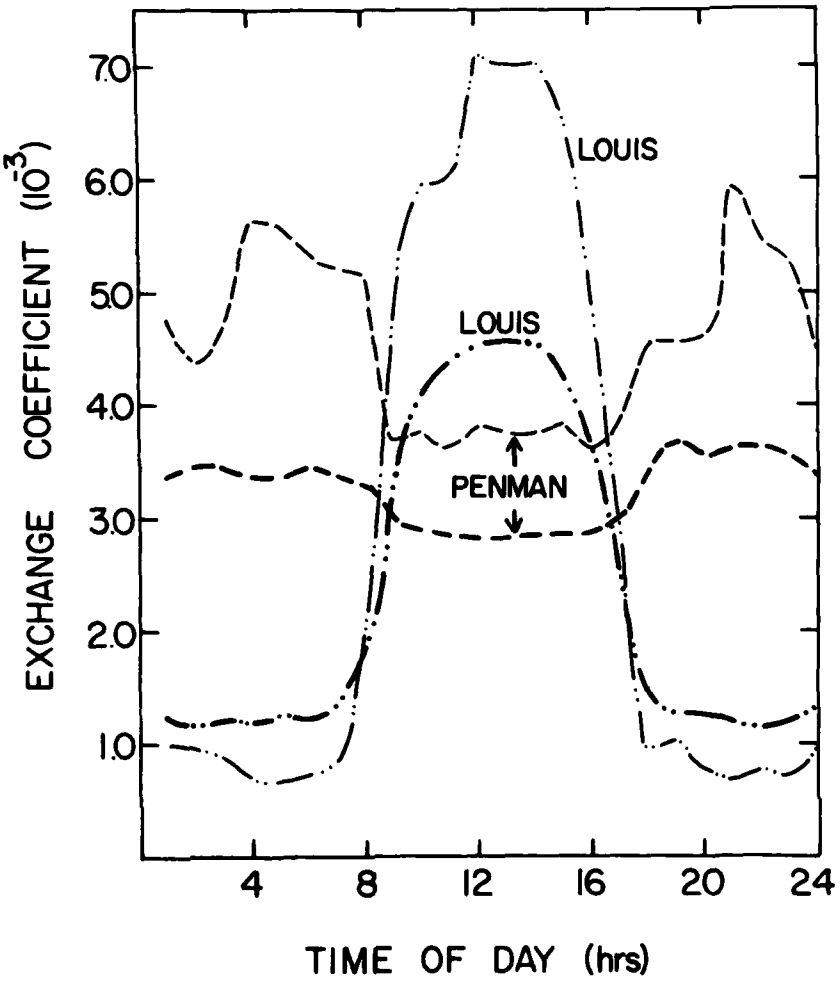

Fig. 2 Averaged diurnal variation of the exchange coefficient as computed from the Louis formulation (thick dot-dash), and as inferred from the original Penman wind function f(u)/u (thick broken). Also shown are averages for the nine days with significant afternoon instability (thin dot-dash and thin broken).

increases in the morning to a maximum value occurring in the early afternoon, dropping off rapidly later in the afternoon to an almost time-independent nocturnal value. The inferred Penman exchange coefficient $C_{qp} = f(u)/u$, where $f(u)$ is the original Penman wind function, reaches a minimum in the afternoon violating physical expectations.

Values are also averaged for days on which significant instability (Obukhov length <10m) occurred in the afternoon. Nine such days are found. On these days, the afternoon exchange coefficient exceeds that inferred from the Penman relationship by almost a factor of two (Fig. 2).

The diurnal variation of wind function $f(u)=C_q u$ corresponding to the stability-dependent aerodynamic expression exhibits significantly greater diurnal variation than the wind function of the unmodified Penman relationship even when averaged over all days (Fig. 3). Here the Penman wind function follows a diurnal pattern close to that corresponding to that wind function with a constant neutral value of the exchange coefficient, but with a smaller decrease at night.

Fig. 4 shows the diurnal variation of the radiation term and the various aerodynamic terms. The radiation expression peaks around noon, whereas the aerodynamic expressions peak in early afternoon. The aerodynamic terms are as large or nearly as large as the radiation term in contrast to some unstable summertime cases where the radiation term is significantly larger than the aerodynamic term.

As expected, the aerodynamic term using the stability-dependent exchange coefficient C_q exhibits, on the average, considerably more diurnal variation than the aerodynamic term of the original Penman relationship. The aerodynamic term of the original Penman relationship is similar to that aerodynamic term with a constant neutral exchange coefficient. Averaged over all days, the

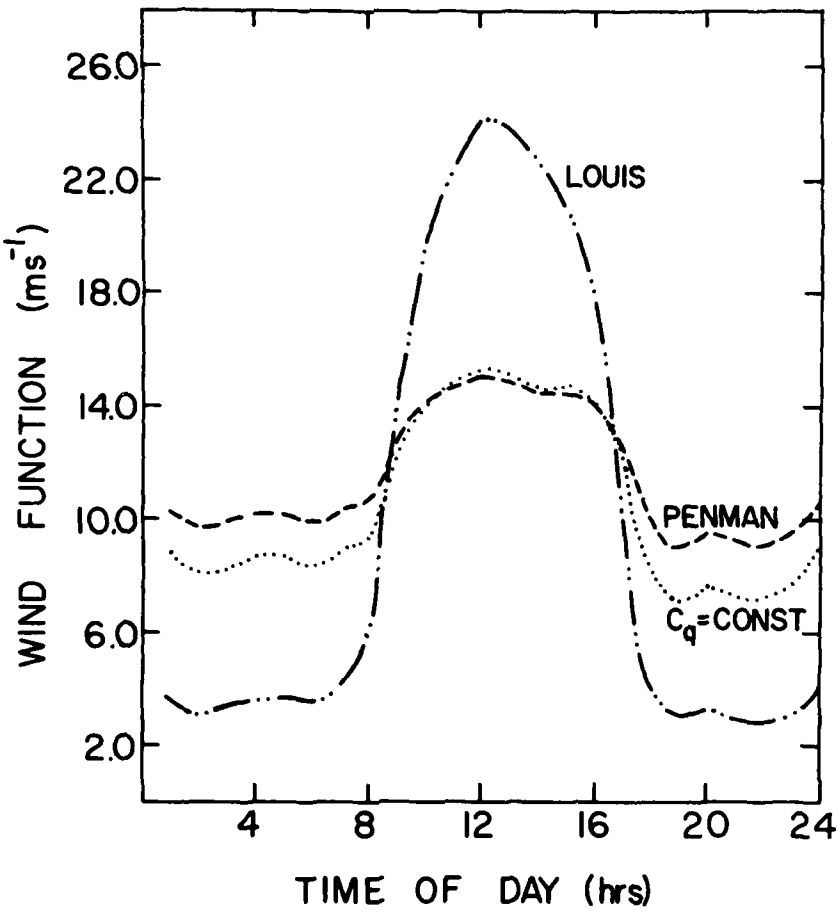

Fig. 3. The averaged diurnal variation of the wind function as computed from the Louis stability-dependent exchange coefficient (dot-dash), the original Penman formulation (broken) and constant exchange coefficient (dotted).

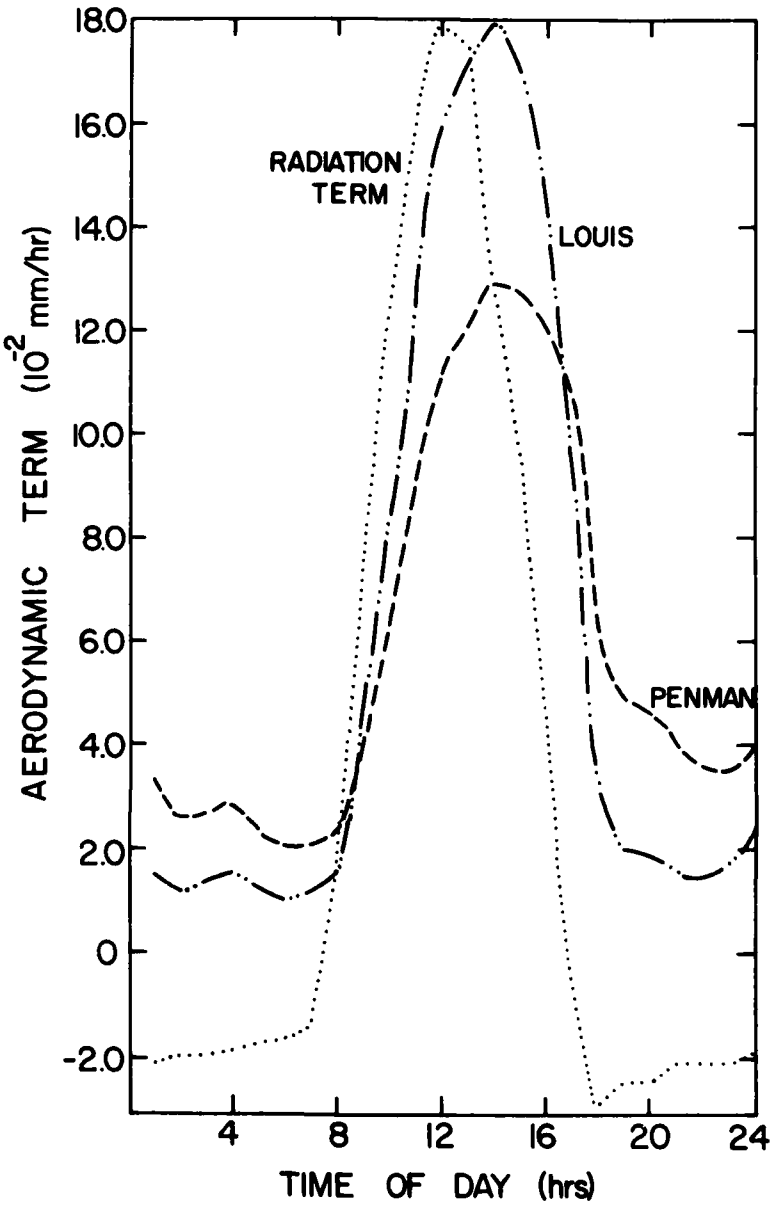

Fig. 4. The averaged diurnal variation of the aerodynamic term as computed from the Louis stability-dependent exchange coefficient (dot-dash), the unmodified Penman aerodynamic term (broken) and the radiation term (dotted).

stability-dependent Penman relationship predicts the afternoon aerodynamic term to be about 40% greater than that of the original Penman relationship in the afternoon and about 50% less than that of the original Penman relationship during the night.

6. Nonlinear diurnal dependence

In most applications of the Penman relationship, the daily total evaporation is estimated by using daily averages of wind speed, net radiation, humidity deficit, and temperature and neglecting the influence of atmospheric stability. Such calculations will incur errors due to neglect of stability influences and due to the nonlinear interaction (correlation) between the diurnal variation of variables which appear as products in the Penman relationship. For example, Jobson (1972) found that nonlinear interaction between the diurnal variation of vapor pressure and wind speed could occasionally lead to significant errors with use of daily-averaged variables in Dalton's relationship. However, on 90% of the days, such an error was found to be less than 10%. This error remains generally less than 25% even when monthly-averaged variables are used (Hage, 1975).

The results of Doorenbos and Pruitt (1977), also discussed by Stigter (1980), indicate that use of the Penman relationship for predicting 24-hour evapotranspiration from a well-watered grass reference crop could incur errors of 50% or more. The Penman relationship was found to usually underestimate water loss with strong wind speed and weak radiative heating. This underestimation decreased or reversed to an overestimation with weak wind speeds and strong surface radiative heating. Although stomatal resistance may have been a factor, the above variation of errors is consistent with the influence of atmospheric

stability on potential evaporation through the stability-dependent exchange coefficient and its correlations with other variables in the aerodynamic term.

We now consider the difference between calculating daily potential evaporation from daily-averaged variables versus summing potential evaporation values computed from hourly variables. We refer to the first case as "linearized potential evaporation" and the latter as "integrated potential evaporation." The original Penman relationship without stability influences is relationship (10) after converting from vapor pressure to specific humidity using relationship (A-3) in the Appendix.

Table 2 summarizes the differences between different expressions averaged over the 40 days of the Wangara experiment. We first note that the linearized radiation term averages 13% less than the integrated radiation term. This underestimation is due to correlation between the diurnal variation of the radiation (less soil heat flux) and the temperature-dependent coefficient of the radiation term.

Table 2. The daily aerodynamic term averaged over the 40 Wangara days (mm).

Method	Averaged Value	% Difference from Integrated Modified	Averaged Absolute Difference
Linearized Penman	1.35	-4%	15%
Integrated Penman	1.42	+1%	12%
Linearized Stability-Dependent	0.89	-36%	36%
Integrated Stability-Dependent	1.40	--	--

The linearized and daily-integrated versions of the aerodynamic terms of the original Penman relationship average within 5% of each other. The average absolute difference between the two versions is only 6%. Even the maximum difference of the 40 individual days is only 11%. This indicates that the linearization due to use of daily-averaged values does not lead to significant errors in the original Penman relationship.

However, the linearization of the stability-dependent aerodynamic term does create significant errors. Here the linearized aerodynamic term averages less than 60% of the integrated aerodynamic term. Differences on some individual days with large variations in stability exceeded 90% of the integrated term. It is concluded that use of the daily-averaged exchange coefficient causes large underestimation of the daily potential evaporation as is explicitly shown in the next section. We also found that use of a netural value of the exchange coefficient, corresponding to a logarithmetic wind profile, underestimates the daily evaporation as previously concluded by Stricker and Brutsaert (1978).

The aerodynamic term of the integrated original Penman averages, perhaps fortuitously, lies within 1% of that of the integrated stability-dependent Penman with an absolute difference averaging only 12%. A maximum individual daily difference of only 24% of the integrated modified term is found on a day with a large diurnal variation in stability.

The daily values of the original Penman relationship agree rather closely with the more complete version partly due to cancellation of underestimation in the daytime and overestimation at night. This agreement can also be attributed to the fact that the estimated roughness of 1.2mm is close to the 1.37mm thought to be representative of pan conditions used to calibrate the original Penman relationship (Thom and Oliver, 1977). However, similarity of roughness lengths

may be a lesser factor since the potential evaporation does not seem to be especially sensitive to the roughness length (Thom and Oliver, 1977).

Similarly, the linearized aerodynamic term of the original Penman equation approximates the aerodynamic term of the integrated, stability-dependent Penman relationship reasonably well. The difference between them averages only 4% and the absolute difference averages only 15%. The maximum individual difference, about 28% of the integrated term, also occurs on a day with a large diurnal variation in stability. We conclude that for the data considered here, the original Penman relationship has been effectively calibrated to predict the daily total evaporation even though it performs poorly on an hourly basis. We further conclude that when only 24-hour averages are available, the original Penman is preferable to the stability-dependent Penman at least without further calibration.

7. Interactive terms

To study the source of errors due to use of daily-averaged variables, each variable has been partitioned into a daily mean denoted with an overbar and an hourly deviation from the daily mean denoted with a prime. Diurnal variations of density and specific latent heat are much smaller than diurnal variations of other parameters and are therefore assigned to be constant with values of $\bar{\rho} = 1.275$ kg/m^3 and $\bar{L}_v = 2.5 \times 10^6$ J/kg. Considering the coefficients $1/(\Delta+1)$ and $\Delta/(\Delta+1)$ each to be a single variable and substituting the partitioned variables into the Penman relationship, we obtain

$$\bar{E} = \bar{E}_R + \bar{\rho}\bar{L}_v \underbrace{\left(\frac{\bar{1}}{\Delta+1}\right)(\overline{q^*-q})}_{(1)} \underbrace{(a+\bar{b}\bar{u})}_{(2)} + \underbrace{b\left(\frac{\bar{1}}{\Delta+1}\right)\overline{u'\,(q^*-q)'}}_{(3)} + \underbrace{b(\overline{q^*-q})\left(\frac{\bar{1}}{\Delta+1}\right)'u'}_{(4)} + \underbrace{(a+b\bar{u})\left(\frac{\bar{1}}{\Delta+1}\right)'(q^*-q)'}_{(5)} + \underbrace{b\left(\frac{\bar{1}}{\Delta+1}\right)'u'\,(q^*-q)'}_{(6)} \tag{13}$$

for the original Penman relationship where $a=3.9\times10^{-3}$ and $b=2.1\times10^{-3}$; for the stability-dependent Penman

$$\overline{E}_a = \overline{E}_R + \overline{\rho L_v}\,\left(\frac{\overline{1}}{\Delta+1}\right)\overline{C}_q\,\overline{u}\,\overline{(q^*-q)} + \left(\frac{\overline{1}}{\Delta+1}\right)\overline{C}_q\,\overline{u'\,(q^*-q)'} + \tag{1}$$

$$\left(\frac{\overline{1}}{\Delta+1}\right)\overline{u}\;\overline{C_q'(q^*-q)'} + \left(\frac{\overline{1}}{\Delta+1}\right)\overline{(q^*-q)}\;\overline{C_q'u'} \tag{2}$$

$$\left(\frac{\overline{1}}{\Delta+1}\right)\overline{C_q'\,u'\,(q^*-q)'} + \overline{C}_q\,\overline{u}\,\overline{\left(\frac{1}{\Delta+1}\right)'\,(q^*-q)'} + \tag{3}$$

$$\overline{C}_q\,\overline{(q^*-q)}\,\overline{\left(\frac{1}{\Delta+1}\right)'\,u'} + \overline{C}_q\,\overline{\left(\frac{1}{\Delta+1}\right)'u'(q^*-q)'} + \tag{4}$$

$$\overline{u}\,\overline{(q^*-q)}\,\overline{\left(\frac{1}{\Delta+1}\right)'\,C_q'} + \overline{u}\,\overline{\left(\frac{1}{\Delta+1}\right)'\,C_q'(q^*-q)'} + \tag{5}$$

$$\overline{(q^*-q)}\,\overline{\left(\frac{1}{\Delta+1}\right)'\,C_q'u'} + \overline{\left(\frac{1}{\Delta+1}\right)'\,C_q'\,u'(q^*-q)'} \tag{6}$$

where

$$\overline{E}_R = \left[\overline{\frac{\Delta}{\Delta+1}\,(R_n-S)} + \overline{\left(\frac{\Delta}{\Delta+1}\right)'\,(R_n-S)'}\right]. \tag{15}$$

Table 3 summarizes the magnitude of the various terms averaged over the 40 Wangara days.

The nonlinear interaction term in the radiation expression averages about 13% of the linear term averaged over all 40 days and may exceed 25% of the linear term on days with large diurnal variation of temperature and net radiation (less soil heat flux).

Table 3. Daily summer nonlinear terms averaged over the 40 Wangara days (mm).

term	averaged-value	ratio to linear term
Original Aerodynamic Term		
(1)	1.45	1.00
(2)	0.13	.09
(3)	-0.02	-.02
(4)	-0.11	-.08
Modified Aerodynamic Term		
(1)	1.03	1.00
(2)	0.14	.14
(3)	0.23	.29
(4)	0.18	.19
(5)	0.03	.04
(6)	-0.08	-.08
(7)	-.03	<.01
(8)	-.01	-.01
(9)	-.05	-.05
(10)	-.01	-.02
(11)	-.01	-.01
(12)	-.02	-.02

In the original Penman aerodynamic expression, the nonlinear interaction between wind and specific humidity deficit (term 2) and between specific humidity deficit and the temperature-dependent coefficient (term 4) are found to be the most significant of the nonlinear terms, approximately 9% and -8% of the linear term, respectively. On a day with large diurnal variation of atmospheric variables, these terms reach about 20% of the magnitude of the linear term. These two nonlinear terms result from higher wind speed, temperature and specific humidity deficit during the afternoon compared to nocturnal periods. Note that these two nonlinear terms are of opposite sign and approximately cancel. This explains why use of the daily-averaged values in the original Penman did not cause significant errors, at least with data analyzed here.

Of the eleven nonlinear terms in the stability-dependent aerodynamic term, seven are found to be relatively unimportant, (terms 5, 7-12), summing to less than -9% of the linear term. The correlation between the exchange coefficient (C_q) and specific humidity deficit (q^*-q), and the correlation between the exchange coefficient (C_q) and wind (u) lead to the most important nonlinear terms which average 29% and 19% of the linear term, respectively. On a day with particularly high diurnal variation of atmospheric variables, these two nonlinear terms are found to be 57% and 26% of the linear term, respectively. This strong correlation between diurnal variations of the stability-dependent exchange coefficient, wind, and humidity accounts for the large errors resulting from the use of daily-averaged variables in the stability-dependent Penman relationship.

8. Iterative results

The Louis formulation is expected to incur errors associated with the approximation of the original similarity theory. Errors also result from the

use of the layer Richardson number between one and four meters in lieu of the Richardson number evaluated between the surface roughness height and the standard level of 2m. Note that in modelling situations, surface temperature is usually determined from the surface energy balance and is often quite different from the air temperature even if measured down at the roughness height. This is an unavoidable inconsistency in modelling situations whenever a bulk aerodynamic relationship is used in conjunction with a surface energy budget. That is, similarity theories do not apply to the actual surface temperature of the ground even when such temperatures can be defined.

As a check on the modelled stability influence used here, we have compared it with the original similarity expressions of Businger et al. (1971). We have integrated the similarity theory between the surface roughness height and two meters for wind and one and four meters for temperature and then used several iterative approaches cited in the Introduction. The Louis relationships used here seem to lead to a small over-estimation of the exchange coefficient in unstable situations during the Wangara experiment, although this disagreement varied somewhat with the choice of iterative scheme. In addition, the original similarity expressions are uncertain in cases of large instability or large stability. Lower limits on the Obukhov length must be imposed for stable situations in order to insure physically realistic behavior and in some cases insure convergence of the iterative scheme.

We conclude that the qualitative differences between the original Penman relationship and those modified to include stability dependencies are not critically dependent on the stability formulation as also concluded by Stricker and Brutsaert (1978). However, even the modified formulations are only approximate and a precise quantitative evaluation of the original Penman relationship is not possible.

9. Radiation-Richardson number

The iterative procedure may be too cumbersome for many applications while the evaluation of the Richardson number requires temperature at two levels, not typically available in modelling and routine observational situations. The Richardson number can be modified by replacing the temperature difference with a dependence on radiation. The resulting parameter is more "external" than the usual Richardson number, since the temperature difference and turbulent fluxes are directly coupled. The surface heat flux is uniquely related to net radiation under conditions of potential evaporation and negligible heat flux to the soil. However, in general, the evaporation is less than potential and the ratio of the heat flux to the surface net radiation varies.

A "radiation-Richardson" number can be developed by beginning with the flux Richardson number

$$R_f \equiv \frac{g/\theta \; \overline{w'\theta'}}{\frac{\partial \bar{y}}{\partial z} \; \overline{w'y'}} \tag{16}$$

where $\overline{w'\theta'}$ is the surface temperature flux, $\overline{w'\underset{\sim}{v}'}$ is the surface momentum flux and $\bar{\underset{\sim}{v}}$ is the mean flow vector. We replace the seldom-measured surface heat flux with the radiative temperature flux less soil heat flux

$$R = \frac{(R_n - S)}{\rho c_p} \; . \tag{17}$$

R_n is positive with net downward radiative flux and is expressed in watts/m^2 in which case R is in units of K ms^{-1}. In most practical situations, S would be neglected. Scaling velocity fluctuations with u, the wind speed at height z, a scale value for the flux Richardson number (16) becomes proportional to the radiation-Richardson number

$$Ri_{Rad} \equiv (g/\theta)\ R\ z/u^3\ . \qquad (18)$$

The relationship between the radiation-Richardson number and atmospheric stability depends on the actual evaporation rate so that the radiation-Richardson number is only a crude estimate of atmospheric stability. However, since the main variation of the exchange coefficient occurs in the transition between stable and unstable cases, the crude estimate of stability based on the radiation-Richardson number will be of utility.

To develop the intended use of the radiation-Richardson number, we regress z/L on the radiation-Richardson number where L, the Obukhov length, is computed iteratively using the similarity relationships of Businger et al. (1971). The height z is again 2m. Cases where net radiative heat gain is positive and z/L is stable and vice versa are eliminated since these cases normally occur in transitional periods when similarity theory is not expected to apply. Fortunately, potential evaporation rates are small during such periods.

The radiation-Richardson number and z/L are linearly correlated with a coefficient of .95 for the unstable cases and .57 for stable cases. However, distributions of these parameters are strongly skewed. The cube root of z/L and the radiation-Richardson number are more normally distributed and will be used for the regression relationships. Note that $(z/L)^{1/3}$ is inversely related to

the surface friction velocity while $(Ri_{Rad})^{1/3}$ is inversely proportional to the wind speed, so that the resulting regression relationship is analogous to a resistance law.

The cube root of z/L is correlated to $(Ri_{Rad})^{1/3}$ with a correlation coefficient of .90 in the unstable case and .77 in the stable case. The regression relationships for the stable and unstable cases are:

$$\begin{aligned} (z/L)^{1/3} &= -\ 8.64\ (Ri_{Rad})^{1/3} - .09; \text{ stable case} \\ (z/L)^{1/3} &= -15.29\ (Ri_{Rad})^{1/3} - .13; \text{ unstable case.} \end{aligned} \tag{19}$$

Both relationships predict that z/L approaches about -10^{-3} as the net radiation vanishes. This small constant has no special significance for the near neutral case but rather improves the fit over the range of the values of the radiation-Richardson number. A higher order model is not justified because of the very approximate nature of this development.

The above regression relationships (19) were used to estimate z/L and subsequently to compute the exchange coefficients for the Wangara data. These exchange coefficients averaged over the forty days appear to lead to an underestimation of the stability influence (Fig. 5). With wetter surface conditions, this technique may overestimate the stability influence. However, these simple explicit relationships based on the radiation-Richardson number should be a significant improvement upon complete neglect of the influence of atmospheric stability and at the same time do not require additional observations as with other stability parameters.

10. Penman-Monteith

To include the influence of stomatal control, the Penman relationship is often multiplied by a plant coefficient which is generally less than unity. As

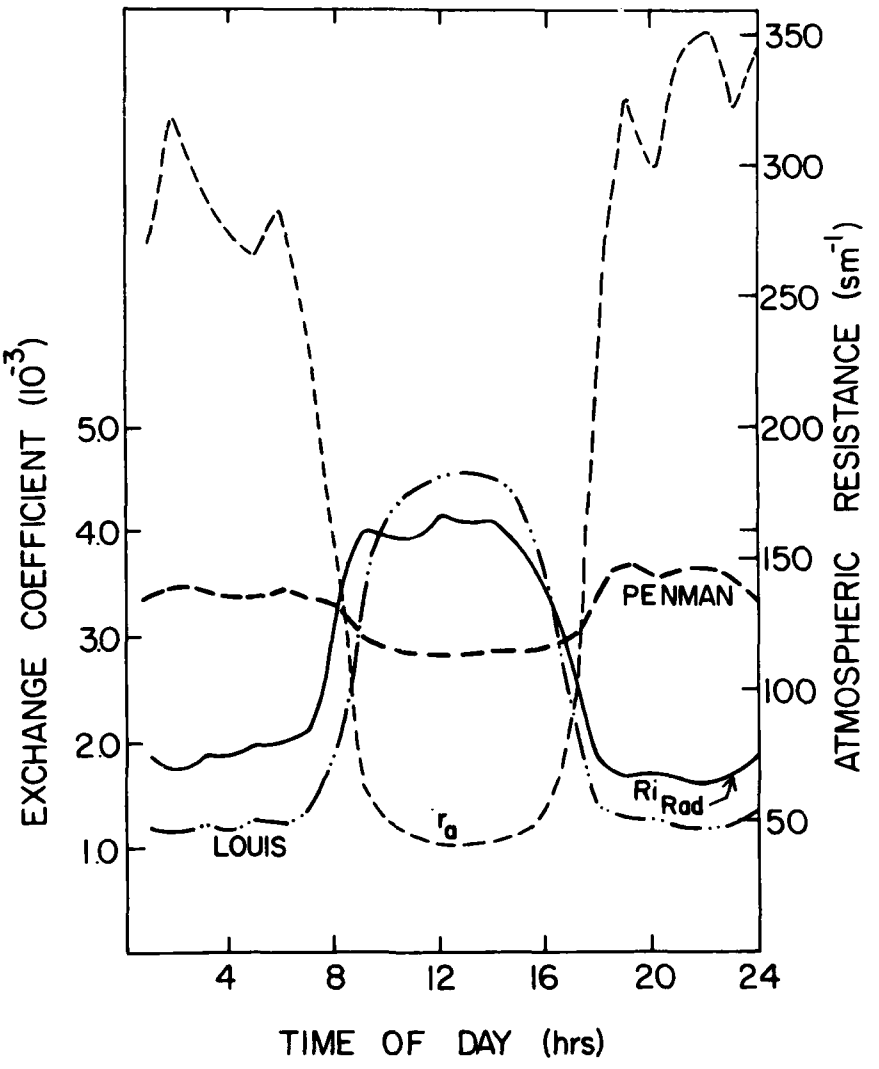

Fig. 5. The averaged diurnal variation of the exchange coefficient based on the Louis formulation (dot-dash), the radiation-Richardson number-regression relationship (solid) and as inferred from the Penman wind function (broken). Also shown is the atmospheric resistance coefficient (thin-broken).

an alternative, the Penman-Monteith relationship (Monteith, 1965) is frequently used. This approach introduces the influence of vegetation properties through a surface resistance factor r_s and the aerodynamic exchange coefficient is absorbed into a coefficient for aerodynamic resistance to atmospheric vapor flux r_a through the relationship

$$r_a = 1/(C_q u) \tag{20}$$

where C_q is parameterized according to (11). Thus the resistance coefficient is sensitive to atmospheric stability. We have computed the diurnal variation of the resistance coefficient from the exchange coefficient averaged over all the days for each hour. The resistance coefficient cannot be averaged directly since during very stable conditions, the resistance coefficient becomes orders of magnitude greater than typical values and theoretically can become infinite.

Diurnal variations of r_a, as computed from the Wangara data, are plotted in Fig. 5. Since the diurnal variation of r_a is substantial, the neglect of stability and nonlinear interactions in the Penman-Monteith expression is expected to lead to large errors. The diurnal variation of r_a could in turn be used to assess the diurnal variation of the coefficient α in the Priestly-Taylor model by employing the model of de Bruin (1983).

Relationship (20) along with either (11), (19) or the procedure in Section 8 would allow inclusion of the stability influence in the Penman-Montieth expression.

11. Conclusions

The potential evaporation, as related exclusively to atmospheric variables, is found to be quite sensitive to the diurnal variation of the exchange

coefficient appearing in the bulk aerodynamic relationship (Dalton's law). The usual neglect of such diurnal variations of stability leads to a factor of two smaller estimates of the values for the aerodynamic term on afternoons with modest instabilities although the differences are reduced substantially when averaged over all of the days in the Wangara experiment (Section 5). Strong instability (very small Obukhov length) did not occur with the data analyzed here due to the relatively low winter sun angle and generally significant airflow. In many summer mid-latitude situations, the diurnal variation of stability will be greater than found here. Over a fully vegetated surface with moist soil and significant airflow, the diurnal variation will often be less than found here.

Although responding inadequately to diurnal variations, the original Penman relationship predicted daily totals of the potential evaporation which are in good agreement with values predicted by the more complete relationship. This can be attributed to partial cancellation of the daytime and nocturnal influences in atmospheric stability and the similarity between the roughness length in the Wangara experiment and that corresponding to the original calibration of the Penman relationship. Use of daily-averaged variables in lieu of summing hourly estimates from the original Penman relationship led to little error.

We have also developed a new formulation for computing the stability-dependent exchange coefficient by defining a "radiation-Richardson number" (Section 9). Although less accurate, this simple formulation uses only variables which are already required for evaluation of the unmodified Penman relationship. Variations of atmospheric stability may also lead to significant day-to-day and regional variations of total potential evaporation.

Appendix: Relationships between specific humidity and vapor pressure

The Penman relationship was originally derived and generally applied in terms of Dalton's law which relates moisture flux to the gradient of vapor pressure. Turbulent transport is better related to a conservative moisture variable such as specific humidity as used in the bulk aerodynamic approach. Here we relate the two approaches.

Specific humidity is related to vapor pressure through the approximate relationship

$$q \approx \varepsilon e/p \qquad \text{(A1)}$$

where ε is the ratio of the molecular mass of vapor to that of dry air, equal to approximately 0.622.

Changes in specific humidity are then

$$dq = \frac{\varepsilon de}{p} - \frac{\varepsilon e dp}{p^2} \quad . \qquad \text{(A2)}$$

Changes of vapor pressure between the surface and some standard level, such as 2m, can be $O(10^{-1})e$ in cases of significant moisture flux. The same can be said of fluctuations of vapor pressure due to turbulence. On the other hand turbulent pressure fluctuations near the surface can be expected to be $O(10^{-4})p$ so that the ratio of the first term to the second term in (A2) is large in which case

$$dq = \varepsilon \frac{de}{p} \quad . \qquad \text{(A3)}$$

The dependence of saturation specific humidity on temperature is related to the dependence of saturation vapor pressure on temperature through (A2) such that

$$\frac{dq^*}{dT} = \frac{\varepsilon}{p}\frac{de^*}{dT} - \varepsilon\frac{e^*}{p^2}\frac{dp}{dT} . \qquad \text{(A4)}$$

The ratio of the second term to the first one is

$$\frac{e^*}{p}\frac{dp}{dT} \Big/ \frac{de^*}{dT} . \qquad \text{(A5)}$$

The relationship between pressure and temperature is restricted by the ideal gas law and thermodynamic relationship. In the case of adiabatic motion of turbulent elements the relationship between temperature and pressure is

$$dT = \frac{\kappa\theta p^{\kappa-1}}{p_o^{\kappa}}\, dp . \qquad \text{(A6)}$$

Using the definition of potential temperature

$$\frac{dp}{dT} = p_o/T\kappa \qquad \text{(A7)}$$

where $\kappa = .286$ and $p_o = 1000$ mb.

Relationship (A7) implies that the ratio (A5) is

$$\frac{dT}{T} \Big/ \kappa\frac{de^*}{e^*} . \qquad \text{(A8)}$$

Using the Clausius-Clapeyron equation,

$$\frac{de^*}{e^*} = \frac{L_v}{R_v} \frac{dT}{T^2} \tag{A9}$$

the ratio (8) becomes

$$\frac{R_v T}{\kappa L_v} \quad . \tag{A10}$$

Where R_v is the specific gas constant for water vapor and L_v is the latent heat of condensation. This ratio has a maximum value of about .2. Then the second term in (A5) can be neglected for a rough approximation in which case

$$\frac{dq^*}{dT} = \frac{\varepsilon}{p} \frac{de^*}{dT} \quad . \tag{A11}$$

Integrating this relationship from the surface temperature to the temperature at some standard level, we obtain

$$q^* - q^*_{sfc} = \frac{\varepsilon}{p} (e^* - e^*_{sfc}) \tag{A12}$$

where the height-dependent pressure can be replaced with the pressure measured at the standard level with an error of only $\leq 10^{-3}$. Integrating (A3) at a constant pressure level produces the same relationship for the general case where saturation is not assumed. Eq. (A12) verifies that the same approximation holds with saturation as represented by the Clausius-Clapeyron equation. Thus we can write

$$q - q_{sfc} = \frac{\epsilon}{p} (e - e_{sfc}) \qquad \text{(A13)}$$

which is valid with or without saturation.

In terms of the exchange coefficient, Dalton's law can then be expressed as

$$\overline{(w'q')}_{sfc} = C_q u \frac{\epsilon}{p} (e - e^*_{sfc}) \ . \qquad \text{(A14)}$$

In the development of this chapter, Dalton's law is not used. This appendix shows that the use of Dalton's law is equivalent to use of the bulk aerodynamic relationship which neglects the stability dependence of the exchange coefficient.

References

Berkowicz, R., and L.P Prahm, 1982: Sensible heat flux estimated from routine meteorological data by the resistance method. J. Appl. Meteor., 21, 1845-1964.

Bouchet, R.J., 1963: Evapotranspiration reelle, evapotranspiration potentielle, et production agricole. Ann. Agron., 14, 743-824.

Brochet, P., and N. Gerbier, 1972: Une methode practique de calcul de l'evapotranspiration potentielle. Ann. Agron., 23, 31-49.

Brutsaert, W.H., 1982: Evaporation and the Atmosphere. D. Reidel Publ. Co., Dordrecht, 299 pp.

Businger, J.A., 1956: Some remarks on Penman's equations for evapotranspiration. Neth. J. Agric. Sci., 4, 77-80.

Businger, J.A., J.C. Wyngaard, Y. Izumi, and E.F. Bradley, 1971: Flux-profile relationships in the atmospheric surface layer. J. Atmos. Sci., 28, 181-189.

Clarke, R.H., A.J. Dyer, R.R. Brook, D.G. Reid, and A.J. Troup, 1971: The Wangara Experiment: Boundary layer data. Tech. Paper No. 19, Div. Meteor. Phys., CSIRO, Australia.

de Bruin, H.A.R., 1983: A model for the Priestley-Taylor parameter α. J. Climate Appl. Meteor., 22, 572-578.

DeHeer-Amissah, A., U. Hogstrom, and A.S. Smedman-Hogstrom, 1981: Calculation of sensible and latent heat fluxes, and surface resistance from profile data. Bound.-Layer Meteor., 20, 35-49.

Doorenbos, J., and W.O. Pruitt, 1977: Guidelines for predicting crop water requirements. FAO Irrigation and Drainage Paper #24. Rome, FAO, 178 pp.

Federer, C.A., 1970: Measuring forest evapotranspiration - theory and problems. U.S.D.A. Forest Service Research paper NE-165.

Fuchs, M., C.B. Tanner, G.W. Thurtell, and T.A. Black, 1969: Evaporation from drying surfaces by the combination method. Agron. J., 61, 22-26.

Hage, K.D., 1975: Averaging errors in monthly evaporation estimates. Water Resour. Res., 11, 359-361.

Jobson, H.E., 1972: Effect of using averaged data on the computed evaporation. Water Resour. Res., 8, 513-518.

Louis, J.F., 1979: A parametric model of vertical eddy fluxes in the atmosphere. Bound.-Layer Meteor., 17, 187-202.

_____, M. Tiedtke, and J.F. Geleyn, 1982: A short history of the operational PBL - Parameterization of ECMWF. Workshop on planetary boundary layer parameterization, European Centre for Medium Range Weather Forecasting, Shinfield Park, Reading, Berks, U.K.

Monteith, J.L., 1965: Evaporation and environment. Symp. Soc. Exp. Biol., 19, 205-234.

Morton, F.I., 1975: Estimating evaporation and transpiration from climatological observations. J. Appl. Meteor., 14, 488-497.

Penman, H.L., 1948: Natural evaporation from open water, bare soil, and grass. Proc. Roy. Soc. A., 193, 120-195.

Priestly, C.H.B., and R.J. Taylor, 1972: On the assessment of surface heat flux and evaporation using large-scale parameters. Mon. Wea. Rev., 100, 81-92.

Seguin, B., 1975: Etude comparee des methodes d'estimation d'ETP en climat Mediterraneen du Sud de la France (Region de'Avignon). Ann. Agron., 26, 671-691.

Stewart, J.E., and A.S. Thom, 1973: Energy budgets in pine forest. Quart. J. Roy. Meteor. Soc., 99, 154-170.

Stigter, C.J., 1980: Assessment of the quality of generalized wind functions in Penman's equations. J. Hydrol., 45, 321-331.

Stricker, H., and W. Brutsaert, 1978: Actual evapotranspiration over a summer period in the "Hupsel Catchment". J. Hydrol., 39, 139-157.

Thom, A.S.,and H.R. Oliver, 1977: On Penman's equation for estimating regional evaporation. Quart. J. Roy. Meteor. Soc., 103, 345-357.

Verma, S.B., N.J. Rosenberg, B.L. Blad, and M.W. Baradas, 1976: Resistance-energy balance method for predicting evapotranspiration: determination of boundary layer resistance and evaluation of error effects. Agron. J., 68, 776-782.

Yu, T.W., 1977: Parameterization of surface evaporation rate for use in numerical modeling. J. Appl. Meteor., 16, 393-400.

III. A Two-Layer Model of Soil Hydrology

Abstract

A two-layer model of soil hydrology is developed for applications where only limited computer time and complexity are allowed. Volumetric soil water is computed in a thin upper layer for use in calculation of surface evaporation. Storage of water is computed for an underlying deeper layer.

In an effort to identify the influence of significant asymmetric truncation errors in the two-layer model, this model is compared with the 100-level model of Boersma et al. (1983). Comparisons are made for modelled soils with clay, loam and sand properties for various time dependencies of potential evaporation and precipitation. Truncation errors in the resulting two-layer model appear to be modest at least compared to errors asociated with difficulty in estimation of the hydraulic diffusivity and its strong dependence on soil water content.

Minimization of the influence of truncation errors requires: 1) choosing the upper layer to be sufficiently thin, 2) allowing the soil water gradient to directly control surface evaporation and 3) using suitable numerical implementation for the evaluation of internal soil water flux.

1. Introduction

The goal of this study is to develop a model of soil hydrology which is simple enough to use in concert with atmospheric general circulation models, forecast models and various operational situations where computer time and allowed complexity are restricted. At the same time a certain minimum physics seems necessary to include for most applications. For example, surface evaporation is related to soil moisture near the surface while storage of soil water and transpiration are related to soil moisture in a deeper layer. Therefore at least two layers including a thin upper layer seem desirable. This geometry was proposed in Deardorff (1977) where the thickness of the upper layer was regarded as vanishingly small.

The strong dependence of hydraulic diffusivity on soil water content is a second necessary inclusion for most applications. As a result of this dependence, the hydraulic diffusivity can vary by orders of magnitude with depth or with time at a given level during the diurnal drying cycle. In the two-layer model of Deardorff (1977), this dependence appeared to be indirectly included as a result of calibration of an empirical evaporation function using observations of drying in Adelanto loam (Jackson, 1973). This indirect calibration would probably have to be significantly altered for other soil types since the hydraulic diffusivity is also sensitive to soil type.

Jersey (1982) more directly includes the dependence of hydraulic diffusivity on soil water content in a two-layer soil model by using the basic soil water transport relationships. These equations form the basis of the high-resolution soil models (Nimah and Hanks, 1973; Feddes et al., 1974; McCumber and Pielke, 1981; Camillo et al., 1983; and Boersma et al., 1983).

A third crucial feature is suitable representation of the relationship between soil evaporation and the atmospheric potential evaporation. The

usual technique of relating evaporation to layer average soil water content is not very well posed. Use of information on near-surface soil water flux is much preferable since it allows control by the soil moisture profile.

Using this modelling approach for evaporation, we develop a two-layer model of soil hydrology from the basic transport equations cited above. As in Deardorff (1977), the upper layer is chosen to be thin so as to better approximate the large, near-surface gradients associated with the diurnal drying cycle. The use of basic transport equations in place of the force-restore approach allows relating surface evaporation to basic characteristics of the soil.

The truncation errors associated with any two-layer model require special attention since they are large and of different nature from the usual truncation errors in higher resolution models. Here we study the behavior of truncation errors by comparing this two-layer model with the high resolution model of Boersma et al. (1983). The depth of the upper layer and the method for implementing the numerical calculation of internal water flux significantly affect the magnitude of the truncation errors.

In this study, we do not consider the influences of vertical temperature gradients on soil water flux as in Camillo et al. (1983) and Jersey (1982). Distinction is not made between liquid transport and the generally less important vapor transport. Since the model is one-dimensional, horizontal inhomogeneity is excluded. While soils are virtually everywhere inhomogeneous in a significant way, it is assumed that a suitable hydraulic diffusivity exists for approximating vertical transport of water over a reference area.

2. Basic model

a. Layer-integration

Neglecting root uptake, the transport of water in the soil can be described by the equation (e.g., Hillel, 1980)

$$\frac{\partial \theta}{\partial t} = + \frac{\partial}{\partial z}\left(D(\theta)\frac{\partial \theta}{\partial z}\right) + \frac{\partial K(\theta)}{\partial z} \tag{1}$$

where θ is the volumetric water content, $D(\theta)$ is the soil water diffusivity, $K(\theta)$ is referred to as the hydraulic conductivity although it has units of velocity and negative z is increasing downward. Integrating (1) over the upper layer of depth z_1 (Fig. 1) we obtain

$$(z_1)\frac{\partial \theta_1}{\partial t} = - D(\theta)\left.\frac{\partial \theta}{\partial z}\right|_{-z_1} - K(\theta)_{-z_1} + I - E_{dir}$$

$$\theta_1 \equiv \frac{1}{(z_1)} \int_{-z_1}^{0} \theta dz \ . \tag{2}$$

E_{dir} is the direct evaporation of soil water to the atmosphere. I is the infiltration rate which is zero in the absence of precipitation and otherwise is equal to the precipitation rate up to a maximum infiltration rate. This maximum rate is parameterized in terms of the estimated flux at the surface under conditions of saturation, approximated as

$$I_{max} = D(\theta_{sat})\ (\theta_{sat} - \theta_1)/\frac{z_1}{2} + K(\theta_{sat}) \ . \tag{3}$$

Here the gradient near the surface has been estimated in terms of a linear variation between the saturation value at the surface and a layer mean value

assumed to occur at the mid-point of the upper layer. Any precipitation which cannot infiltrate or re-evaporate is specified to be runoff. In the case of heavy precipitation and a large time step such as one hour or greater, it may be necessary at the end of the time step to remove any soil water in excess of saturation as additional runoff.

We obtain for the lower layer (see Fig. 1):

$$(z_2 - z_1)\frac{\partial \theta_2}{\partial t} = D(\theta)\left.\frac{\partial \theta}{\partial z}\right|_{-z_1} + K(\theta)_{-z_1} - K(\theta)_{-z_2}$$

$$\theta_2 \equiv \frac{1}{(z_2 - z_1)} \int_{-z_2}^{-z_1} \theta dz \qquad (4)$$

where $K(\theta)_{-z_2}$ is the moisture loss due to "gravitational" percolation through the bottom of the lower layer. For simplicity, the diffusion of soil water across the bottom of the lower layer $z=-z_2$ is neglected since gradients and resulting fluxes at this depth are generally unimportant on the time scale of a few weeks or less. Exceptions include a high water table and the advance of a deep "wetting front." In the latter case, the thickness of the model should be increased.

b. Model geometry

For evaluation of surface evaporation, the upper layer should be chosen as thin as possible so as to be representative of the water content at the surface. However, assigning the layer to be too thin has two disadvantages. First direct comparison with observations are more difficult since vertical gradients and horizontal inhomogeneity may be extremely large near the surface making the water content difficult to define from observations. Secondly, a

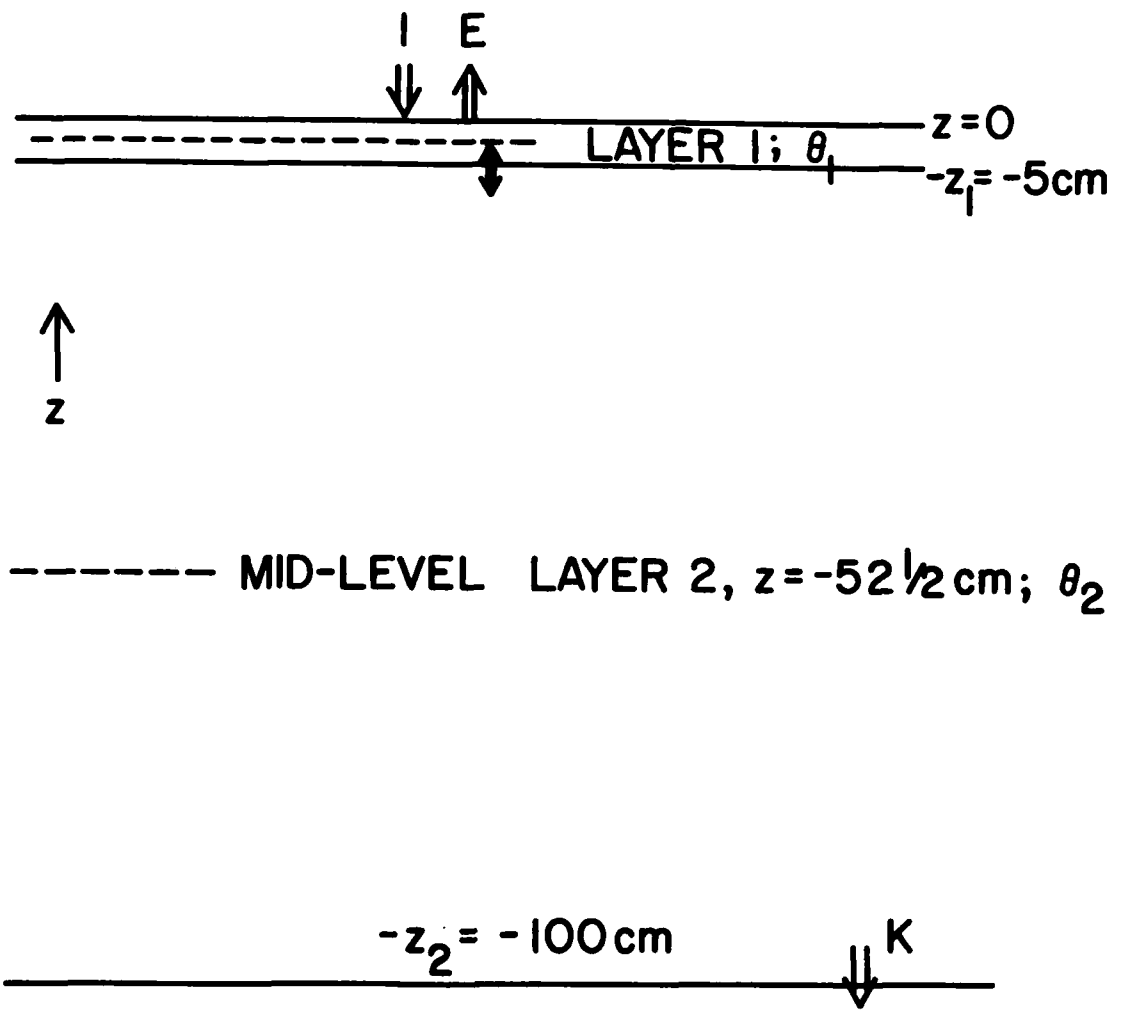

Fig. 1. Geometry of two-layer model. Double arrows indicate location of computed fluxes while dashed lines indicate location of computed soil water content.

large difference in thickness between the two layers leads to asymmetric finite differencing and generally more complicated truncation errors in the approximation of vertical gradients between the two layers. As a compromise between these considerations and cognizance of usual observational levels, we tentatively choose the thickness of the upper layer to be 5 cm and the thickness of the lower layer to be 95 cm.

Implicit time differencing is used with respect to evaluation of the vertical gradient. The time step is 30 minutes.

c. Flux parameterization

The hydraulic conductivity and diffusivity are not properties of the soil but rather strong functions of the water content and history of soil wetting and drying. The rapid decrease of hydraulic conductivity and diffusivity with decreasing volumetric soil water content found in several previous studies is shown in Figs. 2-3. These figures show the large differences between soil types but do not include hysteresis effects due to dependence on soil history.

We will assume that the conductivity and diffusivity behave in a sufficiently organized fashion such that its dependence on water content can be approximated with simple functions. As in Boersma et al. (1983) (hereafter referred to as B), we parameterize the hydraulic diffusivity and conductivity with piecewise log-linear fit to data from Gardner (1960). We have also operated the two-layer model with the hydraulic relationships presented in Clapp and Hornberger (1978) and Campbell (1974) and applied in McCumber and Pielke (1981). These relationships are based on a convenient mathematical format adopted in Gardner et al. (1970). Such relationships allow easy application to a variety of soil types. Here we use the fit to data from Gardner (1960) to facilitate comparison with B.

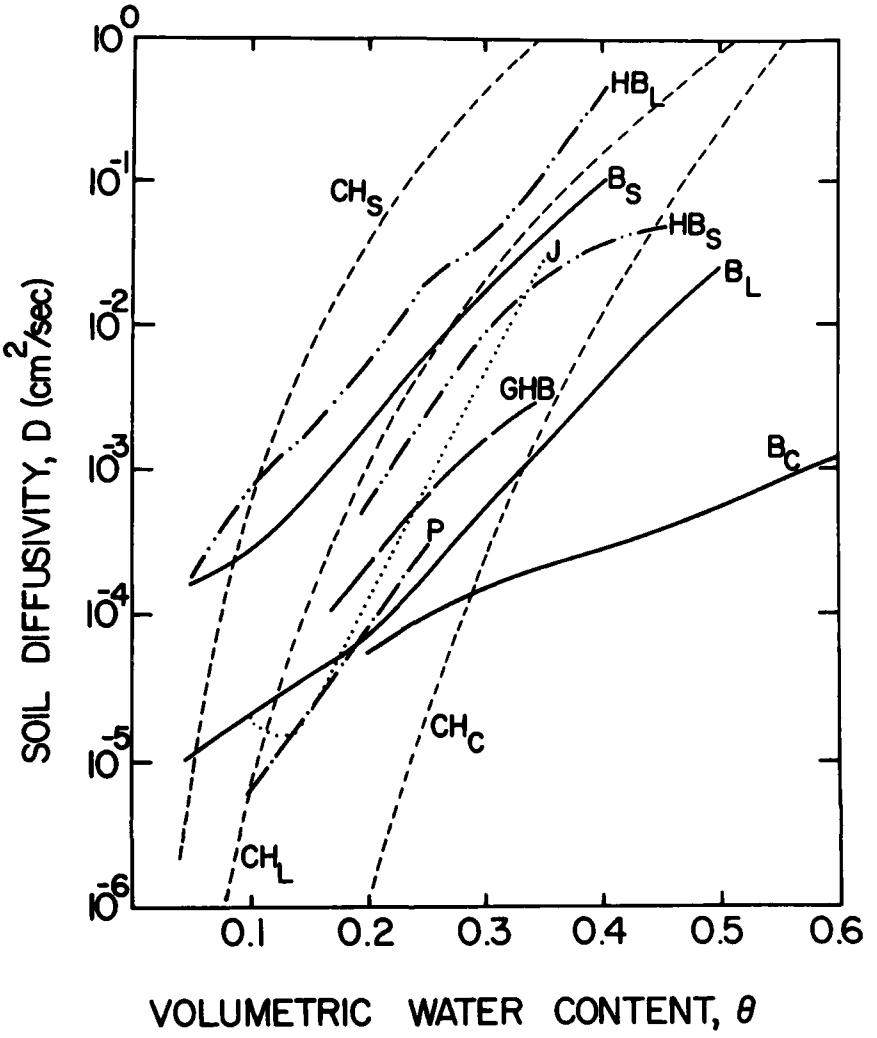

Fig. 2. Examples of the dependence of soil hydraulic diffusivity on volumetric soil water content from loam, (HB_L, Hanks and Bowers, 1962); (J, Jackson, 1973); (GHB, Gardner et al., 1970); silt loam (HB_S, Hanks and Bowers, 1962); clay (P, Passioura and Cowan, 1968); results approximated from Gardner (1960) for sand (B_S), loam (B_L) and clay (B_C); relationship from Clapp and Hornberger (1978) for sand (CH_S), loam (CH_L) and clay (CH_C).

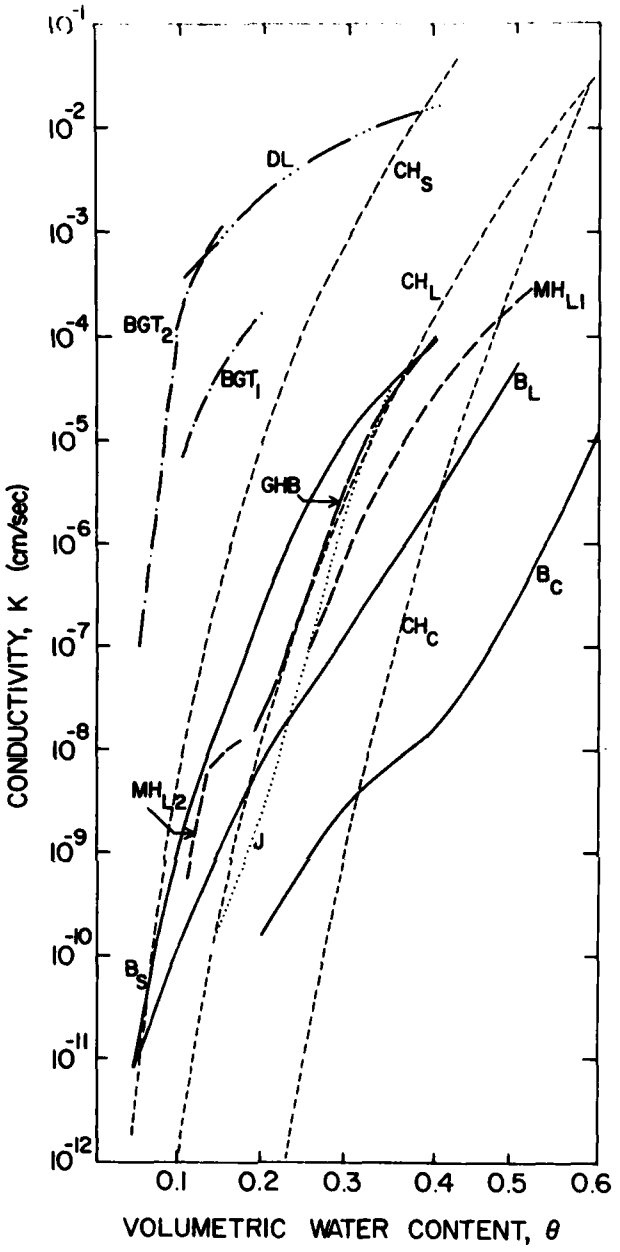

Fig. 3. Examples of the dependence of hydraulic conductivity on volumetric soil water content for sand, (DL, Day and Luthin, 1956); (Black et al., 1970, 0-50 cm-BGT_1, 50-150 cm-BGT_2), loam (J, Jackson, 1973); (MH_{L1} and MH_{L2}, Marshall and Holmes, 1979); (GHB, Gardner et al., 1970); results approximated from Gardner (1960) for sand (B_S), loam (B_L) and clay (B_C); relationship from Clapp and Hornberger (1978) for sand (CH_S), loam (CH_L) and clay (CH_C).

The gradient of soil water at the interfacial level, $-z_1$, is approximated by assuming that the layer-averaged water content occurs at the layer mid-level in which case the present approach becomes equivalent to the usual finite differencing without layer-integration. Assuming linear variation between the two mid-levels we obtain

$$\left|\frac{\partial\theta}{\partial z}\right|_{-z_1} = 2\left[\frac{\theta_1 - \theta_2}{z_2}\right] \tag{5}$$

where $z_2/2$ is the distance between mid-levels. This approximation will normally significantly underestimate the gradient of soil water at the interfacial level in periods of evaporation when the gradient decreases rapidly with depth.

Due to this decrease with depth, linear interpolation between mid-levels will also significantly underestimate the soil water content at the interface and therefore underestimate the diffusivity at the interface. During evaporation periods, the change in water flux with depth is typically a small difference between two much larger effects, one being the rapid decrease of the water content gradient with depth and the other being the rapid increase of hydraulic diffusivity with depth. To minimize truncation errors due to the large distance between mid-levels, it is important that the computed values of the diffusivity and gradient are self-consistent or represent approximately the same level. This is more important than insisting that the estimate of the flux

coincides with the interfacial level. Because of the curvature of the water content profile, the bulk gradient (5) is representative of the gradient well within the lower layer. We found that during drying, use of the hydraulic diffusivity and conductivity corresponding to the water content of the lower layer instead of use of interpolated or vertically averaged values produced results closer to the high resolution model B (Section 4).

After periods of weak evaporation when the soil water varies slowly with depth, the various methods of estimating the interfacial water flux will produce comparable estimates. In the case of precipitation, the downward advance of the wetting front is determined more by the hydraulic properties of the upper wetted soil. Using the diffusivity and conductivity of the upper layer of the two-layer model during precipitation events (Section 5) appeared to minimize truncation errors.

Therefore, when the lower layer is more moist, the diffusivity and hydraulic conductivity at the interface z, (Fig. 1) is evaluated using the soil water content of the lower layer θ_2 so that

$$(K_{z_1}, D_{z_1}) = [K(\theta_2), D(\theta_2)]; \ \theta_2 > \theta_1 . \tag{6}$$

When the upper layer is more moist, the diffusivity and hydraulic conductivity at the interface z are evaluated from the water content of the overlying upper layer θ_1 in which case

$$(K_{z_1}, D_{z_1}) = [K(\theta_1), D(\theta_1)]; \ \theta_1 > \theta_2 . \tag{7}$$

For the cases considered here, this procedure reduces truncation errors as effectively as the finite element approach and does not require the more

complicated boundary conditions needed for the finite element approach. The infiltration condition (3) is consistent with (6-7) in that the diffusivity and hydraulic conductivity are evaluated from "upstream" water content.

3. Vertical structure

We first study the bulk vertical structure of soil water, its dependence on evaporation and precipitation and resulting truncation errors associated with the estimate of the interfacial gradient (5). The magnitude of potential truncation errors in low resolution models will be estimated using the high resolution model B where truncation errors are expected to be small. In B, (1) is evaluated at each of 100 levels. The vertical resolution varies from 1/2 cm near the surface to 2 cm near the bottom (158 cm).

As a single index for potential truncation errors in low resolution models, we define the ratio of the local gradient at 5 cm to the bulk gradient between 2 1/2 cm and 52 1/2 cm, both computed from model B. The local gradient at 5 cm is computed by differencing between the 4 and 6 cm levels in B. The ratio of gradients will allow quick interference of the behavior of truncation errors due to profile curvature of the water content.

Comparisons are made for Chino Clay, a soil with very low hydraulic diffusivity and Pachappa sand which has large hydraulic diffusivity. Two types of experiments are run, one with specified constant potential evaporation (atmospheric demand) of .1 cm/hour, typical of moderate daytime evaporation, and one where the potential evaporation is specified to be constant (.1 cm/hour) for six hours, zero for eighteen hours and so forth. The latter experiments allow examination of the soil response to changes of potential evaporation, and when viewed over several days, crudely simulate diurnal variations of evaporation. Numerical experiments were also run for the case of sinusoidal variation of

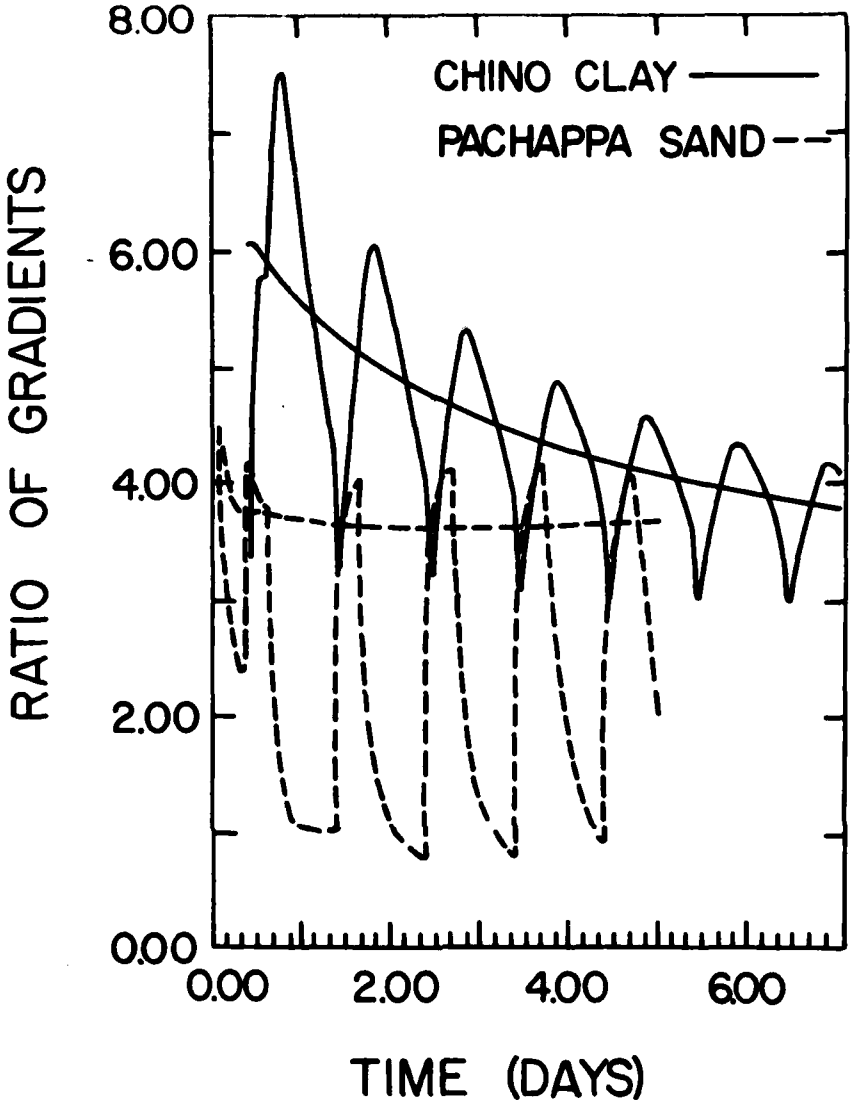

Fig. 4. Ratio of the bulk gradient of volumetric water content to the local gradient at 5 cm as computed from the high-resolution model. Ratio values significantly greater than one reflect the failure of the bulk gradient to recognize the strong curvature near the surface which is induced by surface evaporation. Deviations of the ratio value from unity indicate potential truncation errors in the two-layer model. See text for further explanation.

evaporation. Initial conditions are chosen to be the same as those in B; θ=.29 for Pachappa sand and θ=.47 for Chino Clay.

Fig. 4 indicates that the actual gradient at 5 cm is significantly larger than the bulk gradient during evaporation periods since surface drying induces a moisture gradient which is large at the surface and decreases rapidly with depth. The ratio of the two moisture gradients decreases with time as the influence of surface drying "diffuses" to lower levels. After about 5 hours with constant potential evaporation, the ratio of the local gradient at 5 cm to the bulk gradient in the Pachappa sand has decreased to a nearly time-independent value of about 3.75. This ratio appears to approach the same asymptotic value in the Chino Clay but requires a much longer time due to lower diffusivity. Without considering errors in the diffusivity, this ratio implies that the between-layer flux computed in the two-layer model will be underestimated by a factor of almost four.

In the diurnal simulations, both the daily-averaged ratio of gradients and the diurnal amplitude of the ratio quickly reach an equilibrium value in the Pachappa sand but slowly decrease with time in the Chino Clay. The asymptotic, diurnally-averaged value of the ratio of the local to the bulk gradient appears to be about 3.5 for Chino Clay but closer to 2.5 in the case of Pachappa sand. The ratio of gradients and curvature decrease during non-evaporating periods because large near-surface gradients induced by the evaporation are spreading downward due to transport of soil water, and strong surface gradients are no longer generated by surface evaporation. In fact, during non-evaporating periods in the Pachappa sand, the bulk gradient becomes comparable to that of the 5 cm gradient corresponding to a condition where the vertical moisture gradient varies only slowly with depth and truncation errors are minimal. When the potential evaporation is increased from .1 mm/hr to .3 mm/hr, an appropriate

geophysical upperbound, the ratio of gradients and the curvature are higher but behave in a similar fashion.

The smaller ratio of gradients and smaller curvature in the case of Pachappa sand reflect the greater penetration of the influence of drying due to larger diffusivity. In the case of constant diffusivity, the penetration depth scale for the influence of sinusoidally varying evaporation is $\sqrt{2D/\omega}$ where ω is the frequency of variation. For a diurnal time scale and variations of hydraulic diffusivity for Chino Clay, ranging from $10^{-4}cm^2s^{-1}$ to $10^{-3}cm^2s^{-1}$, the penetration depth scale ranges from 1.7 cm to 5.2 cm. For variation of hydraulic diffusivity in Pachappa sand, ranging from $3x10^{-4}s^{-1}$, to $10^{-1}cm^2s^{-1}$, the diurnal penetration depth scale ranges from 2.8 cm to 52 cm.

These rough calculations and the behavior of the ratio of gradients (Fig. 4) suggest that truncation errors in the computed flux for clay soils are large unless the upper layer is made quite thin. This expectation is demonstrated in Section 5.

4. Direct evaporation

In meteorological models, the surface moisture flux is usually parameterized in terms of a single soil water content as suggested by Thornwaite and Mather (1955) and Budyko (1956) (see Eagleson (1982) for a recent survey of such models). As the volumetric water content decreases below the saturation value, evaporation is usually modelled to continue at the potential rate until the water content decrease below a critical or reference value. Then the modelled evaporation is assumed to decrease linearly with decreasing water content vanishing at some small nonzero value of the water content. Such models appear to be in qualitative agreement with observations collected in Fig. 5.

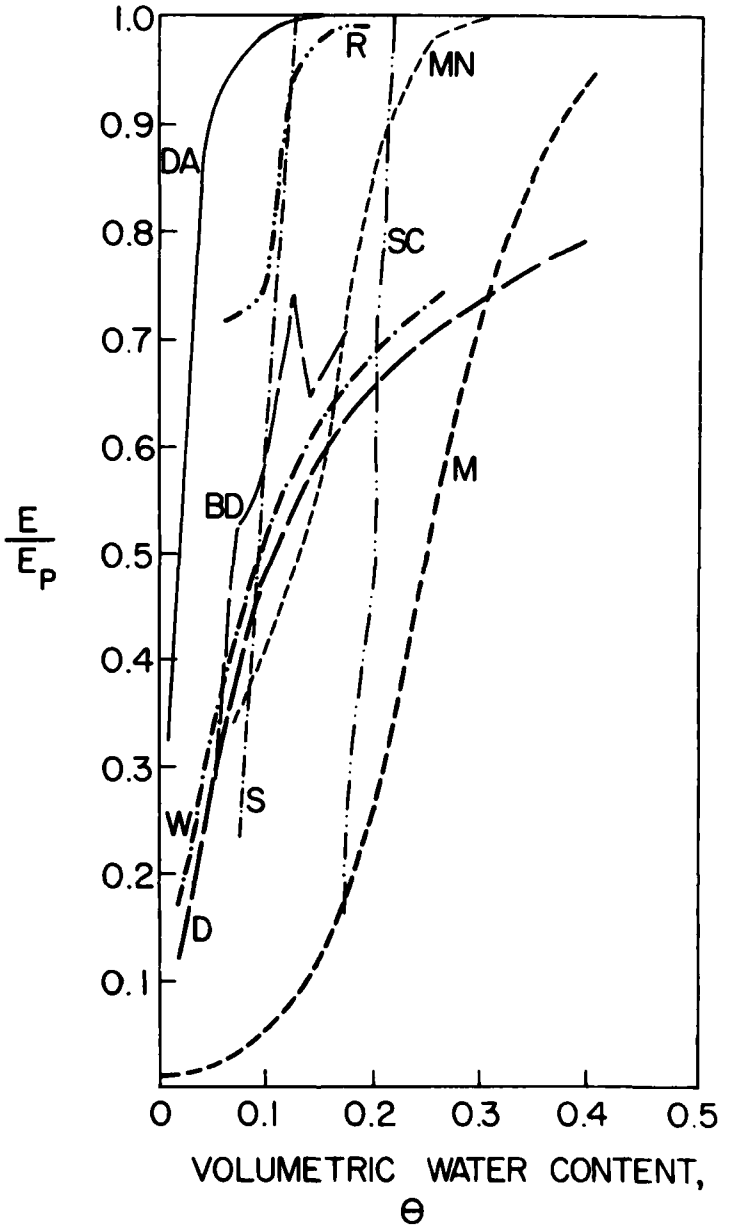

Fig. 5. Examples of observed evaporation scaled by the potential value as a function of soil water content. Thick lines represent cases where transpiration was thought to be of minimal importance. Individual curves are: (M), 5 cm layer of 50-60% sand covered by little vegetation (Marsh et al., 1981); (DA), 5 cm layer of sandy loam covered by ryegrass (Davies and Allen, 1973); (R) 1.5 m layer of sandy loam, vegetation recently burned (Rouse et al., 1977); (D), 1 or 2 cm layer of soil, vegetation recently burned (Barton, 1979); (W), 5 cm layer of soil covered by dry rangeland grass (Williams et al., 1978); (MN), 10-20 cm layer of heavy clay covered by shallow rooted grass (Mukammal and Neuman, 1977); (BD), 25 cm layer of sandy loam with soybean crop (Bailey and Davies, 1981); (SC), 37 cm layer of sandy clay loam with wheat crop (Seaton et al., 1977); (S), 37 cm layer of sandy loam with wheat crop (Seaton et al., 1977).

The dependence of evaporation on water content as determined from B is illustrated in Fig. 6. The relationship between evaporation and averaged soil water content is very sensitive to the averaging depth. The critical water content where evaporation begins to decrease with decreasing soil water occurs at a higher moisture value when a deeper layer is considered (Fig. 6). That is, the drying of a surface sub-layer decreases the evaporation even though the average water content of the entire layer may suffer only a slight decrease. These results imply that attempts to develop models of evaporation based on observations of volumetric soil water must take into account any differences between model levels and soil observational levels.

The relationship of evaporation to layer-averaged soil water content is more complicated in the case of on-off evaporation. On succeeding days of evaporation, the evaporation first starts to decrease at a higher soil water content compared to the previous day. This hysteresis is due to decreasing moisture at lower levels and generally smaller and more diffuse gradients.

For similar reasons the relationship between surface evaporation and layer-averaged soil moisture also depends on the potential evaporation rate E_p (Fig. 7). In particular, E/E_p, for a given layer-averaged soil water content, decreases with increasing potential evaporation. High potential evaporation leads to strong gradients near the surface so that the water content at the surface is less for a given layer-averaged value. With high potential evaporation rate, the soil has greater difficulty transporting water sufficiently fast to meet the atmospheric demand.

These results demonstrate some of the disadvantages of choosing the upper soil layer to be too thick when relating evaporation to soil moisture; namely that the evaporation becomes over-sensitive to the layer-averaged moisture value

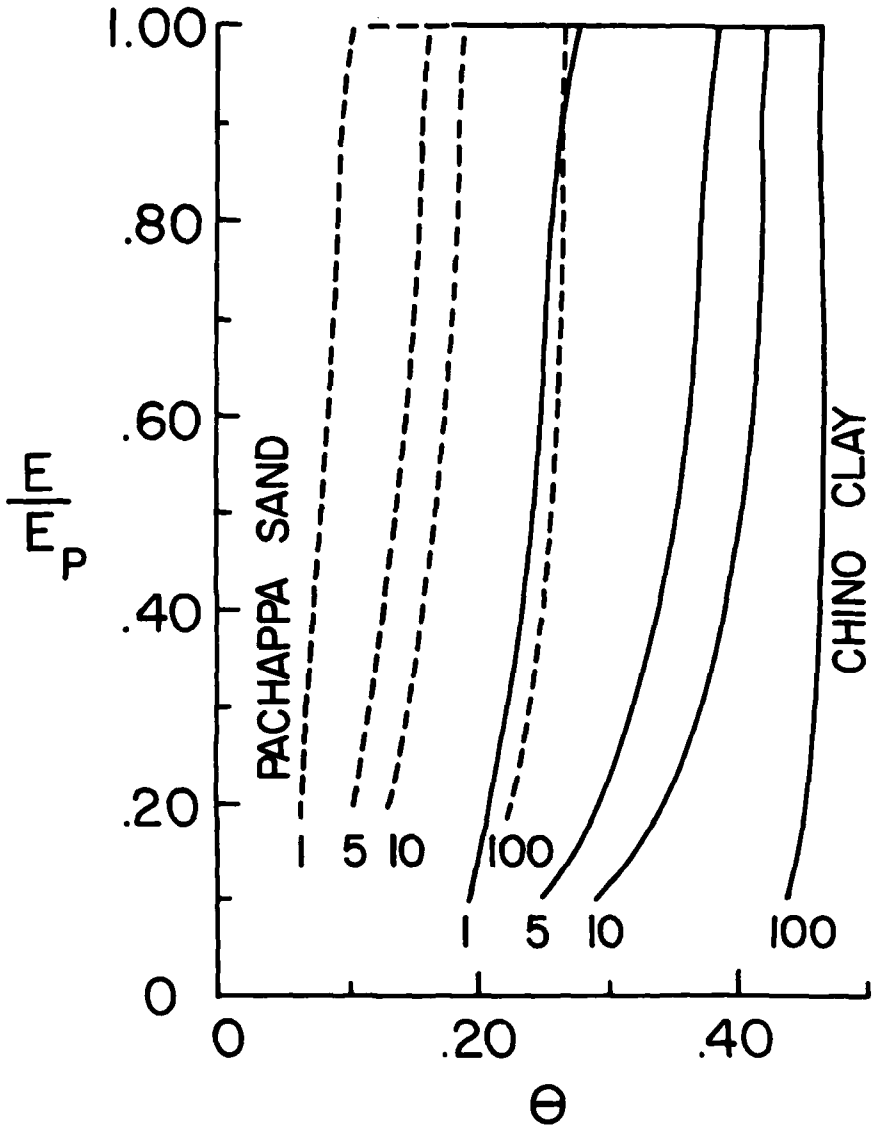

Fig. 6. Evaporation as predicted by model B for constant potential evaporation E_p = .1 cm/hr as a function of the volumetric water content averaged over layers of various depth labelled in cm.

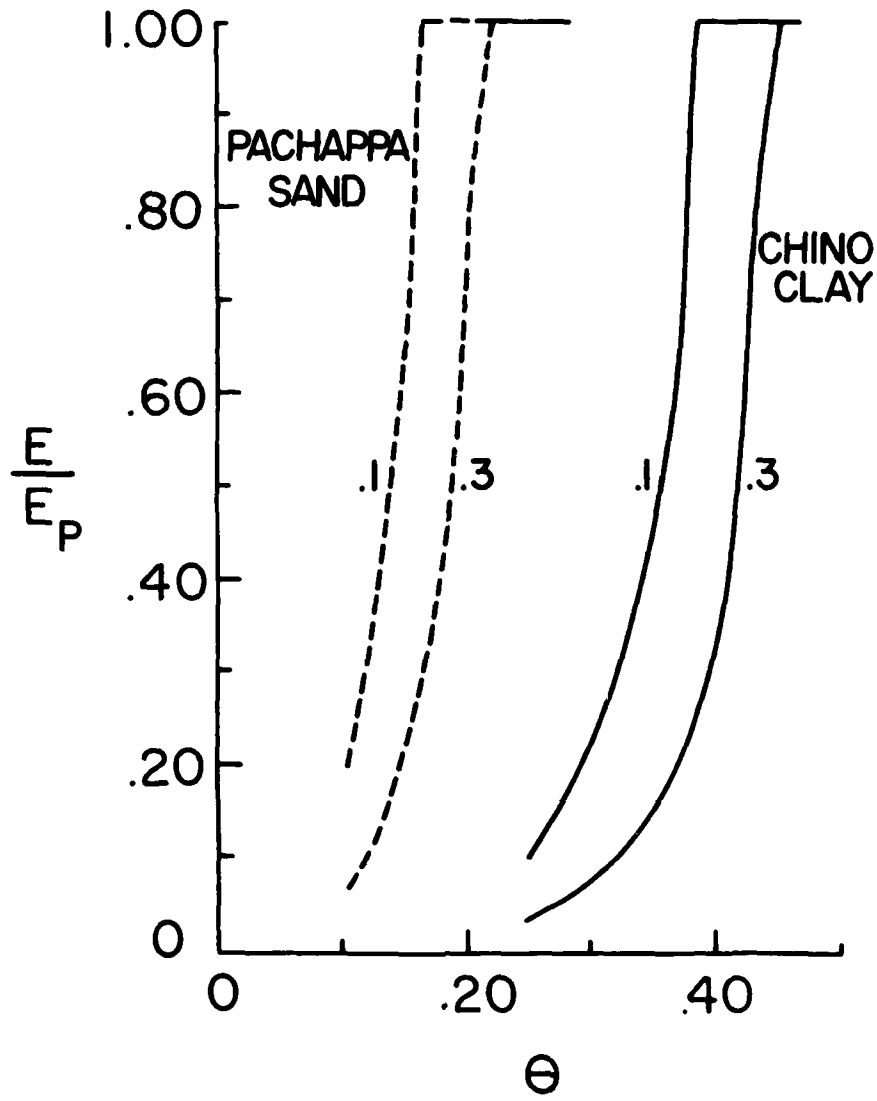

Fig. 7. Evaporation as predicted by model B for constant potential evaporation rates of E_p = .1 cm/hr and .3 cm/hr, as a function of the average volumetric water content θ of the upper 5 cm.

in the case of constant potential evaporation and becomes ambiguously related to the layer-averaged moisture value in the case of variable potential evaporation.

In fact, to completely avoid these problems, extremely thin soil layers would be required near the surface where vertical gradients are large during evaporation. In practice, the surface water content and vertical gradient must be defined over a finite depth which is unfortunately large enough to cause ambiguity between evaporation and water content. With a thinner surface layer, the measurement of water content becomes undefinable due to both the large vertical and horizontal gradients which typically occur near the surface.

An alternate approach is to employ an expression which assumes equilibrium between the soil water content at the surface and the relative humidity of the adjacent air as applied in McCumber and Pielke (1981) and Camillo et al. (1983). The predicted relative humidity allows determination of the surface evaporation using a bulk aerodynamic formulation.

There is no guarantee that the soil can meet the demand imposed by the bulk aerodynamic relationship even though this demand for unsaturated soil is less than the potential evaporation predicted from the bulk aerodynamic relationship with 100% surface relative humidity. McCumber and Pielke (1981) proceed with an iterative procedure which allows matching of near-surface soil water flux and the evaporation into the atmosphere.

Another approach can be constructed by assuming that evaporation proceeds at the potential rate until the surface soil water content decreases to an "air-dry" value (Hanks et al., 1969; Nimah and Hanks, 1973; Feddes et al., 1974). At the air-dry value, the water film is so thin, perhaps only one molecule thick, that electrostatic forces prevent evaporation from continuing at

the potential rate[1]. Then the evaporation is determined by the flux from below and consequently less than the potential rate.

This concept was implemented through an iterative algorithm in model B where the surface water content and soil water flux are iteratively adjusted. In the two-layer model, we proceed by replacing the iterative procedure with an analogous two step approach. We first tentatively demand the evaporation to be potential in which case

$$D(\theta)[\theta_{sfc} - \theta_1]/[(z_1/2)] + K(\theta) = E_p \ . \tag{8}$$

The left-hand side is the finite difference estimate of the water flux. We then compute θ_{sfc} from (8), where θ_{sfc} is that surface water content required to induce the necessary gradient to produce a soil water flux equal to the potential evaporation rate. If the resulting θ_{sfc} is greater than the air-dry value θ_d, then the evaporation rate is equated to the potential rate. If θ_{sfc} is less than the air-dry value θ_d, in violation of physical expectations, the potential evaporation cannot be met. Then the surface evaporation rate is controlled by the soil water profile and the surface water content is equal to the air-dry value in which case

$$E = D(\theta)[\theta_d - \theta_1]/(z_1/2) + K(\theta) < E_p \ . \tag{9}$$

[1]With this particular interpretation of the air-dry soil water content, the increase of density of water molecules in the first 5-10 molecular layers from the soil particle is assumed to not significantly influence the evaporation rate. The particular air-dry value defined in terms of a single molecular layer can be computed from the estimate of surface area of the soil particles which is an increasing function of percent clay content.

Comparisons with B indicated that using D and K values averaged between the surface and upper layer mid-level performed well. One could also analytically integrate the flux relationship between the surface and the mid-level of the upper layer. However, this did not improve the results of the 2-layer model. The air-dry value was chosen to be .05 for Pachappa Sand and .16 for Chino Clay as in B. As in Feddes et al. (1974), model results were found to be insensitive to the choice of air-dry value.

In contrast to use of an air-dry value, the approach based on an equilibrium humidity relationship leads to an immediate reduction of evaporation after the surface soil water decreases below saturation. However, this reduction is generally very slight until the soil surface becomes quite dry depending on the choice of coefficient values required for this approach. Then this approach behaves similarly to the method defined by (8-9).

It must be remembered that the surface soil water content or surface matric potential used in these two evaporation approaches is an internal model parameter with no clear geophysical analog. At the actual air-soil interface, soil water content and relative humidity are characterized by extremely large gradients in both the horizontal and vertical so that such properties are difficult to define. That is, the distribution of H_2O molecules changes significantly even on a molecular scale. However, the adjustment of the "surface" soil water content or matric potential in the above two approaches does not significantly violate the water budget since these surface properties are theoretically defined over an infinitesimally thin layer.

The choice between the above two approaches appears to be less important than the choice of hydraulic properties. In this study we use the latter approach (8-9) since it facilitates evaluation of truncation errors by comparison with B and because it is simpler. In fact, we will march in time by using

hydraulic properties from the previous time step in which case iteration can be avoided completely with use of (8-9). This leads to substantial savings of computer time but has the disadvantage of potentially large truncation errors. These errors result from the fact that the hydraulic diffusivity may vary substantially over a single time step. Comparisons in the next section indicate that such truncation errors are not serious with modest time steps.

5. Model comparison

Clearly, a simple two-layer model of soil hydrology must necessarily suffer significant truncation errors in the flux between layers and could be considered inadequate for many purposes. However, errors in the instantaneous between-layer flux generally translate into smaller errors in the surface evaporation particularly in the case of diurnal variations. The evaporation depends on the soil moisture near the surface which is more sensitive to long term errors in the between-layer flux and less sensitive to diurnal variations of the error in this flux. Additional truncation errors occur in the implementation of the surface moisture flux conditions (8-9). While truncation errors in the two-layer model should dominate the difference in the predictions between the two-layer model and B, other differences include the fact that model B is 158 cm deep whereas the two-layer model is one meter deep.

The between-layer flux and evaporation for the cases of Chino Clay and Pachappa sand are shown for potential evaporation specified to be constant (Figs. 8-9) and specified with on-off dependence on time (Figs. 10-11). For Pachappa sand forced by constant potential evaporation, the two-layer model predicts the total upward flux between layers to be comparable to the 5 cm flux in B for the first 24-hour period although some phase error occurs. After the first day, the 2-layer flux decreases more slowly with time than that in the

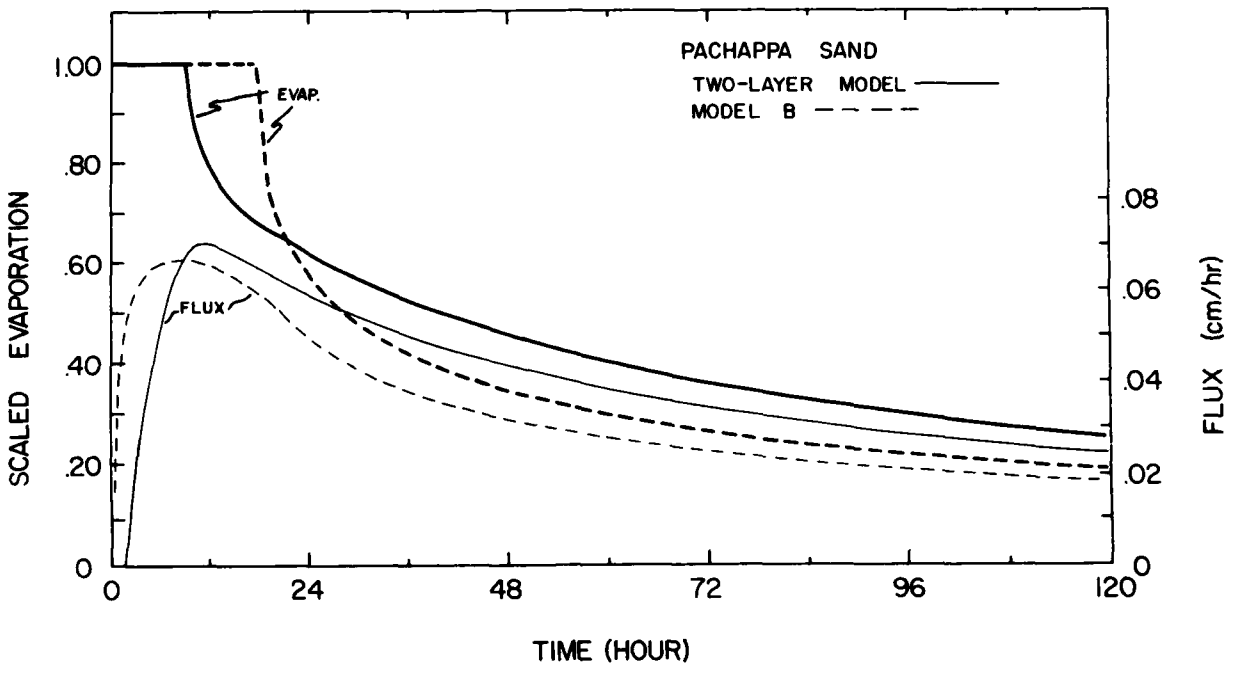

Fig. 8. Evaporation rate (thick solid) and between-layer flux (thin solid) for Pachappa sand forced by constant potential evaporation of .1 cm/hr for the two-layer model with an upper layer of 5 cm. Also shown are the corresponding evaporation rate from B (thick dashed) and the 5 cm water flux (thin dashed).

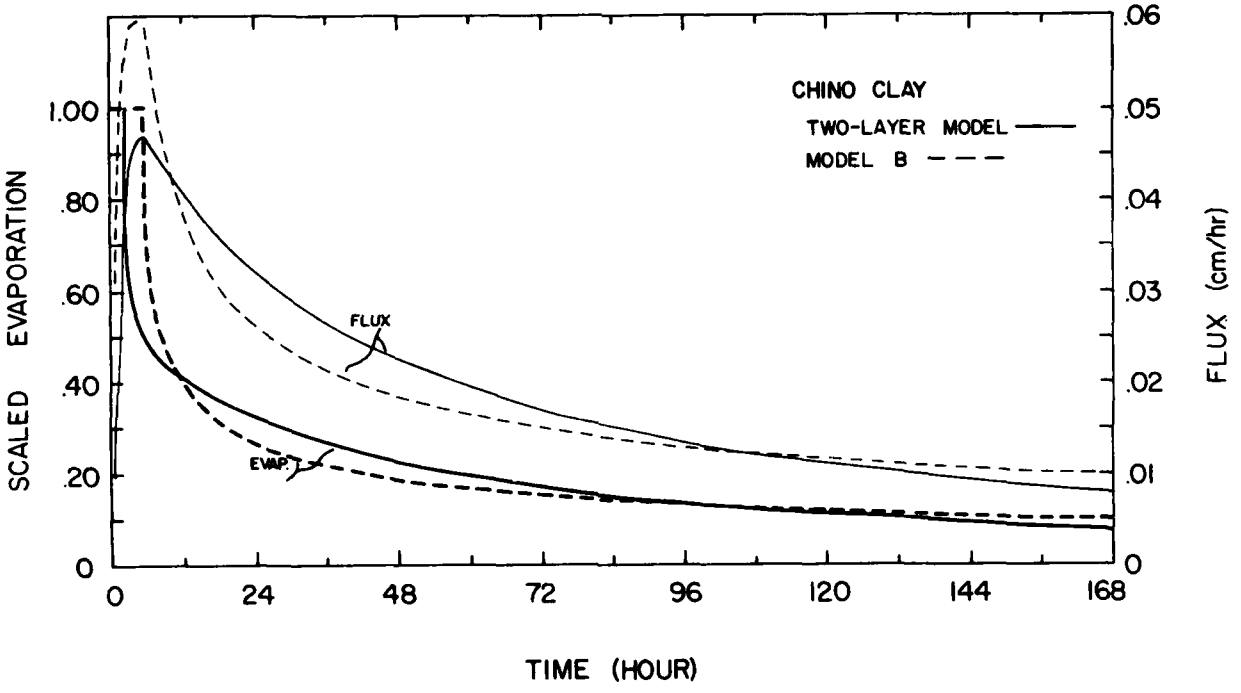

Fig. 9. Evaporation rate (thick solid) and between-layer flux (thin solid) for Chino Clay forced by constant potential evaporation of .1 cm/hr for the two-layer model with an upper layer of 1 cm thickness. Also shown are the corresponding evaporation rate from B (thick dashed) and 1 cm water flux (thin dashed).

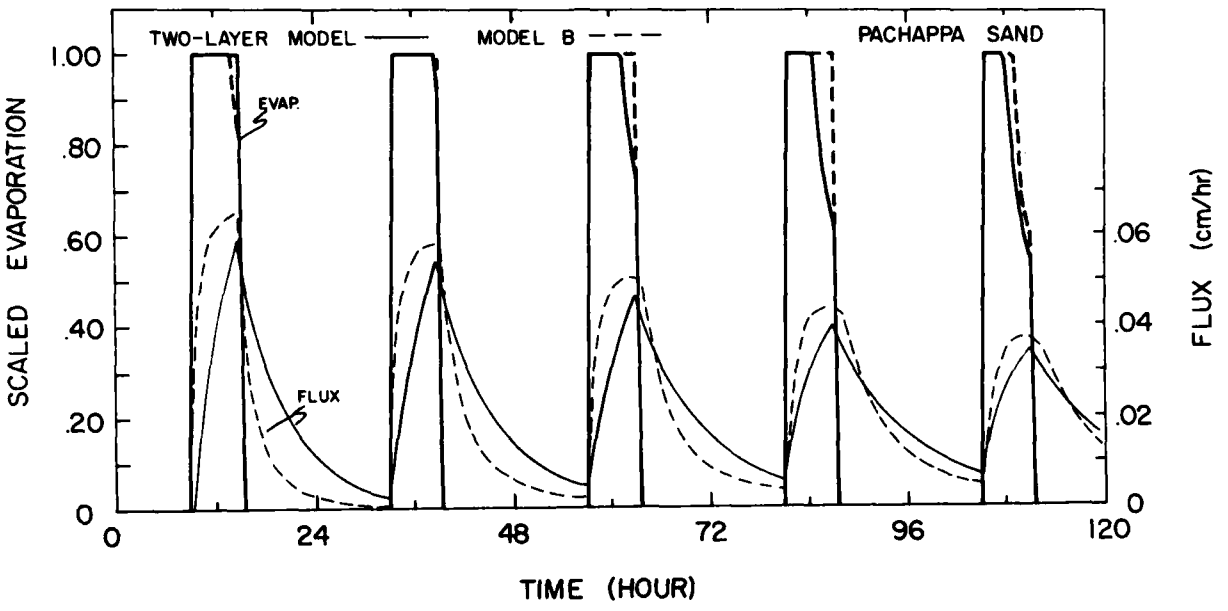

Fig. 10. Evaporation rate (thick solid) and between-layer flux (thin solid) for Pachappa sand forced by on-off evaporation for the two-layer model with a 5 cm upper layer. Also shown are the corresponding evaporation rate from B (thick dashed) and 5 cm flux (thin dashed).

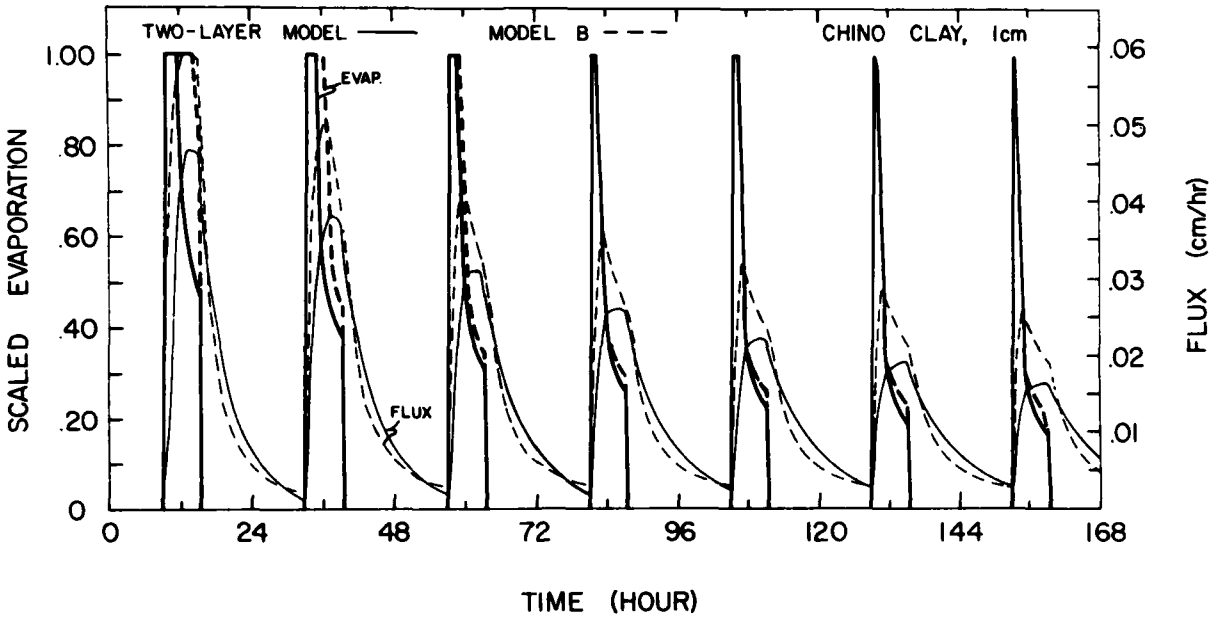

Fig. 11. (a) Evaporation rate (thick solid) and between-layer flux (thin solid) for Chino Clay for on-off evaporation with a 1 cm upper layer. Also shown are the evaporation rate from B (thick dashed) and corresponding 1 cm flux. After 72 hours the two evaporation rates generally coincide.

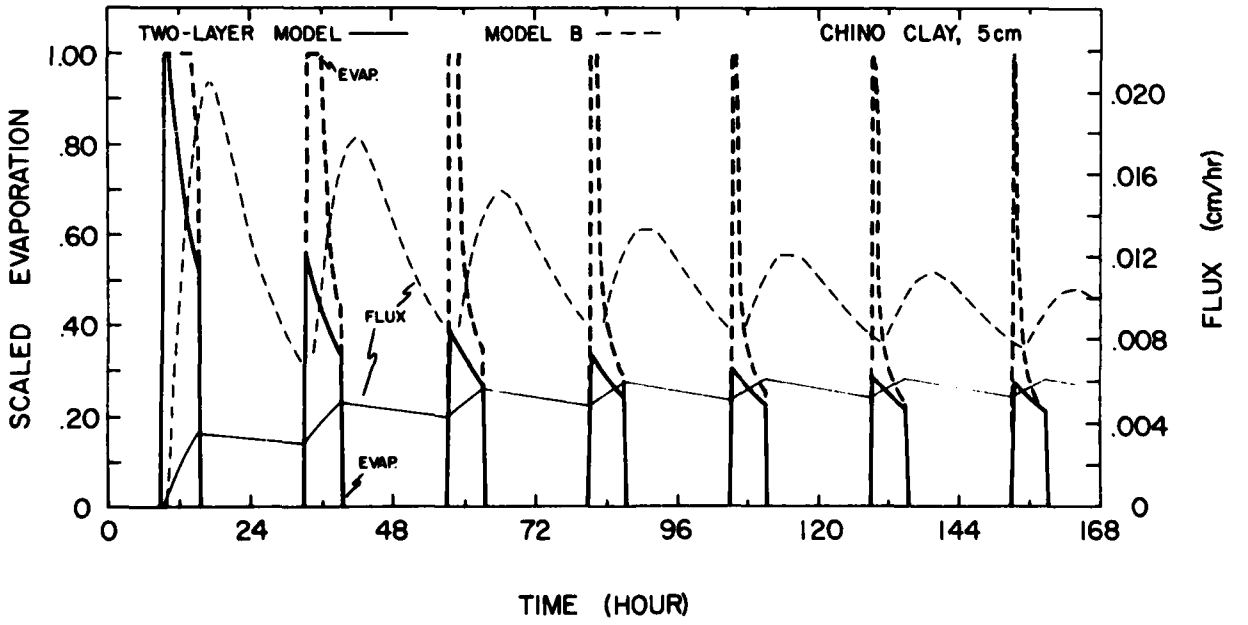

Fig. 11. (b) Same as (a) except for a 5 cm upper layer and 5 cm flux from B.

high-resolution model B. This overestimation of upward water flux eventually leads to an overestimation of the evaporation rate by about 30%. The error in the total accumulated evaporation is significantly less.

When the modelled Pachappa sand is forced by on-off evaporation, the upward water flux between the two layers lags the 5 cm flux in B by several hours (Fig. 10). However, the underestimation of the "daytime" flux is approximately compensated by an overestimation of flux during non-evaporation periods. As a result, the 24-hour between-layer flux predicted by the two-layer model is close to that predicted by the high-resultion model B. Both models predict near potential evaporation for the duration of the numerical experiment.

For the case of modelled Chino Clay, the depth of the upper layer is reduced from 5 cm to 1 cm while the depth of the lower layer is reduced from 95 cm to 19 cm. This change recognizes the small diffusivity and small diurnal penetration depth in clayey soils as discussed in Section 3. Note that the diffusivity for Chino Clay is particularly small (Fig. 2). If the original 5 cm and 95 cm thicknesses are retained for Chino Clay, the two-layer model substantially underestimates the between-layer flux and evaporation as is illustrated for the case of on-off evaporation (Fig. 11b). With the reduced layer thickness (Fig. 11a), the underestimation of the between-layer flux is substantially less although still significant. The evaporation rate predicted by the two-layer model and B become almost identical after the first two days. The evaporation rates predicted by the two models are also in relatively close agreement for Chino Clay forced by constant potential evaporation with the same 1 cm thickness for the upper layer (Fig. 10).

An additional on-off evaporation experiment was conducted where evaporation on the fourth day is replaced with precipitation at a rate of .3 cm/hr. The

two-layer model somewhat underestimates the resulting downward flux of soil water for both soil types. Results for Pachappa sand, which responds more rapidly than Chino Clay, are shown in Fig. 12. Recall that in the case of downward water flux, formulation (6-7) automatically uses the hydraulic diffusivity and conductivity of the upper layer. This substantially reduces the net truncation error.

The truncation errors revealed by the above comparisons can be reduced further by adjusting the depth of the upper layer although this adjustment is dependent on situation. As the thickness of the upper layer is decreased, the time step must be reduced. However, for most applications, the above truncation errors will be smaller than errors resulting from the estimate of soil type and corresponding dependence of diffusivity on soil water content. From the above model comparisons, truncation errors in the between-layer flux appear to be generally less than 30%, particularly when averaged over a 24-hour period. For comparison, inspection of Fig. 2 indicates that minor errors in the estimation of soil type or percent clay content would lead to larger errors in the water flux.

6. Conclusions

At the onset, we concluded that at least two soil layers are required in order to simultaneously include the dependence of evaporation on near-surface soil water content and include the storage of soil water which occurs in a deeper layer. Since more than two layers cannot be accommodated in many modelling situations, we have evaluated the behavior of truncation errors in the two-layer model by comparing with the high resolution model of Boersma et al. (1983).

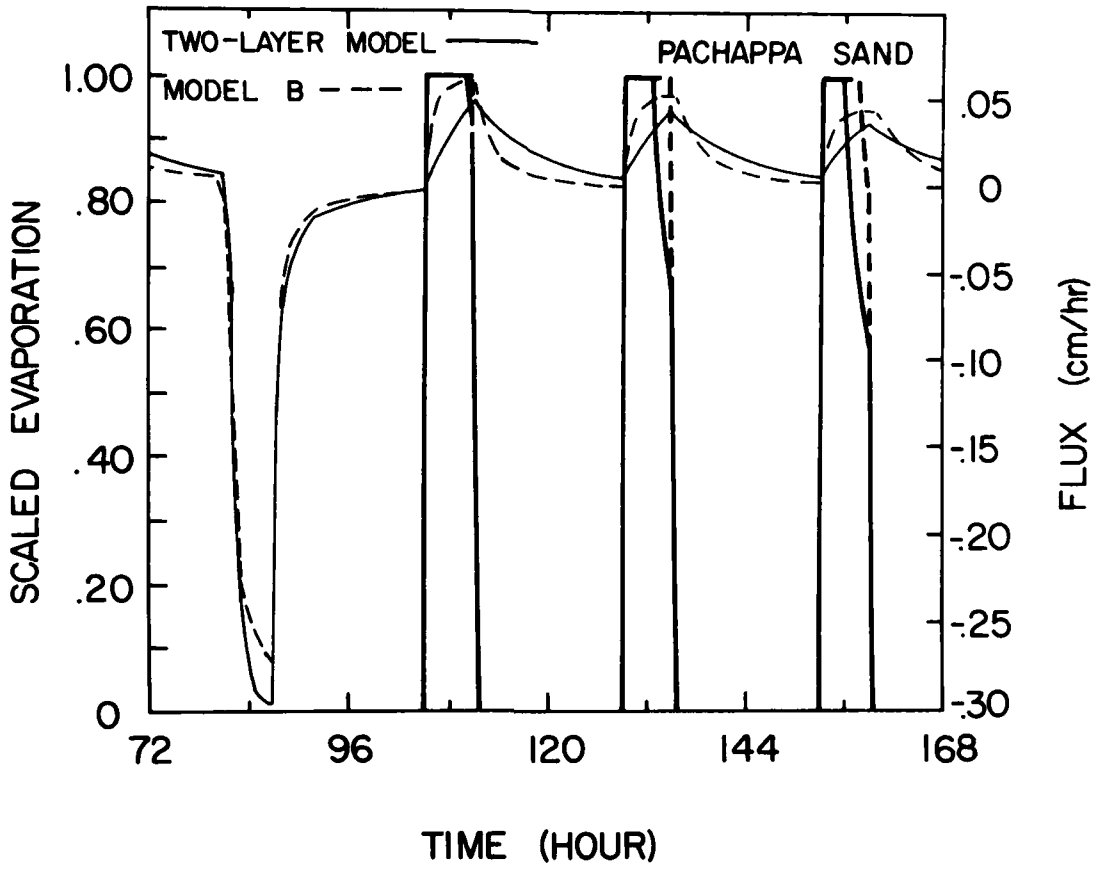

Fig. 12. Evaporation rate (thick solid) and between-layer flux (thin solid) for Pachappa sand (5 cm upper layer) for on-off evaporation with precipitation on the fourth day between 78 and 84 hours.

These comparisons indicate that the two-layer model will typically underestimate the water flux within the soil (Section 5) due to truncation errors. However, the impact of such truncation errors on interfacial water flux can be minimized by choosing the upper layer to be sufficiently thin and by using the diffusivity corresponding to the water content of the layer from which the water flux originates. The reduced truncation errors are still significant and increased resolution would be required for many research situations. However, the truncation errors are probably small compared to errors in estimating the behavior of the hydraulic diffusivity for actual soil applications without extensive measurements. In particular, area-averaged soil properties must be estimated for use in atmospheric and hydrological models. Since the soil hydrology is very nonlinear, it is not clear how to determine such an average even if sufficient soil data were available. Soils often exhibit extreme horizontal variations on small scales.

In Section 4, a surface moisture flux algorithm was developed which allows control by the soil moisture profile near the surface yet does not require iteration. This procedure is found to be preferable to the usual practice of relating evaporation to the layer-averaged soil moisture content.

Since transpiration is related to soil moisture in the root zone and not sensitive to the surface value, it could be most simply included by evaluating formulations similar to those surveyed in Eagleson (1982) (see also Fig. 5) using the layer-averaged moisture. In such a manner, a model of evapotranspiration could be constructed from the present soil model which would be suitable for many modelling situations where simplicity is required.

7. Application to the AFGL model

It is our opinion that the physics of the one-layer model is sufficiently inadequate to be of use in the AFGL general circulation model. The two-layer model is able to include the most important physics, namely that the evaporation is related to the near-surface soil moisture while storage of water is related to the soil moisture in a deeper layer.

Unfortunately, the two-layer model suffers significant truncation errors. However, these truncation errors are not likely to be larger than uncertainties in the variation of soil type both geographically and with respect to depth. The initial soil model will contain "universal" properties which will be comparable to those of loam of intermediate clay content.

The role of vegetation and organic debris (dead plant material on the soil surface) also leads to significant uncertainties in the modelling of the hydrological budget. As a result of this uncertainty and difficulty in estimating soil type, we have concluded that reducing truncation errors by installing more than two layers does not justify the increased computer time.

For this reason, future research on the soil models of general circulation models would best concentrate on parameterizing vertical structure through profile functions and should also concentrate on the behavior of moisture transfer content in the immediate vicinity of the air-soil interface. Inclusion of the thermodynamics of the two-layer soil model is also worth investigating further since it is not particularly complicated and could be important in special circumstances.

For initial use in the AFGL soil model, we have decided upon the Clapp and Hornberger (1978) model for hydraulic diffusivity and conductivity. Which is of the form

$$K = K_s(\theta/\theta_s)^{2b+3}$$

$$D = \frac{bK_s\psi_s}{\theta_s}(\theta/\theta_s)^{b+3} \quad .$$

Where K_s is the saturation hydraulic conductivity, ψ_s the saturation matric potential, θ_s the saturation volumetric water content, and b, a coefficient which depends on soil type. If we assume a "universal soil type" to have average characteristics comparable to sandy clay loam (28% clay) then b=7.12, K_s=1.6 x 10^{-5} cm/min, θ_s=.42, and ψ_s=29.9 cm. The categorization of soil type according to grid point location is a possible future refinement.

The addition of root uptake and transpiration is carried out in Chapter IV, Sections 2-3.

References

Bailey, W.G., and J.A. Davies, 1981: The effect of uncertainty in aerodynamic resistance on evaporation estimates from the combination model. Bound.-Layer Meteor., 20, 187-199.

Barton, I.J., 1979: A parameterization of the evaporation from non-saturated surfaces. J. Appl. Meteor., 18, 43-47.

Black, T.A., C.B. Tanner, and W.R. Gardner, 1970: Evapotranspiration from a snap bean crop. Agron. J., 62, 66-69.

Boersma, L., M.J. Ungs, and E.L. Mccoy, 1983: Transfer problems in soils. Ag. Exp. St., Oregon State University, Corvallis, 97331, U.S.A.; see also: W.F. Ames, (ed.), Proceedings IMACS World Congress on systems simulation and scientific computation. 8-13 August 1982. Montreal, Canada. International Association for Mathematics and Computers in Simulation.

Budyko, M.I., 1956: Teplovoi Balans Zemnoi Poverkhnosti, Gidrometeoizdat, Leningrad; Heat balance of the earth's surface, translated by N.A. Stepanova, U.S. Weather Bureau, Washington, D.C., 1958.

Camillo, P., R. Guerney, and T.J. Schmugge, 1983: Soil and atmosphere boundary layer model for evapotranspiration and soil moisture studies. Water Resour. Res., 19, 371-380.

Campbell, G.S., 1974: A simple method for determining unsaturated conductivity from moisture retention data. Soil Science., 117, 311-314.

Clapp, R.B., and G.M. Hornberger, 1978: Empirical equations for some soil hydraulic properties. Water Resour. Res., 14, 601-604.

Davies, J.A., and C.D. Allen, 1973: Equilibrium, potential and actual evaporation from cropped surfaces in southern Ontario. J. Appl. Meteor., 12, 649-657.

Day, P.R., and J.N. Luthin, 1956: A numerical solution of the differential equation of flow for a vertical drainage problem. Soil Sci. Soc. Am. Proc., 20, 443-447.

Deardorff, J.W., 1977: A parameterization of ground-surface moisture content for use in atmospheric prediction models, J. Appl. Meteor., 16, 1182-1185.

Eagleson, P.A., 1982: Dynamic hydro-thermal balances at macroscale. 289-360. Proceedings of World Meteorological Organization. Presented at JSC Study Conference on Land Surface Processes in Atmospheric General Circulation Models. Jan 5-10, 1981.

Feddes, R.A., E. Bresler, and S.P. Neuman, 1974: Field test of a modified numerical model for water uptake by root systems. Water Resour. Res., 10, 1199-1206.

Gardner, W.R., 1960: Dynamic aspects of water availability to plants. Soil Sci., 89, 63-73.

Gardner, W.R., D. Hillel, and Y. Benyamini, 1970: Post-irrigation movement of soil water, 2. Simultaneous redistribution & evaporation. Water Resour. Res., 6, 1148-1153.

Hanks, R.J., and S.A. Bowers, 1962: Numerical solution of the moisture flow equation for infiltration into layered soils. Soil Sci. Soc. Am. Proc., 26, 530-534.

Hanks, R.J., A. Klute, and E. Bresler, 1969: A numeric method for estimating infiltration redistribution, drainage, and evaporation of water from soil. Water Resour. Res., 5, 1064-1069.

Hillel, D., 1980: Fundamentals of soil physics, Academic Press, 413 pp.

Jackson, R.D., 1973: Diurnal changes in soil water content during drying. Field Soil Water Regime, 3, 37-55.

Jersey, Gilbert R., 1982: Incorporation of a simple evapotranspiration parameterization in an efficient model of the atmospheric boundary layer. Masters thesis, Dept. of Meteorology, The Pennsylvania State University, University Park, PA.

Marsh, P., W.R. Rouse, and M.-K. Woo, 1981: Evaporation at a high Arctic site. J. Appl. Meteor., 20, 713-716.

Marshall, T.J., and J.W. Holmes, 1979: Soil Physics. Cambridge University Press, Cambridge, 345 pp.

McCumber, M.C., and R.A. Pielke, 1981: Simulation at the effects of surface fluxes of heat and moisture in a mesoscale numerical model. J. Geophys. Res., 86, 9929-9938.

Mukammal, E.I., and H.H. Neumann, 1977: Application of the Priestly-Taylor evaporation model to assess the influence of soil moisture on the evaporation from a large weighing lysimeter and class A pan. Bound.-Layer Meteor., 12, 243-256.

Nimah, M.N., and R.J. Hanks, 1973: Model for estimating soil water, plant, and atmospheric interrelations: I. Description and sensitivity. Soil Sci. Soc. Amer. Proc., 37, 522-527.

Passioura, J.B., and I.R. Cowan, 1968: On solving the non-linear diffusion equation for the radial flow of water to roots. Agric. Meteor., 5, 129-134.

Rouse, W.R., P.F. Mills, and R.B. Stewart, 1977: Evaporation in high latitudes. Water Resour. Res., 13, 909-914.

Seaton, K.A., J.J. Landsberg, and R.H. Sedgley, 1977: Transpiration and leaf water potentials of wheat in relation to changing soil water potential. Aust. J. Agric. Res., 28, 355-367.

Thornwaite, C.W., and J.R. Mather, 1955: The water balance. Publications in climatology, 8, Laboratory of Climatology, Centerton, NJ, 86 pp.

Williams, R.J., K. Boersma, and A.L. van Ryswyk, 1978: Equilibrium and actual evapotranspiration from a very dry vegetated surface. J. Appl. Meteor., 17, 1827-1832.

IV. Canopy-Transpiration Budget

Abstract

This chapter summarizes extensive literature surveys of models of the canopy water budget and formulations of the relationship between actual evapotranspiration and potential evaporation. A new model for the canopy water budget is developed which is simple, consistent with other parts of the model and avoids certain asymptotic difficulties of previous models.

The dependence of transpiration on potential evaporation and soil moisture deficit is formulated with a plant coefficient and a functional dependence on the soil volumetric water content. This formulation is based on a large number of observational studies reported here in Chapter IV and also in Chapter III. Interdependence between transpiration, direct evaporation from the soil, and evaporation of intercepted water from the canopy is formulated in a manner to insure self-consistency and certain asymptotic conditions for the total evapotranspiration.

1. Canopy water budget

a. Introduction

The amount of water that is captured and retained by vegetation and evaporated back to the atmosphere without adding moisture to the mineral soil is defined as the inteception loss. This definition excludes water that is temporarily captured by the vegetation before dripping to the ground or flowing down the stems and trunks to the ground. Transpiration is not included as interception.

Tree canopies, grasslands, crops and decaying organic material on the ground (litter) all intercept water. Fig. 1 shows relative magnitudes of the hydrological cycle of a vegetation-soil system, including interception and interception loss (shaded areas). These losses may be a significant addition of water vapor to the atmosphere. Reevaporation of intercepted water from a conifer forest canopy can amount to 20-40% of the total annual precipitation falling on the stand and 10-20% for a hardwood forest (Zinke, 1967). In some instances the annual loss can range up to 70% (Pearce et al., 1980). For individual light precipitation events, a dense canopy could intercept nearly 100% of the rain or snow. Litter interception losses, not shown, would normally be a small quantity, about half the soil evaporation or less.

When water is retained on a leaf, transpiration is suppressed. It has been suggested that evaporation of intercepted water exactly compensates the suppressed transpiration such that there is no net loss of water (Leyton and Carlisle, 1959; Penman, 1963). If this is the case, then water could be evaporated from the wetted portion of the canopy and transpired from the dry portion of the canopy at the same rate, regardless of the total wetness of the canopy.

AD-A144 224 A BOUNDARY LAYER PARAMETERIZATION FOR A GENERAL MODEL (U) OREGON STATE UNIV CORVALLIS DEPT OF ATMOSPHERIC SCIENCES L MAHRT ET AL. MAR 84 AFGL-TR-84-0063 2/2

UNCLASSIFIED F19628-81-K-0046 F/G 8/13 NL

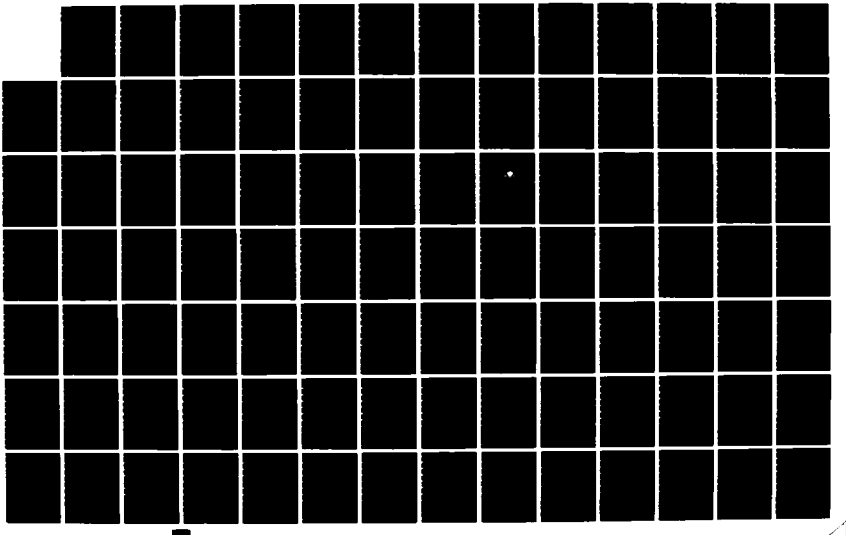

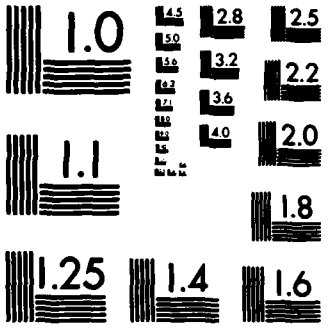

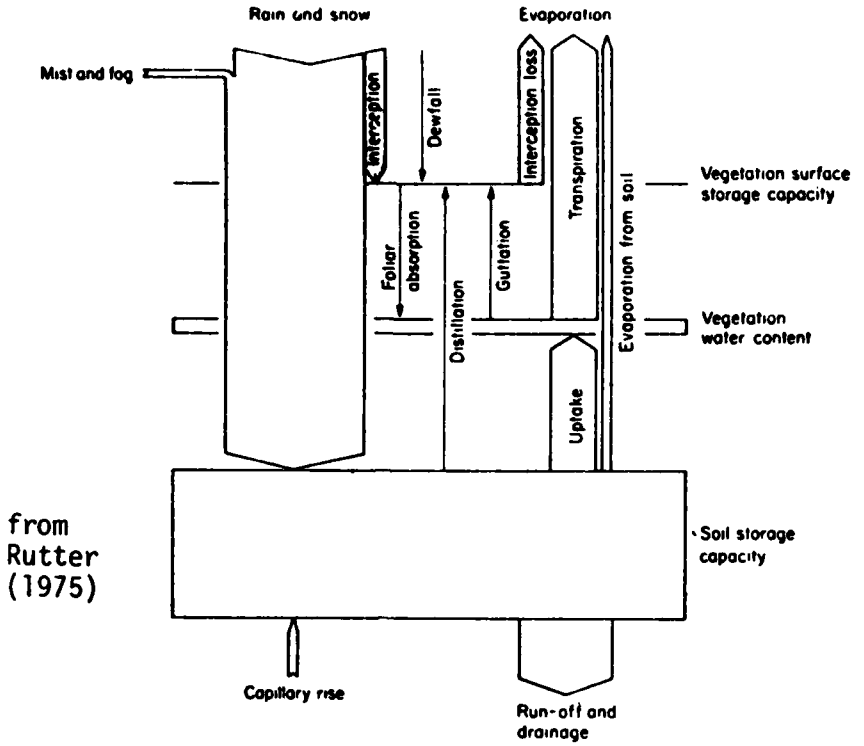

Fig. 1. The hydrological cycle in a vegetation-soil system; components approximately to scale for annual rainfall 100 mm and evaporation 500 mm.

However, recent research has indicated that the rate of evaporation of intercepted water from a canopy could be three times or more greater than the transpiration rate (e.g., Thorud, 1967; Waggoner et al., 1969; Stewart, 1977; Singh and Szeicz, 1979), thus the total evaporation from a canopy could exceed the potential evaporation. Potential evaporation is a reference evaporation which is modified by plant type and maturity, time of year, and soil moisture content to determine the actual evaporation of the plant. For short vegetation, such as grasses, transpiration rates of dry surfaces are large enough to equal evaporation of intercepted water, such that there would be nearly no net addition of water to the atmosphere.

In this section we will attempt to determine the canopy capacity of various types of vegetation and then proceed with a critical survey of models available with the purpose of defining a model to determine the amount of water evaporated from a canopy back to the atmosphere.

b. Canopy capacity

The amount of water retained on a canopy after rainfall and drip drainage have ceased in the absence of wind is defined as the canopy capacity, S. This value, expressed either as depth of water or depth of water per projected unit area of the canopy, is dependent on meteorological and climatic conditions, species, and leaf or needle characteristics. Zinke (1967) provides an extensive review of capacity values for various American species. Table 1 presents

Table 1. Average canopy capacity values, $\bar{S}$, for various vegetation types. n is the number of different values used to determine $\bar{S}$.

Type (n)	$\bar{S}$ (mm)	Reference(s)
Conifers		
Pine (8)	0.95	Zinke, 1967; Gash and Morton, 1978
Spruce (2)	2.00	Leyton et al., 1967; Hancock and Crowther, 1979
Douglas Fir (1)	1.20	Robins, 1974
Mixture (1)	2.00	Bringfelt and Harsmer, 1974
Hardwoods		
Eastern No. Am. Hardwoods	0.30-1.60	Helvey and Patric, 1965
Mixture		
Leafy (4)	0.90	Zinke, 1967; Leyton et al., 1967;
Leafless (4)	0.50	Thompson, 1972.
Shrubs (5)	1.20	Zinke, 1967
Grasses (2)	1.30	Zinke, 1967
Tropical Highland Forest (1)	1.00	Jackson, 1975

average canopy capacity values for rainfall for various vegetation types. These values should be used with caution since they are averages and deviations should be expected according to genus, climatic conditions, rainfall duration and intensity, and dislodging forces such as wind.

Zinke (1967) speculates that capacity values of 1.3 mm for rain for most grasses, shrubs and trees would be a reasonable average. Snowfall required to attain canopy capacity ranged from 2.3 mm to 9.1 mm (for 4 cases) for conifers, with 3.8 mm reported as a reasonable average. Snowfall on hardwoods is not reported, but should be minimal.

c. Interception models

Regression models

Horton (1919) introduced a model for total-storm interception of rainfall which fills the canopy to capacity according to

$$I = S + kEt_r \qquad (1)$$

where I is the interception in water depth on the projected crown area, S the canopy capacity in the same units, E the evaporation rate in water depth per unit time, and t_r the duration of the storm. The ratio of vegetal surface to its ground projection, k, is analogous to leaf area index as defined by Ross (1975) and generally exceeds 1.0. This equation states that the total interception during a storm is equal to the canopy capacity plus evaporative losses; i.e., evaporation increases the amount intercepted when the canopy is filled to capacity.

Eq. (1) assumes that the canopy fills to capacity during the storm. For a storm where the capacity is not reached, the amount intercepted does not exceed the total rainfall and could be expressed as

$$I = Pt_r \qquad (2)$$

where P is the precipitation rate.

Horton also suggests relating total interception to total gross precipitation P_g, according to

$$I = a + b\,P_g \qquad (3)$$

where a and b are constants for individual species. Hydrologists have used this method quite often to determine the hydrology of a catchment or basin, determining a and b through regression analysis. The disadvantages of this approach are discussed later.

Some of the models presented in the literature are shown in Table 2.

Table 2. Regression models relating interception, I, to precipitation characteristics. P_g is the gross rainfall, D duration and R intensity.

Vegetation	Model	Reference
Northern Hardwoods East of 100th meridian (average over many models)		
Growing Season	$I=0.083\ P_g + 0.036$	Helvey and Patric, 1965
Dormant Season	$I=0.059\ P_g + 0.020$	
Old-growth Douglas Fir, Oregon	$I=0.17\ P_g + 0.046$	Rothacher, 1963
Eastern White Pine (western No. Carolina)	$I=0.14\ P_g + 0.06$	Helvey, 1967
Ponderosa Pine Laws.	$I=0.06\ P_g + 0.11$ for $P_g > 0.5$ in.	Rowe & Hendrix, 1951
Tropical Forest (east Africa)	$I=0.85 + 0.542 \ln P_g$ $I=0.764 + 0.521 \ln D + 0.50 \ln R$ (P_g in mm)	Jackson, 1975

Zinke's (1967) review paper of U.S. vegetation presents additional models and interception amounts as percentage of gross precipitation. Molchanov (1960) presents results for eastern Europe.

Jackson (1975) related interception to various precipitation characteristics using linear, quadratic and logarithmic models. He found that as little as 20% and as much as 60% of the variance of the interception observations could be explained by the various models. The models in Table 2 are two that gave satisfactory results, explaining 46% (relating I to P_g) and 56% (relating I to D and R) of the variance.

The regression models, while simple to use, suffer some serious disadvantages. First, all do not apply until the precipitation exceeds a threshold value. In the case of linear models, P_g must exceed a/(1-b) where a is the intercept and b the slope. Secondly, the regression coefficients are usually determined for a specific stand of trees and probably do not apply to the same species in another climate or stand with different characteristics. Finally, the models provide little insight into the physics of the interception process.

Aston model

Aston (1979) proposed a model for a single-storm event which fills the canopy to capacity. The gross interception is expressed as

$$I = S\{1 - \exp[(1 - p)\ P_g/S]\} + kEt_r \qquad (4)$$

where p is the throughfall fraction or fraction of the canopy which allows precipitation to pass through to the ground, i.e., gaps in the canopy, and the other variables are as defined previously. The last term on the right is a

general evaporation term, identical to the term used by Horton (1919) and discussed earlier. No attempt by Aston is made to further define this term.

Gash model

Gash (1979) developed a model that computed the total interception over a number of storms with sufficient time between storms to allow the canopy and trunk to dry completely. In addition he assumed meteorological conditions from storm-to-storm are similar so that mean precipitation and evaporation apply to all storms, that there is no drainage from the canopy when C < S and for C > S, C = S within 20-30 minutes after rainfall ceases, independent of C at the time rainfall ceases where C is the actual canopy water content. The model for total interception loss over n+m storms is

$$\underset{j=1}{\overset{n+m}{\Sigma}} I_j = \underset{\text{I}}{(1-p-p_t)\underset{j=1}{\overset{n}{\Sigma}} P'_j} + \underset{\text{II}}{(1-p-p_t)\underset{j=1}{\overset{m}{\Sigma}} P_j} + \underset{\text{III}}{(\bar{E}/\bar{R})\underset{j=1}{\overset{n}{\Sigma}} (P_j - P'_j)} + \underset{\text{IV}}{qS_t} + \underset{\text{V}}{p_t \underset{j=1}{\overset{n+m-q}{\Sigma}} P_j} \qquad (5)$$

where P is the gross rainfall, P' the rainfall necessary to fill the canopy to capacity, p the free throughfall coefficient for the forest stand, P_t the water diverted and retained on stems and trunk, $\bar{E}$ and $\bar{R}$ the average evaporation and rainfall, respectively, computed from those hours when the canopy is saturated. S_t is the stem and trunk capacity, n the number of storms sufficient to fill the canopy capacity, m the number of storms not sufficient to fill the canopy and q the number of storms of the total, n+m, that fill the trunk to capacity. Terms I and II are contributions to total interception from storms that fill and do not fill the canopy capacity, respectively, term III is the

additional amount intercepted due to evaporation when the canopy is full and terms IV and V are contributions from trunk and stems, respectively. The evaporation from each storm is estimated from the Monteith (1965) equation.

The amount of water required to attain canopy capacity is given by

$$P'_g = S(-\bar{R}/\bar{E}) \ln \{1-(\bar{E}/\bar{R}) (1-p-p_t)^{-1}\}. \quad (6)$$

This model is the most complete of the interception models, separating and computing interception losses resulting from evaporation during rainfall and from canopy characteristics. A drawback is the need to know values of p, p_t and S_t, for which little or no observations exist for various species. Use of this model would then require a guess at these values. Also long term observations to compute $\bar{E}$ and possible $\bar{R}$ for forest stands may not exist and empirical values of $\bar{E}$ and $\bar{R}$ may be necessary.

Water balance models

The amount of water on a canopy is charged by gross precipitation and depleted by evaporation and drip drainage (or blowoff in the case of snow). In the previous section gross amounts of intercepted water per storm period were determined, primarily by relating interception to gross precipitation. This section will present models that determine changes in time of water storage on a canopy by considering drip and evaporation from the vegetal surfaces. Most of the models consider only evaporation of intercepted water and not transpiration since they are concerned with the hydrology of a watershed rather than the amount of water evaporated back to the atmosphere. These models could be extended to include transpiration.

Rutter model

Rutter et al. (1971) proposed a single-layer canopy model to describe interception loss in pine canopies by calculating a running balance in time of rainfall, evaporation, throughfall which includes drip drainage, and changes in canopy storage.

The change in canopy storage of water, ΔC, for any period within a storm, is given by

$$\Delta C = \Sigma R - \Sigma T - \Sigma E \qquad (7)$$

where ΣR is total rainfall, ΣT total throughfall and ΣE total evaporation. These values are expressed as equivalent depth of water. Total throughfall is the sum of total drip drainage, ΣD, and "free" throughfall or rainfall through gaps in the canopy

$$\Sigma T = \Sigma D + p\Sigma R \qquad (8)$$

where p is proportion of rain falling through the canopy. Substituting (8) into (7) yields

$$\Delta C = (1-p)\ \Sigma R - \Sigma D - \Sigma E. \qquad (9)$$

Drip is assumed not to begin until the amount of water on the canopy, C, exceeds the capacity of the canopy, S. After C > S then the drip rate D (in mm/unit time) is given by

$$D = K \exp(\bar{b}C)$$

where $\bar{b}$ is an empirically derived constant and $K = \exp(\ln(0.002) - \bar{b}S)$. When the canopy water is reduced to 0, this parameterization incorrectly continues to produce a finite drip, at a rate equal to K. Improvements to this are discussed later in other models.

The evaporation rate E (in mm/unit time) is assumed to be

$$E = \begin{cases} E_p & \text{if } C > S \\ E_p \cdot \frac{C}{S} & \text{if } C \leq S \end{cases}$$

where E_p is the potential or reference evaporation rate. This is a crude assumption since the canopy is assumed to be one layer and the same amount of water C could be distributed differently, thus changing the evaporation. A possible modification to this is presented in Section 3 of this Chapter.

In both of the above we note that C could exceed S. Rutter neither explains how this is possible or by how much C should be allowed to exceed S. Physically, some excess water could temporarily be detained on the canopy before dripping through. Evidence of canopy water exceeding capacity is the drip occurring after rainfall ceases and in the absence of wind or other dislodging forces.

The final form of Rutter's model for computing changes in canopy water storage during rainfall is

$$\frac{dC}{dt} = \begin{cases} (1-p)R - K \exp(\bar{b}C) - E_p & C > S \\ (1-p)R - K \exp(\bar{b}C) - E_p \cdot \frac{C}{S} & C \leq S \end{cases} \qquad (10)$$

After rainfall, (1-p)R vanishes and the change in canopy water is due to drip and evaporation. When C > S, it was assumed that there was no drip ($\Sigma T = p\Sigma R$); therefore, the exponential drip term above could be dropped for $C \leq S$. Rutter argues, however, that the drip rate is extremely small, on the order of 10^{-3} mm hr^{-1}, and unimportant when C < S, so retaining it should cause little error.

This model forms the basis for many other models. It follows changes of canopy water with time by considering simplified physics of the interception process. Its major drawback is its treatment of evaporation of water from the canopy. No distinction is made between transpiring and evaporating leaf surfaces or the distribution of canopy water. Rutter et al. (1975) considered a more generalized interception loss model, but did not improve the evaporation computation.

Calder model

Calder (1977) made Rutter's drip term linear to eliminate the finite drip from a dry canopy. His model, using the same notation, is

$$\frac{dC}{dt} = -b_i C + (1-p)R - E \qquad (11)$$

where $b_i = \begin{cases} b_1 & \text{for } C > S \\ b_2 & \text{for } C \leq S \end{cases}$

and E is determined from the Penman-Monteith equation. Using optimization techniques Calder determined the optimum parameters for b_1, b_2, p and S.

Simulated storm results were compared to actual storms for a spruce forest and it was found that S ≈ 1.95mm.

MANTA model

The MANTA model (Sellers and Lockwood, 1981) is a multi-layer crop model that has inputs to and outputs from four levels within a vegetal covering. Although too complex for our needs, important features of the model are that evaporation from the wetted portion of the leaf and transpiration from the dry portion are both considered and that there is a quadratic relationship between wetted area of a leaf layer and C/S for each layer. This latter assumption is discussed in developing a model for our use.

Massman model

Massman (1980) developed a model to predict changes in canopy storage which included the components found in previous models but computed by other methods. His model is of the form

$$\frac{dC}{dt} = I(t) - D_o\left(\frac{e^{\alpha(C/S)}-1}{e^{\alpha}-1}\right) - E_o\left(\frac{e^{\beta(C/S)}-1}{e^{\beta}-1}\right) \qquad (12)$$

where I(t) is the interception intensity, D_o and α drainage constants, and E_o and β evaporation constants, the latter four depending on foliage characteristics and meteorological conditions. E_o could be estimated by a Penman-like equation, D(t) directly proportional to I(t), i.e.,

$$D(t) = I(t)\left(\frac{e^{\alpha(C/S)}-1}{e^{\alpha}-1}\right) \qquad (13)$$

or I(t) assumed to be constant.

A major problem with this method is the lack of definition or quantification of α and β for any vegetation type. Also D(t) proportional to D_o or I(t) depends on foliar wetness and whether or not it is raining. As with the Calder (1977) model, the problem of finite drip from a dry canopy has been eliminated.

NCAR GCM

The National Center for Atmospheric Research (NCAR) general circulation model contains a routine to compute total intercepted water by a canopy within its planetary boundary layer subroutine (Dickinson et al., 1981). The computation is very complex using numerous variables and attempts to include all factors in the interception process. The model, keeping with notation conventions already established, is

$$\frac{\partial C}{\partial t} = (1-p)R - (E_f - E_{tr}) \tag{14}$$

where E_f and E_{tr} are the total evaporation rate including transpiration and the suppressed transpiration of the wetted portion of the canopy, respectively. The factor 1-p is a calculated quantity, dependent on subsurface temperature, and is given by

$$1-p \equiv \sigma_f \approx \begin{cases} \sigma_f \text{ summer} & T_{g2} > 298K \\ \sigma_f \text{ summer} - \{1-FSEAS(T_{g2})\}\Delta\sigma_f & 273K \leq T_{g2} \leq 298K \\ \sigma_f \text{ summer} - \Delta\sigma_f & T_{g2} < 273K \end{cases}$$

where σ_f summer and $\Delta\sigma_f$ are predetermined and tabulated by vegetation type. FSEAS(T_{g2}) is a seasonal adjustment of $\Delta\sigma_f$, depending only on subsurface temperature.

The NCAR model also computes the maximum amount of water a canopy can hold W_{dmax}. This is similar to canopy capacity S except that it apparently includes temporary storage due to drip time lag. W_{dmax} is a vegetation and seasonally adjusted foliage cover coefficient given by

$$W_{dmax} = 0.02\text{cm}\ \sigma_f\ \text{LSAI}$$

where LSAI is a leaf-stem area index defined by LSAI = LAI + SAI (= leaf area index + stem area index). SAI is a tabulated value according to vegetation type since it does not depend on season but LAI is computed by

$$\text{LAI} = \text{LAI}_{min} + \text{FSEAS}\ (T_{g2})\ (\text{LAI}_{max} - \text{LAI}_{min})$$
$$= f(\text{season, vegetation type})$$

and LAI_{max} and LAI_{min} are specified according to vegetation type.

Precipitation is added to the canopy if $C < W_{dmax}$. Otherwise $C = W_{dmax}$ and any excess is added to the soil as rain or snow, depending on the choice of a temperature for rain or snow determination.

E_f represents the total evaporation of moisture from vegetation to atmosphere which is reduced by the total suppressed transpiration, E_{tr}. Both of the above require many computations and are not presented here. An important point in the computations is that each one is adjusted for the proportion of canopy wetness through the factor $(C/W_{dmax})^{2/3}$ and also adjusted for seasonal foliage cover. This is one step further than the MANTA model previously discussed in that seasonal foliage cover is considered.

Stanford Watershed Model

A hydrological model currently used by people interested in the water balance of a watershed is the Stanford Watershed Model, SWM-IV described, in part, in Viessman et al. (1977). In this model all incoming precipitation is intercepted unless the precipitation rate exceeds the interception rate, predefined according to vegetation type and cover, or if the canopy capacity is attained. Evaporation of intercepted water is at the potential rate until the interception storage is depleted.

The model seems to assume that all surfaces of the foliage are wetted or dried at the same rate and that canopy water storage does not exceed the canopy capacity.

d. Litter interception

Litter, the dead and decaying organic material on the forest floor, has not received much attention. The few results available indicate that the amount of water intercepted by litter is a function of stand age. It is estimated that 2-5% of the gross annual rainfall is evaporated from litter (Zinke, 1967). For our purposes interception loss from litter will be assumed negligible. A more important function of litter interception is to reduce direct evaporation from the soil which may be necessary to include in the soil moisture model.

2. Transpiration

For the limited complexity which can be accommodated here, transpiration is best related to potential evaporation by means of a single coefficient or function without explicit representation of stomatal and internal plant resistances. This coefficient is often referred to as the crop coefficient or plant coefficient. This approach is the usual one in routine irrigation management and simple hydrological modelling. As a result there are many studies attempting to determine the value of the plant coefficient; some of these studies are summarized in Table 3.

Table 3. Plant coefficients (PC) for different seasons at different locations. Maximum refers to the maximum for the growing season; growing season is the average for the growing season. General refers to any location where modification by empirical coefficients of climate and geography are necessary for application of PC to a specific location. Necessary for the determination of PC is the way in which PET and ET are obtained. Comb. refers to a combination equation, TB is a thermally based equation, pan is pan evaporation, ETB is an energy and thermally based equation. Lys is a lysimeter measurement and BC refers to an already existing Blaney-Criddle crop coefficient so that no PET measurement was made.

	Season	PC	Location where valid	First author, Date	PET measurement method or equation	ET measurement method
Agricultural plants:						
Crop: Alfalfa						
1.	Spring Summer Fall	.93 .99 .96	Arizona	Van Bavel, 1966	comb.	lys.
2.	Maximum	1.00	Arizona	Van Bavel, 1967	comb.	lys.
3.	Maximum Growing	1.35 1.00	General	Hargeaves, 1974	TB	lys.
4.	Maximum	.85	Semi-arid & Arid locations	Holmes, 1959	---	BC
5.	Maximum Yearly Avg.	1.10 .80	General	USDA*, 1967	---	BC

* United States Department of Agriculture

Table 3. (continued)

Crop: Snap Beans						
1.			Kimberly, Idaho	Wright, 1978	comb.	lys.
2.	Summer	.48	Wisconsin	Black, 1970	comb.	lys.
3.	Maximum Growing Season	1.10 .85	General	USDA, 1967	---	BC
4.	Maximum Growing Season	1.15	General	Hargreaves, 1974	TB	lys.
Crop: Dry Beans						
1.	Maximum Growing Season	1.10 .85	General	USDA, 1967	---	BC
2.	Maximum Growing Season	1.15 .90	General	Hargreaves, 1974	TB	lys.

Table 3. (continued)

Crop: Soy Beans						
1.	Maximum Growing Season	1.05 .65	General	USDA, 1967	---	BC
2.	Maximum Growing Season	.73	India	Vankatachari, 1978	---	BC
3.	Maximum Growing Season	1.15	General	Hargreaves, 1974	TB	lys.
4.	Maximum Growing Season	1.10 .70	Iowa	Stanley, 1978	pan	neutron-probe gravimetric
Crop: Corn						
1.	Summer Late Summer	1.15 1.01	Ohio	Parmele, 1974	comb.	lys.
2.	Maximum Growing Season	1.25 .80	Israel	Lomas, 1974	comb.	lys.
3.	Maximum Growing Season	1.15 .70	Minnesota	Dylla, 1980	ETB	lys.
4.	Maximum Growing Season	.89 .71	India	Vankatachari, 1978	---	BC
5.	Maximum Growing Season	1.15	General	Hargreaves, 1974	TB	lys.
6.	Maximum Growing Season	1.08 .85	General	USDA, 1967	---	BC
Crop: Cotton						
1.	Maximum	.70	Israel	Fuchs, 1963	--	BC
2.	Maximum Growing Season	.81 .60	India	Vankatachari, 1978	---	BC
3.	Maximum Growing Season	1.02 .60	General	USDA, 1967	---	BC
4.	Maximum Growing Season	1.15 .90	General	Hargreaves, 1974	TB	lys.

Table 3. (continued)

Crop: Grain (wheat)						
1.	Maximum	.81	India	Vankatachari, 1978	---	BC
	Growing Season	.72				
2.	Maximum	.95	Eastern Oregon	Bates, 1982	pan	neutron probe
	Growing Season	.70				
3.	Maximum	1.30	General	USDA, 1967	---	BC
	Growing Season	.75				
4.	Maximum	1.15	General	Hargreaves, 1974	TB	lys.
	Growing Season	.90				
Crop: Grain (Barley)						
1.	Growing Season	.76	Denmark	Kristensen, 1974	Penman	neutron probe
Crop: Grain (Sorghum)						
1.	Maximum	.72	India	Vankatachari, 1978	---	BC
	Growing Season	.56				
2.	Maximum	1.08	General	USDA, 1967	---	BC
	Growing Season	.70				
3.	Maximum	1.15	General	Hargreaves, 1974	---	lys.
	Growing Season	.90				
Crop: Grass (short, green)						
1.	Summer	.80	SE England	Thom, 1977	Penman	?
	Winter	.60				
2.	Growing Season	.73	Denmark	Kristensen, 1974	Penman	neutron probe
3.	Maximum	1.00	General	Hargreaves, 1974	TB	lys.
	Growing Season	1.00				
4.	Spring	.75	Wyoming	O'Neill, 1979	---	BC
	Summer	.90				
	Fall	.70				

Table 3. (continued)

Crop: Grass (long)						
1. Growing Season	.74	Denmark	Kristensen, 1974	Penman	neutron probe
Crop: Grass (Pasture)						
1. Summer	.90	Australia	Shepherd, 1972	comb.	lys.
2. Maximum Growing Season	1.50 .85	Netherlands	Stricker, 1978	bulk aerodynamic	energy balance
3. Maximum	1.15	General	Hargreaves, 1974	TB	lys.
Crop: Potatoes						
1. Maximum Growing Season	1.38 .90	General	USDA, 1967	---	BC
2. Summer	.90	Australia	Shepherd, 1972	comb.	lys.
3. Maximum Growing Season	.90 .50	*Eastern Oregon*	Bates, 1982	pan	neutron probe
4. Maximum Growing Season	1.15 .90	General	Hargreaves, 1974	TB	lys.
Crop: Rice						
1. Maximum	1.20	Arid & Semi-Arid Conditions	Holmes, 1959	---	BC
2. Summer	1.02	California/Davis	Lourence, 1971	reference crop	energy balance
Crop: Sugar Cane						
1. Maximum Growing Season	1.25 1.00	General	Hargreaves, 1974	TB	lys.
2. Growing Season	.85	General	USDA, 1967	---	BC

Table 3. (continued)

Crop: Sugar Beets						
1.	Growing Season	.82	Denmark	Kristensen, 1974	Penman	neutron probe
2.	Maximum	1.15	General	Hargreaves,	TB	lys.
	Growing Season	.90		1974		
3.	Maximum	1.25	General	USDA, 1967	---	BC
	Growing Season	.90				
Crop: Field and Oil Crops (Flax, peanuts, safflower, tomatoes)						
1.	Maximum	1.15	General	Hargreaves,	TB	lys.
	Growing Season	.90		1974		
Crop: Citrus Fruits (Orange, lemon grapefruit)						
1.	Maximum	.75	General	Hargreaves,	TB	lys.
	Growing Season	.75		1974		
2.	Maximum	.72	General	USDA, 1967	---	BC
	Yearly Avg.	.70				
Crop: Deciduous Fruits (peaches, plums, walnuts)						
1.	Maximum	1.10	General	Hargreaves,	TB	lys.
	Growing Season	.85		1974		
2.	Maximum	1.00	General	USDA, 1967	---	BC
	Yearly Avg.	.50				
Crop: Grapes						
1.	Maximum	.75	General	Hargreaves,	TB	lys.
	Growing Season	.60		1974		
2.	Maximum	.82	General	USDA, 1967	---	BC
	Yearly Avg.	.50				

Table 3. (continued)

Crop: Summer Vegetables					
1. Maximum	1.15	General	Hargreaves, 1974	TB	lys.
Growing Season	.85				
2. Maximum	.85	General	USDA, 1967	---	BC
Growing Season					
Non-agricultural plants:					
Plant: Spruce, Pine, Fir					
Spring	1.00	France	Assenac, 1972	?	?
Summer	1.00				
Fall	1.00				
Plant: Douglas Fir					
Annual Range	.64 to 1.00	France	Assenac, 1972	?	?
Plant: Prairie grass					
Summer	.90	Canadian Great Plains	Nkemdirim, 1973	Penman	lys/ neutron probe

Table 3. (continued) Seasonal plant coefficients (PC) for irrigated crops from USDA (1967).

Crop	Length of Normal Growing Season of Period (1)	Plant Coefficient (2)
Alfalfa	Between frosts	0.80 to 0.90
Bananas	Full year	.80 to 1.00
Beans	3 months	.60 to .70
Cocoa	Full year	.70 to .80
Coffee	Full year	.70 to .80
Corn (Maize)	4 months	.75 to .85
Cotton	7 months	.60 to .70
Dates	Full year	.65 to .80
Flax	7 to 8 months	.70 to .80
Grains, small	3 months	.75 to .85
Grain, sorghums	4 to 5 months	.70 to .80
Oilseeds	3 to 5 months	.65 to .75
Orchard crops:		
Avocado	Full year	.50 to .55
Grapefruit	Full year	.55 to .65
Orange and lemon	Full year	.45 to .55
Walnuts	Between frosts	.60 to .70
Deciduous	Between frosts	.60 to .70
Pasture crops:		
Grass	Between frosts	.75 to .85
Ladino whiteclover	Between frosts	.80 to .85
Potatoes	3 to 5 months	.65 to .75
Rice	3 to 5 months	1.00 to 1.00
Soybeans	140 days	.65 to .70
Sugar beet	6 months	.65 to .75
Sugarcane	Full year	.80 to .90
Tobacco	4 months	.70 to .80
Tomatoes	4 months	.65 to .70
Truck crops, small	2 to 4 months	.60 to .70
Vineyard	5 to 7 months	.50 to .60

(1) Length of season depends largely on variety and time of year when the crop is grown. Annual crops grown during the winter period may take much longer than if grown in the summertime.

(2) The lower values of plant coefficients for use in the Blaney-Criddle formula are for the more humid areas, and the higher values are for the more arid climates.

Although such studies are ubiquitous, three major uncertainties remain:

(1) The crop coefficient is related to a variety of different definitions of potential evaporation which might significantly influence the value of the plant coefficient.

(2) Values have been estimated primarily for commercial crops. Information on natural plant communities is limited.

(3) Due to the usual observational set up, the plant coefficient usually includes both transpiration and direct evaporation from soil. We will want to distinguish between transpiration and direct soil evaporation because the relationship of these two processes to the soil moisture distribution is different.

a. Plant coefficient

The plant coefficient is formally defined here as the ratio of transpiration to the potential evaporation for the case of insignificant soil water deficit. Unfortunately, the plant coefficient is usually evaluated from measurements as the ratio of the total evapotranspiration to the potential evaporation. However, with significant vegetative cover the contribution due to direct evaporation will usually be small. The plant coefficient accounts for the various ways which plant density and stomatal behavior influence the actual transpiration. We will later partition the influences of vegetative density and stomatal resistance. We leave the two factors combined here since the distinction between them is usually not possible from observations.

Evapotranspiration may be determined by direct or indirect methods. An example of direct measurements of $\overline{(w'q')}$ is the computation from observations of fluctuations of specific humidity q and vertical motion w.

Evapotranspiration may be estimated indirectly by means of the energy budget. Net radiation, soil heat flux and sensible heat flux are determined; the residual term is then equated to latent heat flux (e.g., Fritschen, 1965). The soil moisture budget method equates evapotranspiration to precipitation less change in soil moisture storage, runoff at the surface and infiltration to the ground water zone beneath (Strahler, 1975). Instrumentation used in measuring the change in soil moisture include lysimeters and other gravimetric devices, and the neutron probe. A lysimeter is an isolated block of soil in which soil moisture can be closely monitored. In general, gravimetric methods involve a "before" and "after" soil moisture measurement which is then related to evapotranspiration. The neutron probe is an instrument that measures the scattering of neutrons in the soil and relates this to water content.

b. Measurements

Fig. 2 is an idealized example of the annual variation of potential evapotranspiration, actual evapotranspiration, direct evaporation from the soil, and transpiration. Available information on evaporation of intercepted water does not allow construction of a curve for seasonal variation. Note that the transpiration curve peaks more sharply in summer than the soil evaporation or potential evapotranspiration curves. This is due to the large increase in the plant coefficient mainly associated with increasing plant density. The sum of the soil evaporation and transpiration curves gives the evapotranspiration curve which also peaks sharply. As a result the value of the plant coefficient peaks in summer (Fig. 3). Note the significant decrease of the plant coefficient as the plant approaches maturity.

The plant coefficients in Table 3 represent typical values from numerous studies. Listed are plant coefficients for vegetation types for different times

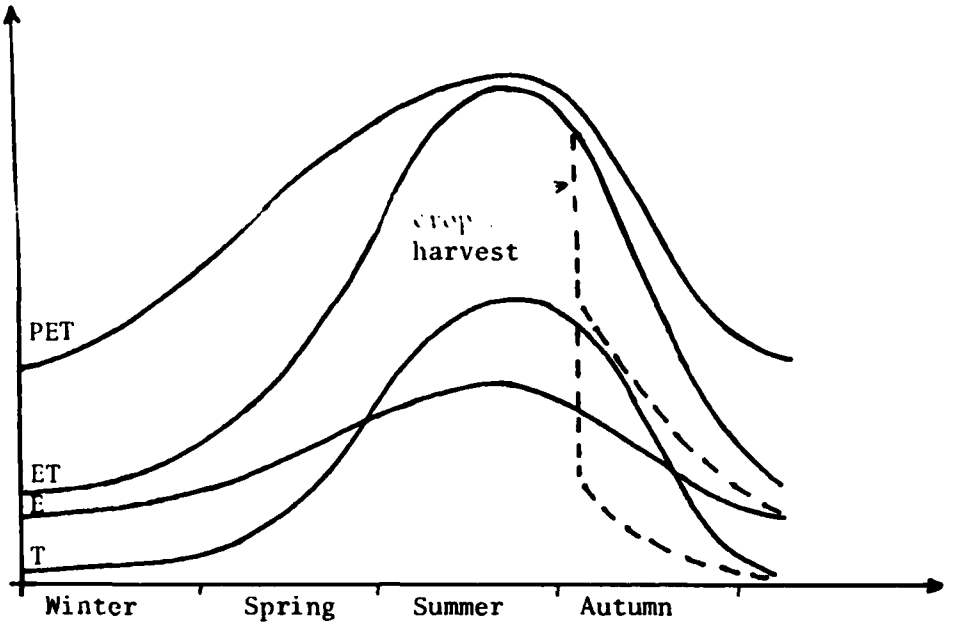

Fig. 2. Typical examples of annual curves of potential evapotranspiration (PET), evapotranspiration (ET), soil evaporation (E), and plant transpiration (T). Curves generalized from Al-Khafaf et al.(1978); Bates et al. (1982); Cuenca et al.(1981); Fritschen (1982); Kanemasu et al. (1976); Nelson and Hwang (1976); Russell (1980).

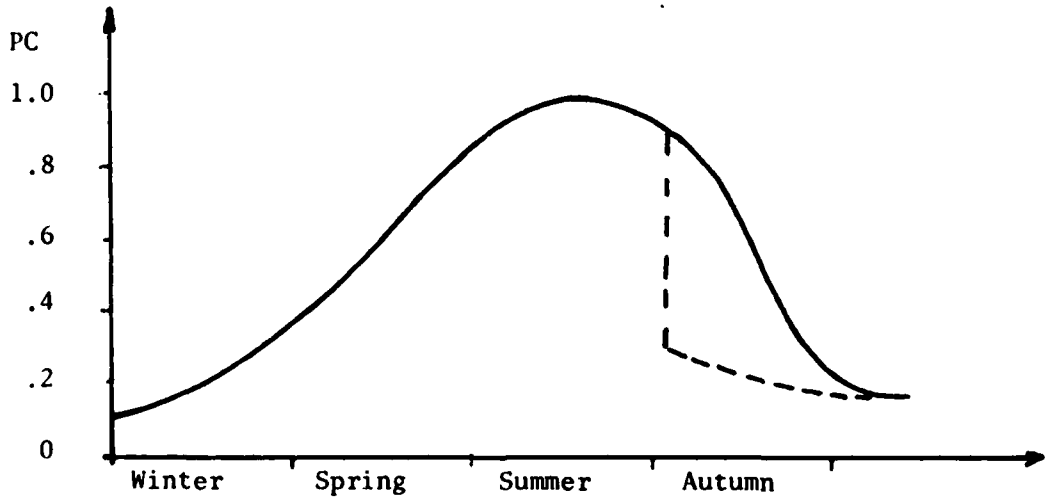

Fig. 3. Typical example of an annual plant coefficient (PC) curve. Dashed line indicates modification due to harvest. Curve generalized from Bates et al. (1982) and Wright and Jensen (1978).

of the year at various geographic locations for the condition of non-limiting soil moisture.

c. Plant coefficient partitioning

From a physical point of view it is useful to separate the influences of stomatal resistance and vegetative density because the latter leads to reduction of direct evaporation from the soil due to decreased solar radiation and air flow at the soil surface.

Therefore, we represent the plant coefficient as

$$E_T/E_p = k_v \sigma_f$$

where E_T is the transpiration, E_p the potential evaporation, k_v a factor due to stomatal resistance analagous to that used in Eagleson (1982) and σ_f a factor representing vegetative density (Deardorff, 1978; Eagleson, 1982) which will be referred to as the shading factor.

The coefficient σ_f, which varies between zero and one, has the advantage that it also represents the percent of solar radiation reaching the soil surface after adjusting for sun angle. The principle disadvantage is that measurements of transpiration have been usually related to the "leaf area index." Some examples are shown in Fig. 4. Fortunately these results are of guidance here since the relation between shading factor and leaf area index has been estimated in several studies (Fig. 5).

The product $k_v \sigma_f$ typically varies between .5 and unity (Table 3). Emphasizing the few observations over grasses and forest, we choose a typical plant coefficient to be .7. In the present model the reduction from unity is attributed entirely to the shading factor while the resistance factor is

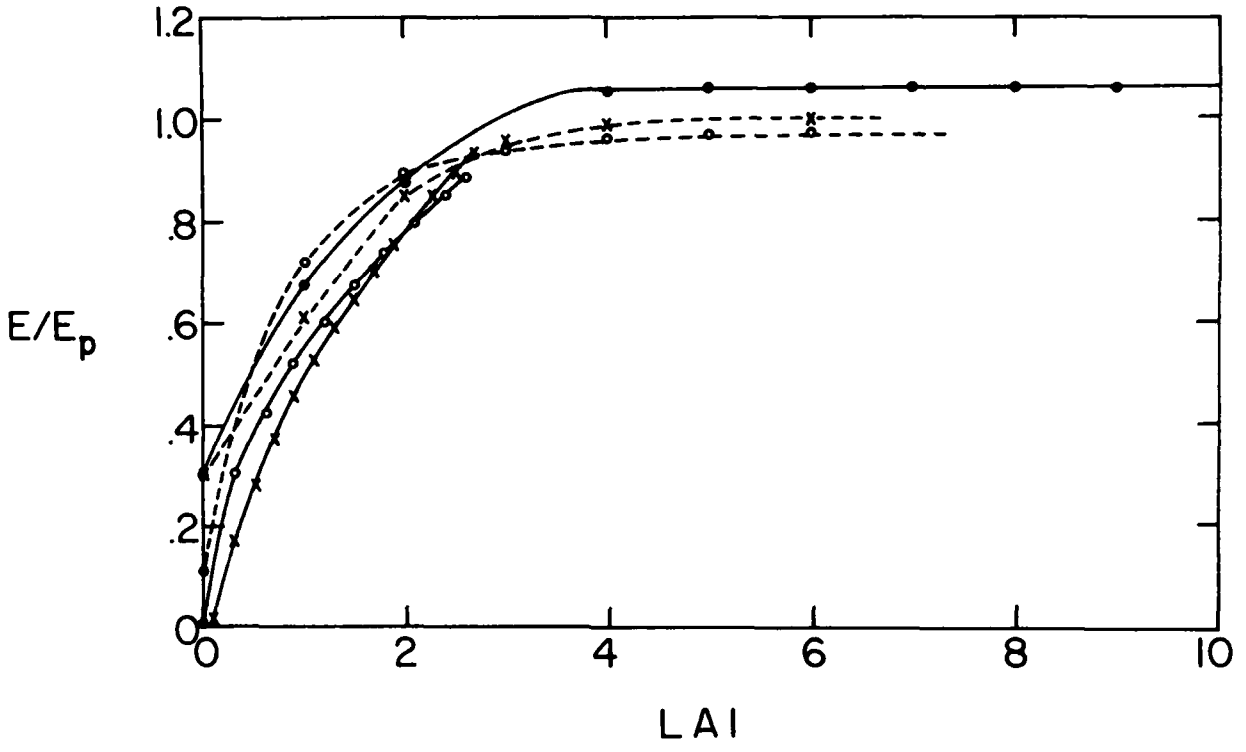

Fig. 4. Relative evapotranspiration as a function of leaf area index from Hanson (1976) (open circle, solid line); Kristensen (1974) (solid circles, solid line); Ritchie and Burnett (1971) (x's, solid line); Eagleson (1978) for k_v=1.0 (open circles, broken line) and k_v=.7 (x's, broken line).

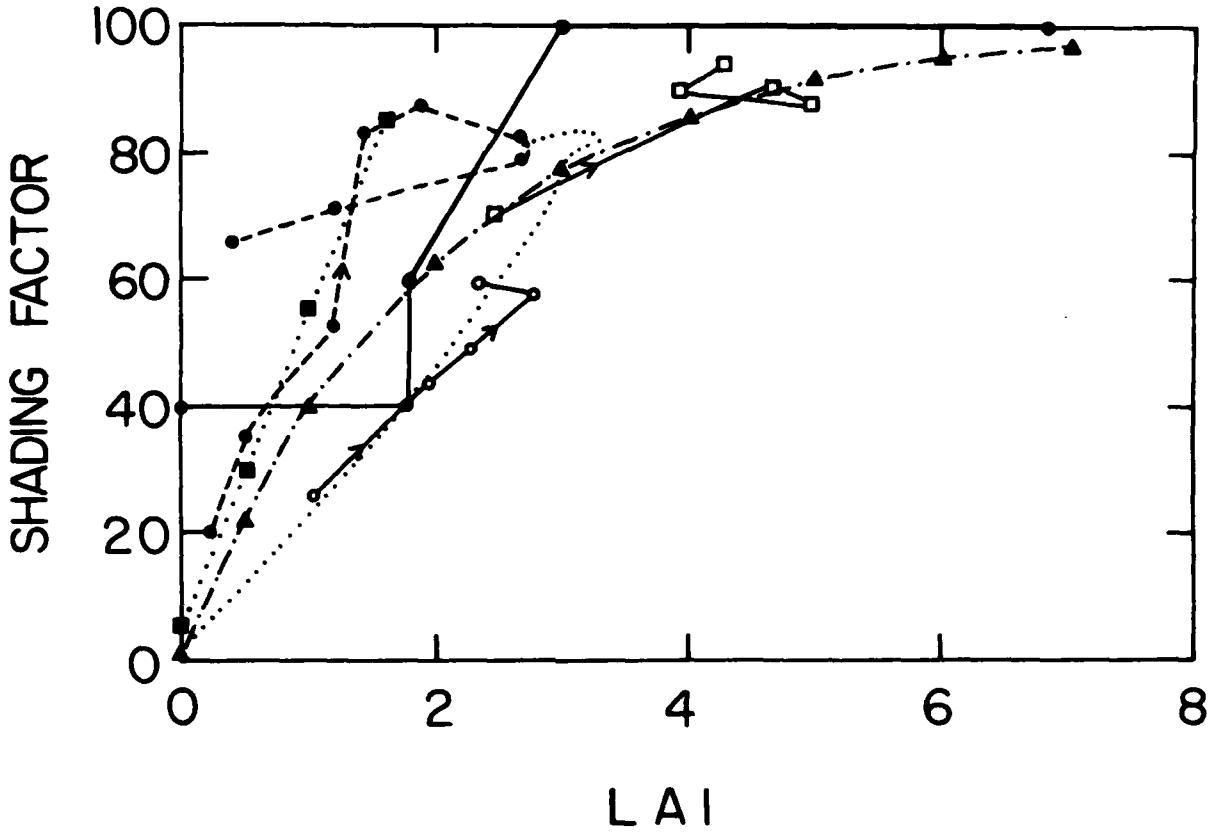

Fig. 5. Shading factor as related to leaf area index from Adams et al. (1976) for sorghum (open circle-100 cm row spacing, open squares-25 cm spacing); Rosenthal et al. (1977) for corn (solid circles, solid line); Heilman and Moore (1980) for barley (solid circles, broken line); Ritchie and Burnett (1971) for cotton (dotted line, no symbols); Conner et al. (1974) for a model with 60° leaf angle (triangles); Tanner and Jury (1976) for potatoes (solid squares).

assigned to be unity. Such values can be altered to accommodate special circumstances or global variations.

d. Dependence on soil moisture deficit

Some examples of the dependence of evapotranspiration on the soil water content are presented in Fig. 5 of Chapter III. While transpiration appeared to decrease continuously with the soil moisture deficit, a sharp decrease begins to occur at moderately low values of soil moisture. The transpiration continues to decrease rapidly until it vanishes at some nonzero value of moisture. The latter is referred to as the wilting point.

As noted in Chapter III, the evapotranspiration is often modelled to be potential until the soil moisture decreases below a reference or critical value, then to decrease linearly, vanishing at the wilting point. We will model the *transpiration part of the evapotranspiration* in this matter as is explicitly recorded in Section 3 of this chapter.

e. Values of soil parameters

Examples of values of the important quantities necessary as inputs to soil moisture for modelling evapotranspiration are briefly summarized in Table 4. Runoff parameters will not be considered at this time. Soil water is expressed in terms of θ, the volumetric soil water content (percent water by volume).

The following symbolism will be used: θ_{cap} = field capacity, θ_{crit} = value above which water is evaporated at the potential rate, θ_{sat} = soil saturation, θ_{pwp} = permanent wilting point, D_i = depth of the soil layer in the model. The following relationship will generally be true

$$\theta_{pwp} < \theta_{crit} < \theta_{cap} < \theta_{sat}$$

but may depend on a particular author's own definition of these terms. Field capacity has uncertain physical meaning but is included here due to its widespread usage.

Table 4. Soil moisture parameters

I. Baier and Robertson, 1966

θ_{cap} = 0.30

θ_{pwp} = 0.15

model soil depth 26 in.

number of layers 6

available water (θ_{cap} - θ_{pwp}) 4 in.

II. Carson, 1982

$\int\theta_{cap}$ range 10-30 cm

$\int\theta_{crit}$ range 5-11.25 cm

III. Clapp and Hornberger, 1978

SOIL TYPE	% CLAY	θ_{sat}
sand	3	0.395
sandy loam	9	0.435
loam	19	0.451
clay loam	34	0.476
sandy clay	43	0.426
clay	63	0.482

(This is only a part of a much larger set of soil types)

IV. Deardorff, 1977

D_0 = 10 cm

D_1 = 50 cm

θ_{crit} = 0.30

θ_{cap} = 0.40

The surface layer, D_0, is contained within the total depth, D_1.

V. Deardorff, 1978

D_0 = 10 cm θ_{pwp} = 0.10 θ_{cap} = 0.40

D_1 = 50 cm θ_{crit} = 0.30

VI. Manabe, 1969

D_0 = 1 m θ_{crit} = .11 θ_{cap} = .15

VII. Marshall and Holmes, 1979

SOIL TYPE	% CLAY	θ_{pwp}	θ_{cap}	θ_{sat}
Sand	3	0.02	0.06	0.4
Loam	22	0.05	0.29	0.5
Clay	47	0.20	0.41	0.6

VIII. McCumber and Pielke, 1981

D_0 = 1 m, 14 levels

SOIL TYPE	θ_{pwp}
Sand	0.068
Sandy Loam	0.114
Sandy Clay	0.219
Peat	0.395

IX. Dickinson et al., 1981

D_0 = 10 cm overlapping layers, where D_0 is the surface

D_1 = 100 cm layer

θ^*_{pwp} = 0.30 (volume of water/volume of water at saturation)

θ^*_{cap} = 0.60

where θ^* is the volume of water in the layer/volume of water in the layer of saturation. With this definition $0 \leq \theta^* \leq 1$ and $\theta^*_{sat} = 1$.

X. Clothier et al., 1981

θ_{sat} = 0.34 for fine sand

θ_{cap} = 0.33 for sandy loam

XI. Lee, 1980

SOIL TYPE	θ_{pwp}	θ_{cap}
Sand	0.025	0.100
Fine Sand	0.033	0.116
Sandy Loam	0.050	0.158
Loam	0.100	0.267
Silty Loam	0.116	0.283
Light Clay Loam	0.133	0.300
Clay Loam	0.150	0.317
Heavy Clay Loam	0.175	0.325
Clay	0.208	0.325

XII. Rutter, 1975

SOIL TYPE	θ_{pwp}	θ_{cap}
Sand	0.02	0.09
Sandy Loam	0.11	0.27
Loam	0.13	0.34
Silt Loam	0.14	0.38
Clay loam	0.16	0.30
Clay	0.22	0.39
Peat	0.25	0.55

XIII. Black, 1979

SOIL TYPE	θ_{pwp}	θ_{cap}	D_1	GROUND COVER
Sandy Loam	0.08	0.215	70 cm	Douglas fir
Sandy Loam	0.11	0.213	85 cm	Douglas fir & salal

3. Canopy water and transpiration model

Normally evapotranspiration is considered collectively without distinguishing between transpiration and direct soil evaporation. Here we want to preserve the distinction since the direct soil evaporation is most appropriately related to the soil moisture of an upper thin layer while water for transpiration originates more from the deeper root zone. The total evaporation can be written as

$$E = E_{dir} + E_T + E_C = F \cdot E_p \tag{15}$$

where E_{dir} is the direct evaporation from the soil, E_T is the transpiration, E_C is the evaporation of precipitation intercepted by the canopy, E_p is the potential evaporation and F is a function whose components are discussed below and summarized in Chapter VI.

a. Reduction of direct evaporation

Vegetation reduces the direct evaporation from the soil by shading the ground and reducing the wind speed near the ground. The reduction of wind speed can be posed in terms of increased surface roughness parameter and increased displacement height. One can further include subcanopy flow dynamics.

The roughness length, displacement height and existence of special subcanopy dynamics depend on the height and density of the vegetation. Both of these effects are presumably dependent on the leaf area index or related shading factor discussed in Section 2. The reduction of solar radiation reaching the ground surface through the vegetation can be expressed as a function of the shading factor; here we do not explicitly include complexities due to varying sun angle.

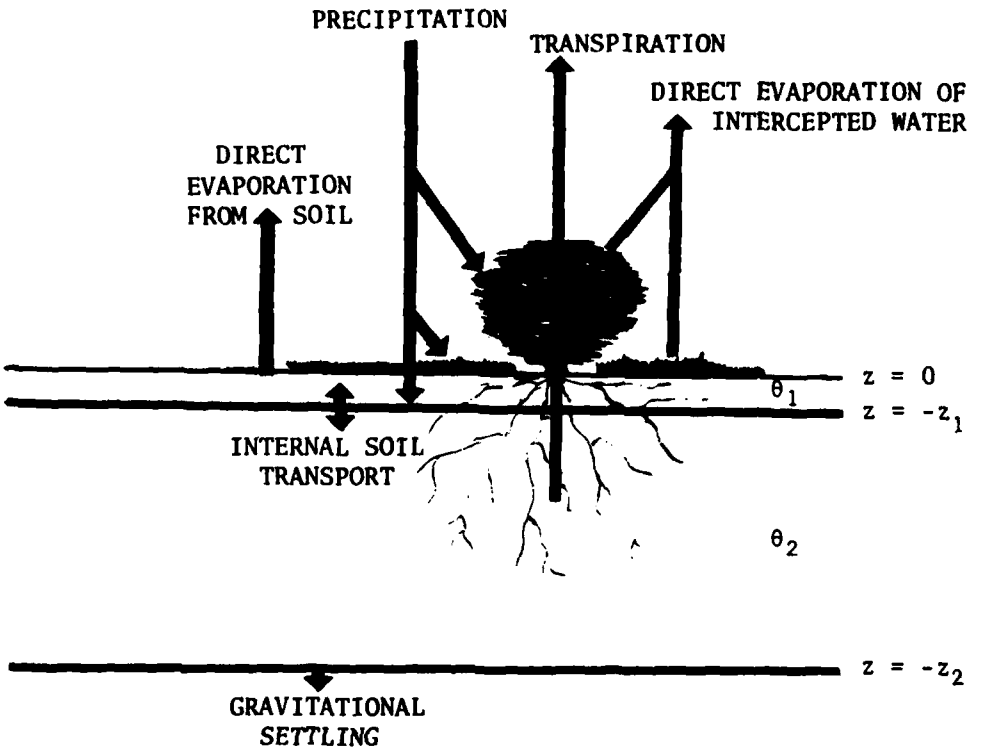

Fig. 6. Schematic illustration of geometry of hydrology model.

To minimize the number of parameters we relate both the influences of shading and wind speed reduction to the shading factor σ_f according to the format

$$E_{dir} = E_{soil} (1-\sigma_f) \tag{16}$$

where σ_f is the shading factor, E_{soil} is the evaporation from the soil model in the absence of vegetation as modelled in Chapter III. The linear dependence on σ_f is based partly on the expected dominance of the importance of radiational forcing of direct soil evaporation under a partial canopy as assumed in Feddes et al. (1974).

b. Transpiration

Transpiration is related to the density of vegetation cover and the stomatal, internal and root resistance of the vegetation and the soil moisture content. Here we detail the transpiration corresponding to the two-layer version of the model although the model is set up to accommodate up to ten layers. These influences are most simply included with the following format for transpiration which is based on discussions in Section 2.

$$E_T = E_p \, k_v \sigma_f \left[\frac{z_1}{z_2} g(\theta_1) + \frac{(z_2-z_1)}{z_2} g(\theta_2) \right] \left[1 - (C/S)^n \right] \tag{17}$$

$$g(\theta) = \begin{cases} 1 & \theta > \theta_{ref} \\ \dfrac{\theta - \theta_{wilt}}{\theta_{ref} - \theta_{wilt}} & \theta \leq \theta_{ref} \\ 0 & \theta \leq \theta_{wilt} \end{cases}$$

Here we have assumed that the root uptake rate is independent of depth within a given layer. The wilting point, θ_{wilt}, where root uptake ceases, is assigned

to be .12. The plants do not die if the water content decreases to the wilting point; transpiration begins again as soon as θ exceeds θ_{wilt}. The parameter θ_{ref} is the soil moisture content where the soil moisture deficit begins to reduce root uptake and transpiration. θ_{ref} is chosen to be .25 which is significantly below the saturation values for most soil types. These soil parameter values are based on results in Section 2d.

C is the canopy water content and S is the canopy water capacity, both of which are discussed in Section 1. The coefficient k_v is the plant resistance factor chosen to be unity and σ_f is specified to be .7. As discussed in Section 2, the product of $k_v\sigma_f$ is similar to the commonly used plant coefficient. The parameter n is chosen to be 1/2 to be consistent with the interception model discussed below.

c. Interception

We have constructed a model for the canopy water budget by considering previous models and any inconsistencies as discussed in Section 1 and recognizing the level of simplicity required here. We propose the following interception model

$$\frac{dC}{dt} = \sigma_f P - E_C \tag{18}$$
$$E_C = \sigma_f (C/S)^n E_p$$

where C is the canopy water storage, S the storage capacity of the canopy, here chosen to be 2 mm, P the precipitation rate, E_p the potential evaporation rate and σ_f the shading factor. This interception model is similar to that of Rutter et al. (1971) except that:

1) the throughfall parameter is replaced with the closely related expression $1 - \sigma_f$ in order to reduce the number of parameters;
2) the evaporation factor C/S is multiplied by σ_f to account for the asymptotic limit that canopy evaporation vanishes as the canopy vanishes; and
3) n is chosen to be less than unity to correspond to a finite time for the canopy to dry following rainfall as modelled in Deardorff (1978).

Based on the work of Leyton et al. (1967), a value of n = 1/2 is inferred which is somewhat less than the n = 2/3 value chosen by Deardorff (1978).

Once the canopy is saturated (C=S), all additional rainfall is assumed to fall through to the ground. This is analogous to assuming that drip processes occur instantaneously so that the canopy is never temporarily "supersaturated."

References

Adams, J.E., G.F. Arkin, and J.T. Ritchie, 1976: Influence of row spacing and straw mulch on first stage drying. Soil Sci. Soc. Am. J., 40, 436-442.

Al-Khafaf, S., P.J. Wierenga, and B.C. Williams, 1978: Evaporative flux from irrigated cotton as related to leaf area index, soil water, and evaporative demand. Agron. J., 70, 912-917.

Assenac, G., 1972: Etude de l'evapotranspiration reelle de quatre peuplements forest revs dans l'est de la France. Ann. Sci. Forest., 29, 369-389.

Aston, A.R., 1979: Rainfall interception by eight small trees. J. Hydrol., 42, 383-396.

Baier, W., and G. Robertson, 1966: A new versatile soil moisture budget. Can. J. Plant Sci., 4, 299-315.

Bates, E.M., F.V. Pumphrey, D.C. Hane, and T.P. Davidson, 1982: Evapotranspiration relationships with pan evaporation of frequently irrigated wheat and potatoes. Oregon State University, Department of Crop Science. Unpublished manuscript.

Black, T.A., 1979: Evapotranspiration from Douglas fir stands exposed to soil water deficits. Water Resour. Res., 15, 164-170.

_____, C.B. Tanner, and W.R. Gardner, 1970: Evaporation from a snap bean crop. Agron. J., 62, 66-69.

Bringfelt, B., and P.-O. Harsmer, 1974: Rainfall interception in a forest in the Velen hydrological representative basin. Nordic Hydrol., 5, 146-165.

Calder, I.R., 1977: A model of transpiration and interception loss from a spruce forest in Plynlimon, central Wales. J. Hydrol., 33, 247-265.

Carson, D., 1982: Current parameterizations of land-surface processes in atmospheric general circulation models. In: JSC Study Conference on Land-Surface Processes in Atmospheric General Circulation Models. 5-10 January 1981, Greenbelt, Maryland, 67-108.

Clapp, R., and Hornberger, 1978: Empirical equations for some soil hydraulic properties. Water Resour. Res., 14, 601-604.

Clothier, B.E., I. White, and G.J. Hamilton, 1981: Constant-rate rainfall infiltration: field experiments. Soil Sci. Soc. Amer. J., 45, 245-249.

Conner, D.J., L.F. Brown, and M.J. Trlica, 1974: Plant cover, light interception, and photosynthesis of shortgrass prairie--a functional model. Photosynthetica, 8, 18-27.

Cuenca, R.H., J. Erpenbeck, and W.O. Pruitt, 1981: Advances in computation of regional evapotranspiration. Proceedings of the ASCE, Water Forum '81, San Francisco, 73-80.

Deardorff, J., 1977: A parameterization of ground-surface moisture content for use in atmospheric prediction models. J. Appl. Meteor., 16, 1182-1185.

_____, 1978: Efficient prediction of ground surface temperature and moisture with inclusion of a layer of vegetation. J. Geophys. Res., 83, 1889-1903.

Dickinson, R.E., J. Jager, W.M. Washington, and R. Wolski, 1981: Boundary subroutine for the NCAR global climate model. NCAR Tech. Note 78-01.

Dylla, A.S., D.R. Timmons, and H. Shull, 1980: Estimating water use by irrigated corn in west central Minnesota. Soil Sci. Soc. Am. J., 44, 823-827.

Eagleson, P.S., 1978: Climate, soil and vegetation. 4. The expected value of annual evapotranspiration. Water Resour. Res., 14, 731-739.

_____, 1982: Dynamic hydro-thermal balances at macroscale. In: JSC Study Conference on Land Surface Processes in Atmospheric General Circulation Models. 5-10 January 1981, Greenbelt, Maryland, 289-357.

Feddes, R.A., E. Bresler, and S.P. Neuman, 1974: Field test of a modified numerical model for water uptake by root systems. Water Resour. Res., 10, 1199-1206.

Fritschen, L.J., 1965: Evapotranspiration rates of field crops determined by the Bowen ratio method. Agron. J., 58, 339-342.

_____, 1982: The vertical fluxes of heat and moisture at a vegetated land surface. In: JSC Study Conference on Land Processes in Atmospheric General Circulation Models. 5-10 January 1981, Greenbelt, Maryland, 169-226.

Fuchs, M., and G. Stanhill, 1963: The use of class A evaporation pan data to estimate the irrigation water requirements of the cotton crop. Israel J. Agric. Res., 13, 63-78.

Gash, J.H.C., 1979: An analytical model of rainfall interception by forests. Quart. J. Roy. Meteor. Soc., 105, 43-55.

_____, and A.J. Morton, 1978: An application of the Rutter model to the estimation of the interception loss from Thetford forest. J. Hydrol., 38, 49-58.

Hancock, N.H., and J.M. Crowther, 1979: A technique for the direct measurement of water storage on a forest canopy. J. Hydrol., 41, 105-122.

Hanson, C.L., 1976: Model for Predicting evapotranspiration from native rangelands in the Northern Great Plains. Amer. Soc. Agric. Engineers Trans., 19, 471-77, 481.

Hargreaves, G.H., 1974: Estimation of potential and crop evapotranspiration. Amer. Soc. Agric. Engineers Trans., 17, 701-704.

Helvey, J.D., 1967: Interception by eastern white pine. Water Resourc. Res., 3, 723-729.

_____, and J.H. Patric, 1965: Canopy and litter interception of rainfall by hardwoods of eastern United States. Water Resourc. Res., 1, 193-206.

Heilman, J.L., and D.G. Moore, 1980: Thermography for estimating rear-surface soil moisture under developing crop canopies. J. Appl. Meteor., 19, 324-328.

Holmes, R.M. and G.W. Robertson, 1959: A modulated soil moisture budget. Mon. Wea. Rev., 87, 101-105.

Horton, R.E., 1919: Rainfall interception, Mon. Wea. Rev., 47, 603-623.

Jackson, I.J., 1975: Relationships between rainfall parameters and interception by tropical forest. J. Hydrol., 24, 215-238.

Kanemasu, E.T., L.R. Stone, and W.L. Powers, 1976: Evapotranspiration model tested for soybean and sorghum. Agron. J., 68, 569-572.

Kristensen, K.J., 1974: Actual evapotranspiration in relation to leaf area. Nordic Hydrol., 5, 173-182.

Lee, R., 1980: Forest Hydrology. Columbia Univ. Pr., New York, 349 pp.

Leyton, L., and A. Carlisle, 1959: Measurements and interpretation of interception by forest stands. Int. Assoc. Hydrol. Sci. Hannoversch-Munden, 48, 111-119.

_____, E.R.C. Reynolds, and F.B. Thompson, 1967: Rainfall interception in forest and moorland. In: Forest Hydrology (W.E. Sopper and H.W. Lull, eds.), Pergamon, Oxford, 163-178.

Lomas, J., E. Schlesinger, and J. Lewin, 1974: Effects of environmental and crop factors on the evapotranspiration rate and water-use efficiency of maize. Agric. Meteor., 13, 239-251.

Lourence, F.J., and W.O. Pruitt, 1971: Energy balance and water use of rice grown in the Central Valley of California. Agron. J., 63, 827-832.

Manabe, S., 1969: Climate and the ocean circulation. I. The atmospheric circulation and the hydrology of the earth's surface. Mon. Wea. Rev., 97, 739-774.

Marshall, T., and J. Holmes, 1979: Soil Physics. Cambridge Univ. Press, Cambridge, 345 pp.

Massman, W.J., 1980: Water storage on forest foliage: a general model. Water Resourc. Res., 16, 210-216.

McCumber, M., and R. Pielke, 1981: Simulation of the effects of surface fluxes of heat and moisture in a mesoscale numerical model. J. Geophys. Res., 86, 9929-9938.

Molchanov, A.A., 1960: The hydrologic role of forests. Izdatel'stvo Akademia Nauk SSR (Translated by Israel Program for Scientific Translations, 1963). 14-39.

Monteith, J.L., 1965: Evaporation and environment. Symp. Soc. Exp. Biol., 19, 206-234.

Nelson, S.H., and K.E. Hwang, 1976: Water usage by cabbage plants at different stages of growth. Can. J. Plant Sci., 56, 563-566.

Nkemdirim, L.C., and P.F. Haley, 1973: An evaluation of grassland evapotranspiration. Agric. Meteor., 11, 373-383.

O'Neill, P., L. Pochop and J. Borrelli, 1979: Urban lawn evapotranspiration-measurement and prediction. Amer. Soc. Agric. Engineers Trans., 22, 1050-1053.

Parmele, L.H., and J.L. McGuinness, 1974: Comparisons of measured and estimated daily potential evapotranspiration in a humid region. J. Hydrol., 22, 239-251.

Pearce, A.J., L.K. Rowe and J.B. Stewart, 1980: Nighttime, wet canopy evaporation rates and the water balance of an evergreen mixed forest. Water Resourc. Res., 16, 955-959.

Penman, H.L., 1963: Vegetation and Hydrology. Tech. Comm. 53, Commonwealth Bur. of Soils, Harpenden, England.

Ritchie, J.T., and E. Burnett, 1971: Dryland evaporative flux in a subhumid climate: II. Plant influences. Agron. J., 63, 56-62.

Robins, P.C., 1974: A method of measuring the aerodynamic resistance to the transport of water vapour from forest canopies. J. Appl. Ecol., 11, 315-325.

Rosenthal, W.D., E.T. Kanemasu, R.J. Raney, and L.R. Stone, 1977: Evaluation of an evapotranspiration model for corn. Agron. J., 69, 461-464.

Ross, J., 1975: Radiative transfer in plant communities. In: Vegetation and the Atmosphere 2v.1 (J.L Monteith, ed.), Academic Press, London, 13-55.

Rothacher, J., 1963: Net precipitation under a Douglas fir forest. Forest Sci., 9, 423-429.

Rowe, P.B., and T.M. Hendrix, 1951: Interception of rain and snow by second-growth ponderosa pine. Amer. Geophys. Union Trans., 32, 903-908.

Russell, G., 1980: Crop evaporation, surface resistance and soil water status. Agric. Meteor., 21, 213-226.

Rutter, A.J., 1975: The hydrological cycle in vegetation. In: Vegetation and the atmosphere, vol. 1 (J.L. Monteith, ed.), Academic Press, London, 111-154.

_____, K.A. Kershaw, P.C. Robins, and A.J. Morton, 1971: A predictive model of rainfall interception in forests, I. Derivation of the model from observations in a plantation of Corsican pine. Agric. Meteor., 9, 367-384.

_____, A.J. Morton, and P.C. Robins, 1975: A predictive model of rainfall interception in forests, II. Generalization of the model and comparison with observations in some coniferous and hardwood stands. J. Appl. Ecol., 12, 367-380.

Sellers, P.J., and J.G. Lockwood, 1981: A computer simulation of the effects of differing crop types on the water balance of small catchments. Quart. J. Roy. Meteor. Soc., 107, 395-380.

Shepherd, W., 1972: Some evidence of stomatal restriction of evaporation from well-watered plant canopies. Water Resour. Res., 8, 1092-1095.

Singh, B., and G. Szeicz, 1979: The effect of intercepted rainfall on the water balance of a hardwood forest. Water Resourc. Res., 15, 131-138.

Stanley, C.D., and R.H. Shaw, 1978: The relationship of evapotranspiration to open-pan evaporation throughout the growth cycle of soybeans. Iowa State J. Res., 53, 129-136.

Stewart, J.B., 1977: Evaporation from the wet canopy of a pine forest. Water Resourc. Res., 13, 915-921.

Strahler, A.N., 1975: Physical Geography, John Wiley and Sons, Inc., New York, pp. 205-208.

Stricker, H., and W. Brutsaert, 1978: Actual evapotranspiration over a summer period in the "Hupsel Catchment." J. Hydrol., 39, 139-157.

Tanner, C.B., and W.A. Jury, 1976: Estimating evaporation and transpiration from a row-crop during incomplete cover. Agron. J., 68, 239-243.

Thom, A.S., and H.R. Oliver, 1977: On Penman's equation for estimating regional evaporation. Quart. J. Roy. Meteor. Soc., 103, 345-357.

Thompson, F.B., 1972: Rainfall interception by oak coppice (Quercus robur, L.). In: Research Papers in Forest Meteorology (J.A. Taylor, ed.), Cambrian News Ltd., Aberystwyth, 59-74.

Thorud, D.B., 1967: The effect of applied interception on transpiration rates of potted ponderosa pine. Water Resourc. Res., 3, 443-450.

United States Department of Agriculture, Soil Conservation Service, Engineering Division, April 1967, Revised September 1970, Irrigation Water Requirements, Technical Release No. 21.

Van Bavel, C.H.M., 1966: Potential evaporation: The combination concept and its experimental verification. Water Resour. Res., 2, 455-467.

_____, 1967: Changes in canopy resistance to water loss from alfalfa induced by soil water depletion. Agric. Meteor., 4, 165-176.

Vankatachari, A., and K.A. Reddy, 1978: Relationship of evapotranspiration with pan evaporation and evaluation of crop coefficient. Acta Agronomica Scientiarium Hungaricae, 27, 107-110.

Viessman, W., J.W. Knapp, G.L. Lewis, and T.E. Harbaugh, 1977: Introduction to Hydrology, Harper and Row, New York, 704 pp.

Waggoner, P.E., J.E. Begg, and N.C. Turner, 1969: The evaporation of dew. Agric. Meteor., 6, 227-230.

Wright, J.L., and M.E. Jensen, 1978: Development and evaluation of evapotranspiration models for irrigation scheduling. Amer. Soc. Agric. Engineers Trans., 21, 88-91.

Zinke, P.J., 1967: Forest interception studies in the United States. In: Forest Hydrology (W.E. Sopper and H.W. Lull, eds.), Pergamon, Oxford, 137-161.

V. A Boundary Layer Formulation for Atmospheric Models

Abstract

A simple model for the atmospheric boundary layer is proposed for use in operational global weather prediction models and other models where simplicity is required. Surface fluxes are represented in terms of similarity theory while turbulent diffusivities above the surface layer are formulated in terms of bulk similarity considerations and matching conditions at the top of the surface layer. The boundary layer depth is represented in terms of a modified bulk Richardson number. Attention is devoted to the interrelationship between predicted boundary layer growth, the turbulent diffusivity profile, "counter-gradient" heat flux and truncation errors. The model is especially suited for use in models where some resolution is possible within the boundary layer, but where the resolution is still insufficient for resolving the detailed boundary layer structure.

As an example application, the model is used to study the influence of surface moisture flux on the boundary layer development.

1. Introduction

The present interest in medium range weather prediction, climate response studies, and limited area forecast models creates a need for development of simple formulations of surface fluxes and transport in the atmospheric boundary layer. A number of boundary layer models with low resolution have been proposed for use in large scale models. One approach is to model the bulk effect of the boundary layer by interpolating pertinent variables from the large scale model without attempting to resolve any boundary layer structure explicitly (Clarke, 1970; Deardorff, 1972; Smeda, 1979; Chang, 1981).

In models where some grid levels are available to resolve boundary layer structure, a more direct approach is usually adopted by expressing turbulent diffusivities in terms of local gradients of the mean profiles. Models of this kind have been used mostly in cases where comparatively high resolution is available (column models), then diffusivities are related directly to the local gradient Richardson number (Zhang and Anthes, 1982), or to a Richardson number adjustment scheme (Chang, 1979), or computed in conjunction with a prescribed mixing length profile (Busch et al., 1976; Louis, 1979). With coarser resolution, the sensitivity of these formulations to small changes in the mean profiles becomes a disadvantage. Inclusion of transport terms by employing the turbulence energy equation (Mailhôt and Benoit, 1982; Troen, 1982) or even higher order closure schemes (Yamada and Mellor, 1975; André et al., 1978) is presently not practical for use in large scale models because of the large computational requirements.

Here we develop a model, where turbulent diffusivities have a prescribed profile shape as a function of z/h and scale parameters derived from similarity arguments where z is the height above ground and h is the boundary layer top.

This approach partially alleviates resolution requirements yet is more flexible than the purely "bulk" models.

Similar approaches for the simulation of the heated boundary layer have been proposed by Pielke and Mahrer (1975), and Yu (1977). The present model, however, differs from these approaches both with respect to the profile formulations and the way the boundary layer height is determined.

In Section 6, the model is used to study interactions between surface evaporation, mixing and boundary layer growth by arbitrarily specifying the relationship of actual surface evaporation to the potential evaporation. The intention is to identify certain physical feedbacks which have not been previously considered.

2. The model

a. The surface boundary layer

The surface layer parameterization scheme devised by Louis (1979) is used to relate surface fluxes of heat, momentum and water vapor to the values of temperature, the wind components and specific humidity, all at the lowest model level. The layer between the surface and the lowest model level is thus considered to be in equilibrium obeying surface layer similarity. The basic advantage of this formulation is computational efficiency, since the formulation avoids an iterative process which is otherwise necessary when employing the original expressions given by Businger et al. (1971) for the usual range of atmospheric stability; however, the correct behavior of such formulations is uncertain in the cases of extreme stability or instability.

b. The boundary layer above the surface layer

Above the surface layer, the diffusion equation is assumed to adequately describe the effect of turbulent mixing in the boundary layer except for the

modification due to a "counter-gradient" term. Thus, model closure simplifies essentially to the determination of the diffusivity profiles.

As in Brost and Wyngaard (1978), the momentum diffusivity is modelled according to the format

$$K_m = u_* \, kz \, \phi_m^{-1} (1 - \frac{z}{h})^p \qquad (1)$$

where u_* is the surface friction velocity, k is the von Karman constant, ϕ_m is the nondimensional shear, and h is again the boundary layer height. Eq. (1) is consistent with surface layer similarity where

$$K_m = u_* \, kz \, \phi_m^{-1} \quad (z/L) \text{ for } z << h. \qquad (2)$$

For stable conditions we use ϕ_m from Businger et al. (1971) given as

$$\phi_m = 1 + 4.7 \, z/L \qquad (3)$$

where L is the Obuknov length.

For $z > L$ we obtain the following asymptotic expression:

$$K_m \equiv 0.09 \, L \, u_* \, (1 - \frac{z}{h})^p \qquad z > L \, . \qquad (4)$$

That is, for the stable case L becomes the relevant length scale and u_* the relevant velocity scale for the entire boundary layer. The boundary layer depth h here only enters as the height at which the turbulence vanishes and does not influence the boundary layer velocity scale.

For unstable conditions

$$\phi_m(z/L) = (1 - 7 \, z/L)^{-1/3}, \qquad z << h \, . \qquad (5)$$

The exponent of -1/3 is chosen to ensure the free convection limit for $z >> L$. With the coefficient chosen to be 7, the difference between Eq. (5) and the original expression given by Businger et al. (1971) as derived from the Kansas

data differs by less than 6% over the range of the original data ($-z/L < 2$). Here we consider the surface layer to extend upward to $z = \varepsilon h$.

Above the surface layer for the unstable case, we assume that the velocity scale is constant and given by

$$w_s = u_* \phi_m^{-1} = (u_*^3 + 7\varepsilon k w_*^3)^{1/3} \tag{6}$$

then (1) becomes

$$K_m = w_s h \, k \frac{z}{h} (1 - \frac{z}{h})^p, \qquad z > \varepsilon h \, . \tag{7}$$

For $h >> -L$, the velocity scale approaches

$$w_s \approx w_* \, (7\varepsilon k)^{1/3} \tag{8}$$

where $w_* = (\frac{g}{T_o} \overline{w'\theta'_o} \, h)^{1/3}$ is the convective velocity scale. For $\varepsilon = .1$, and $h >> -L$, w_s approaches $.65 \, w_*$.

The expression for the mixed layer velocity scale (6) can be compared with the velocity scale developed by Hojstrup (1982) from the Kansas and Minnesota experiments. Hojstrup's expressions for the velocity variances at $z/h = \varepsilon = .1$, reduce to

$$w_s = (\sigma_u^2 + \sigma_v^2 + \sigma_w^2)^{1/2} = 2.26 \, u_* \, (1 + 2.75 \, (0.1 \frac{h}{-L})^{2/3})^{1/2} \, . \tag{9}$$

Apart from a constant factor of proportionality, Eqs. (6) and (9) differ by less than 16% in the range of $h/-L$ between 0 and 5000, in which range w_s changes by a factor of 13.

The factor $(1-z/h)^p$ ensures that the turbulent mixing approaches zero towards the top of the boundary layer. In the convective case, this would correspond to a capping inversion with unimportant turbulent mixing in the overlaying stratified free atmosphere. The eddy diffusivity is zero above the boundary layer top.

3. Determination of boundary layer height

For well-defined diurnal variations, a rate equation for growth of the daytime mixed layer is often used with a separate model for the depth of the nocturnal boundary layer. However, on a day-to-day basis at an arbitrary location, the top of the daytime boundary layer and capping inversion are often not well-defined. The depth of the boundary layer may be constantly adjusting to changing synoptic control in which case the boundary layer growth equations and boundary layer collapse provisions become too specialized. Even in situations with definable mixed layer growth, the vertical resolution in most atmospheric models is inadequate to define a capping inversion.

Alternatively, Busch et al. (1976) choose the boundary layer top to be the lowest model layer where the gradient Richardson number exceeds a critical value. This method, however, still requires good resolution, and even with high resolution may lead to large unphysical oscillations of h due to the sensitivity of the gradient Richardson number to small changes in the mean profiles.

To be consistent with the bulk approach adopted in Section 2, we determine the boundary layer top to be the height where the bulk Richardson number over the whole boundary layer becomes critical, viz.,

$$Ri_B = \frac{g\,(\theta_v(h) - \theta_s)\,h}{T_o\left|\vec{V}(h)\right|^2} = Ri_{cr} \,. \qquad (10)$$

where $\theta_v(h)$ and θ_s are the virtual potential temperatures at the boundary layer top and near the surface, respectively. The bulk Richardson number is frequently used to model the depth of the stable boundary layer. In the heated boundary layer, the predicted boundary layer top occurs just above the well-mixed region. The thickness of the implied entrainment region, between the well-mixed region and predicted boundary layer top, depends on the free flow

stratification and the value chosen for the critical bulk Richardson number. However, the downward heat flux due to entrainment implied by this model also depends on the profile of diffusivity in this region and the way such a diffusivity interacts with the h-formulation and truncation errors. In the case of vanishing wind speed, and thus vanishing shear generation of turbulence by the mean wind, relationship (10) reduces to a purely thermodynamic argument as applied in Holzworth (1964).

The choice of the lower temperature θ_s in (10) plays an important role. Since the largest and most energetic scales of turbulent motion in the convective boundary layer are thermals, it seems more correct to define θ_s as a measure of temperature of the thermals in the lowest part of the boundary layer. This can be estimated from the relevant velocity scale w_s corresponding to a thermal turnover time of h/w_s. The virtual temperature excess near the surface is then

$$\theta_T = C \frac{(\overline{w'\theta'_v})_o}{w_s} \qquad (11)$$

where $(\overline{w'\theta'_v})_o$ is the surface virtual kinematic heat flux and C is a coefficient of proportionality. Use of this temperature excess to estimate the boundary layer top from (10) could be viewed as a parcel approximation which neglects the influence of entrainment and pressure effects on the thermal ascent. This overestimation of thermal ascent would be partially compensated by neglect of penetration of thermals beyond the buoyancy equilibrium level. The attempt to include such complexities in a limited resolution model would not be appropriate due to large truncation errors.

For simplicity, the temperature excess (11) is assumed to occur at the lowest atmospheric level in the model, z_1. Then

$$\theta_s = \theta_v(z_1) + \theta_T \, . \qquad (12)$$

For the unstable case, the modelled boundary layer depth (10-12) depends mainly on the thermodynamics and is insensitive to the choice of the critical Richardson number.

However, as we approach neutral conditions from the unstable side, θ_T in (11) vanishes. Then θ_s becomes equal to the virtual temperature at the first grid level and the modelled boundary layer depth depends significantly on wind speed.

Within the resolution of the model, the boundary layer depth relations (10-11) compared favorably with more sophisticated entrainment models for the data examined here. That is, for sole purpose of approximating the boundary layer growth rate, the main role of the convective heating can be captured rather simply.

Relationships (11) and (12) are not relevant for the stable boundary layer. Since the first model level may be above the nocturnal boundary layer, θ_s is defined to be the surface virtual temperature for the stable case. Here turbulence is generated by shear only and the Richardson number would seem to be a relevant number. Unfortunately, the turbulence in the nocturnal boundary layer is often intermittent and layered so that the turbulence at a given level may be more related to the local Richardson number than the bulk Richardson number.

However, in low-resolution large scale models, the structure of the nocturnal boundary layer cannot be resolved so that only bulk formulations can be implemented. The use of the bulk Richardson number (10) to predict the top of the nocturnal boundary layer has been tested in a number of studies (some of which are surveyed in Mahrt, 1981a), and provides a smooth transition to the unstable case in the present model.

In such studies the critical bulk Richardson number is typically chosen between .3 and 1. Such values are sometimes tested against the depth of the nocturnal inversion which may be considerably thicker than the depth of the layer of continuous turbulence (Mahrt et al., 1979; André and Mahrt, 1982). On the other hand, we must recognize that model fluxes imply both time and horizontal averaging. Such averaging would then include transport induced by mesoscale and terrain induced circulations which seem to be important in the nocturnal boundary layer even over very weak slopes (Wyngaard et al., 1978; Mahrt, 1981b). Furthermore, fluxes may occ locally in space and time even though the Richardson number evaluated from averaged variables is large. These factors suggest choosing a larger critical Richardson number for computing the boundary layer depth. Here we choose a value of unity for the critical bulk Richardson number.

In the stable case, the modelled boundary layer depth is less significant than in the unstable case as is evident from comparison of (4) and (7). That is, the implied length scale of the mixing asymptotically becomes independent of h and proportional to L. In the unstable case, the value of h significantly influences the length scale above the surface layer; however, the value of h becomes insensitive to the bulk Richardson number.

4. The diffusivities for heat and water vapor

We make the usual assumption of equating diffusivities for heat and water vapor. The turbulence Prandtl number $Pr = K_h/K_m$ under unstable conditions is found to be strongly dependent on stability in the surface layer (Businger et al., 1971). In the mixed layer above the surface layer, the Prandtl number is not very well-defined because local gradients may vanish and fluxes become more related to bulk gradients. Thermals and boundary layer scale eddies transport properties according to bulk gradients which may be much larger than, or of opposite sign from, gradients in the boundary layer interior.

The simplest way to include this nonlocality is to incorporate a "counter-gradient" term as discussed by Priestly and Swinbank (1947) and Deardorff (1966). Then the heat flux becomes

$$\overline{w'\theta'} = -K_h \left(\frac{\partial \theta}{\partial z} - \gamma\right) . \tag{13}$$

In the present formulation

$$\gamma = C \frac{\overline{(w'\theta')}_o}{w_s h} . \tag{14}$$

This prescription is consistent with the formulation of the temperature excess for thermals, (11). A similar correction procedure was suggested by Deardorff (1973) and used in the model by Mailhôt and Benoit (1982), except that the free convection velocity scale w_* was chosen to be the velocity scale. The use of the velocity scale w_s is more consistent with the formulation of the eddy exchange coefficient and includes the reduction of thermal buoyancy by mechanical mixing. Since the counter-gradient factor is a correction to the flux predicted by the eddy exchange coefficient, the value of γ and therefore C depend on the formulation of the eddy diffusivity.

This interrelationship is clearest at the level where the potential temperature gradient vanishes as it reverses with height from weakly unstable to

weakly stable. At this level, say $z = z^*$, (13) becomes

$$\overline{w'\theta'} = K_h(z^*)\gamma$$

or using (14)

$$C = \frac{hw_s}{K_h(z^*)} .$$

Thus C cannot be specified independently of the formulation of K_h as has been done in previous studies. Substituting in the formulation for K_h, the expression for C becomes

$$C = \left[Pr\ k \frac{z^*}{h} (1-z^*/h)^p\right]^{-1} .$$

Note that C becomes independent of the choice of the velocity scale w_s. Choosing, for example, $p = 2$, $Pr = 2$ and $z^*/h = 1/2$, one obtains the usual value of $C \approx 10$. We will adopt this value for subsequent computations although the results in this study were found to be insensitive to the numerical value of C.

It seems necessary to adopt a counter-gradient correction term for transport of moisture or any scaler, since thermals also transport according to the bulk moisture gradient and therefore create flux, even where the local mean

gradient vanishes. We then define the counter-gradient factor for moisture by assuming that it can be formulated with the same coefficient C as for heat transport in which case

$$\gamma_q = C \frac{\overline{(w'q')}_o}{h\, w_s} \tag{15}$$

where $\overline{(w'q')}_o$ is the surface moisture flux. An analogous correction for momentum is not adopted. Because of the pressure effects, thermals cannot efficiently transport momentum over large distances and the gradient of momentum often remains significant throughout the mixed layer.

a. Prandtl Number

Busch et al. (1976) assume the Prandtl number to obey surface layer relations for the entire boundary layer while Mailhôt and Benoit (1982) assume that the Prandtl number is independent of height with a value computed at 4 m. In the present development we match heat and momentum fluxes at the top of the surface layer so that

$$u_* \theta_* = -K_h \left(\frac{\partial \theta}{\partial z} - \gamma\right) \tag{16}$$

$$u_*^2 = -K_m \frac{\partial u}{\partial z} \quad .$$

Combining these two relationships, using the definitions of nondimensional gradients (ϕ_m, ϕ_h), substituting for γ from (14) and solving for the Prandtl number, we obtain

$$Pr = \frac{K_h}{K_m} = \left[\frac{\phi_h}{\phi_m} \left(\frac{z}{L}\right) + k \frac{z}{h} C\right]^{-1} \tag{17}$$

where z is the level where matching (16) is applied, here taken as .1h. Lacking other evidence, we assume that the Prandtl number is constant above .1h. Expression (17) has the advantage that it is well behaved for vanishing Obukhov length L.

b. Comparison with Wyngaard and Brost

It is instructive to compare the diffusivity profile used here with the diffusivity profile which can be derived from the large eddy simulations by Wyngaard and Brost (1983). They derive expressions for the gradients of a scalar for the case of vanishing entrainment flux (their Eq. (33)) and for the case of vanishing surface flux (their Eq. (39)). Profile functions were determined by comparing with numerical simulations for the case $-z/L = 64$. When both fluxes are present we can obtain the effective diffusivity from their individual relationships. Assuming the flux in the boundary layer to vary linearly with height, the diffusivity relationship derived from Wyngaard and Brost becomes

$$K = w_* h \frac{(1 - (1 - R)\frac{z}{h})}{R\,(1 - \frac{z}{h})^{-3/2} + 0.4\,(\frac{z}{h})^{-3/2}} \qquad (18)$$

where $R = \left(\overline{w'c'}\right)_h / \left(\overline{w'c'}\right)_o$ and c is the transported quantity.

As discussed by Wyngaard and Brost (1983), this form is not well behaved since the transport by large eddies or thermals is not directly related to the local gradients. The simplest way to effectively include this transport process is to again adopt a gradient correction factor γ such that

$$\overline{w'c'} = -K \left(\frac{\partial \overline{c}}{\partial z} - \gamma_c\right)$$

$$\gamma \equiv C' \frac{(\overline{w'c'})_o}{w_* h} \tag{19}$$

where the prime notation on the coefficient C' indicates that the free convection velocity scale w_* must be used instead of w_s in order to be consistent with (18). Then using the gradient and flux from Wyngaard and Brost (1983), the diffusivity satisfying (19) and the gradient correction γ (14) becomes

$$K = w_* h \frac{\left(1 - (1 - R) \frac{z}{h}\right)}{R \left(1 - \frac{z}{h}\right)^{-3/2} + 0.4 \left(\frac{z}{h}\right)^{-3/2} + C'} \quad . \tag{20}$$

The diffusivity profile modified to include the counter-gradient correction (20) is shown in Fig. 1 for different values of R, the ratio of the entrainment flux to the surface flux . C' has been assigned the value of 10 as in previous studies. Eq. (20) and Fig. 1 show that the addition of the counter-gradient correction makes the diffusivity well-behaved and only moderately sensitive to the value of the ratio R.

c. The exponent p

In the case of the diffusivity for heat, the ratio R is often approximated as -.2 (Tennekes, 1973). The profile for the heat diffusivity based on (17) for values of the exponent p between 2 and 3, exhibits good agreement with

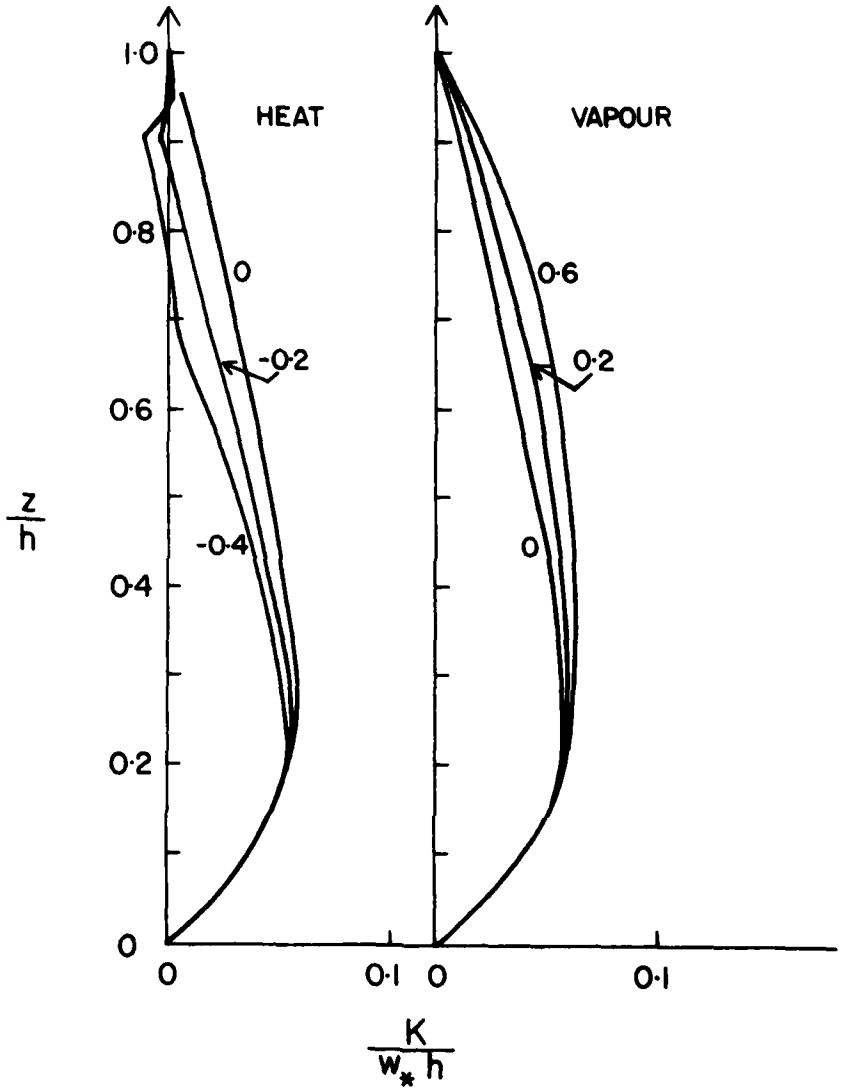

Fig. 1. The profile of diffusivity from eq. (20) for different values of R = ratio of entrainment flux at the top of the boundary layer relative to the surface flux.

the corresponding profile from Wyngaard and Brost (1983) for R=-.2 except the heat diffusivity is somewhat larger in the middle of the boundary layer (Fig. 2).

Near the top of the boundary layer, behavior of the diffusivity determines the importance of the entrainment flux. The exact relation between the heat diffusivity near the top and the flux ratio R is, however, complicated by the way in which the boundary layer height is determined, and is in practice also found to be sensitive to truncation errors in the numerical model. For this reason we use the exponent p as an adjustable parameter chosen to give reasonable values for the flux ratio R in a particular model with a particular resolution. It is obvious that the exponent p could be dependent on stability. For example, Brost and Wyngaard (1978) choose 1.5 for the stable case. For simplicity, and lack of observational evidence, we presently specify p to be independent of stability with a constant value of 2.

5. Numerical technique

The time integration of the change of mean profiles due to boundary layer turbulence reduces to the solution of the diffusion equation

$$\frac{\partial X}{\partial t} = \frac{\partial}{\partial z} K \left(\frac{\partial X}{\partial z} - \gamma\right) \qquad (21)$$

where $X = [u,v,\theta,q]$. At each time step, the mean profiles are used first to calculate drag coefficients c_m and c_h from Louis (1979) and then calculate the surface fluxes. Next, boundary layer height is estimated for computation using (10) with $\theta_s = \theta_o$ where θ_o is the surface virtual temperature obtained from surface energy balance (Appendix). Under convective conditions (positive surface heat flux), Eq. (11) is then used together with (12) and (10) to obtain an improved estimate for the boundary layer height h. Eq. (21) is then used to

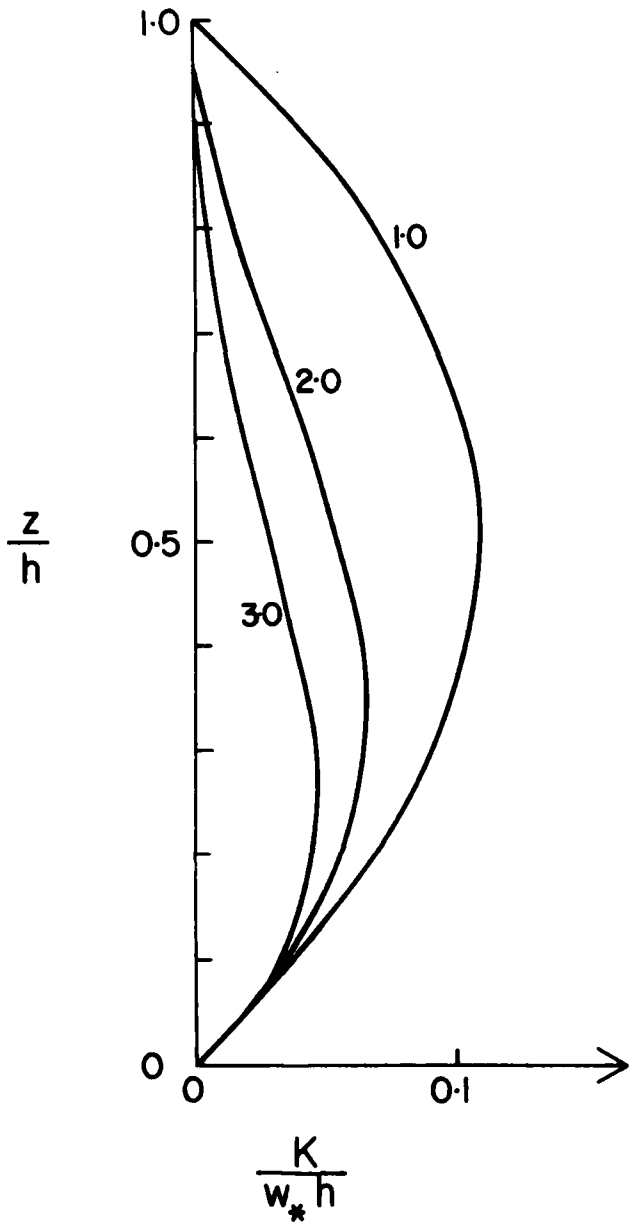

Fig. 2. The profile of diffusivity for heat and water vapor in the present model in the case of a heated boundary layer with parameters taken from Wyngaard and Brost (1983). Numbers on the graphs give the values of p in eq.(1).

step forward one time step using the diffusivity profile (1). The layer between the ground and the first atmospheric level is treated as an equilibrium surface layer and (21) is employed only above this layer. The boundary conditions thus become flux conditions at the lowest model level. The boundary layer height, h, counter-gradient correction term, surface values of temperature, θ_o, and humidity, q_o, are assumed constant during each time step. In order to ensure computational stability with large time steps, it is necessary to use an implicit integration technique; here we use the fully implicit Cranck-Nicholson scheme (or Laasonen scheme) given by

$$X^{(n+1)} - X^{(n)} = \Delta t \frac{\partial}{\partial z} K \frac{\partial}{\partial z} X^{(n+1)} \qquad (22)$$

where the superscripts designate the time level. For the spatial operator, we employ a variation of the finite-element method using Chapeau functions for the mean variables. Some care must be taken to ensure that no unnecessary truncation errors are introduced. The model is intended to be used with only a few grid levels in the boundary layer, say levels at 50, 250, 500, 1000, 2000m. Therefore, the large variation of the diffusivities near the top of the boundary layer will typically not be adequately resolved. To minimize truncation errors from finite differencing of the diffusivity profile, we use the finite element technique with the analytical form of K from (1). The method can be developed as follows: suppose X is written in terms of some expansion in basic functions $\alpha_k(z)$. Multiplying by $\alpha_k(z)$ on both sides of (22) and integrating from the lowest level to the boundary layer top yields

$$A_{ki}\,(X_i^{(n+1)} - X_i^{(n)}) = B_{ki}\,X_i^{(n+1)} \tag{23}$$

with

$$A_{ki} = \int_{z_i}^{z_N} \alpha_k(z)\alpha_i(z)dz$$

$$B_{ki} = \Delta t \int_{z_1}^{z_N} \alpha_k(z)\,\frac{\partial}{\partial z}\,K(z)\,\frac{\partial}{\partial z}\,\alpha_i(z)dz\ .$$

We use Chapeau functions for the basic functions defined on the grid as

$$\alpha_i(z) = \begin{cases} \dfrac{z - z_{i-1}}{z_i - z_{i-1}} & \text{for } z_{i-1} \le z \le z_i \\[2ex] \dfrac{z_{i+1} - z}{z_{i+1} - z_i} & \text{for } z_i \le z \le z_{i+1} \end{cases} \tag{24}$$

and zero outside the interval $z_{i-1} - z_{i+1}$. These functions span all piecewise linear functions on the grid. Using (24) and (1), A_{ki} and B_{ki} are easily computed. Solution of the diffusion step then becomes

$$(A_{ki} - B_{ki})\,X_i^{n+1} = A_{ki}\,X_i^{n}\ . \tag{25}$$

The expansion coefficients X_i are simply the gridpoint values by virtue of our choice for α_i in (24).

We find by integration

$$A_{ii-1} = \Delta z_{i-1}/6$$

$$A_{ii} = \frac{1}{3}(\Delta z_{i-1} + \Delta z_i) \tag{26}$$

$$A_{ii+1} = \Delta z_i/6$$

$$(\Delta z_i \equiv z_{i+1} - z_i) .$$

All other terms are zero.

For B_{ki} we find that

$$B_{ii-1} = \frac{\Delta t}{\Delta z_{i-1}^2} \int_{z_{i-1}}^{z_i} K(z)dz$$

$$B_{ii+1} = \frac{\Delta t}{\Delta z_i^2} \int_{z_i}^{z_{i+1}} K(z)dz \tag{27}$$

$$B_{ii} = -(B_{ii-1} + B_{ii+1}) .$$

The integrals of K over one grid interval are found to be sufficiently accurate when approximated by the center value multiplied by Δz, except for the integral over the interval containing the top of the boundary layer, where we instead use the approximation

$$\int_{k_z}^{z_{k+1}} K(z)dz = \int_{z_k}^{h} K(z)dz \simeq (h-z_k)\, K\left(\frac{h + z_k}{2}\right). \tag{28}$$

6. Sensitivity to surface moisture flux

One of the goals of this study is to develop a boundary layer model sufficiently simple to allow physical analysis of the qualitative response of the boundary layer to external forcing. In this section we will attempt to identify interaction between boundary layer growth and surface evaporation. This interaction is normally removed in mixed layer growth studies by specifying the surface heat flux.

The primary influence of surface evaporation is to decrease surface heating which in turn reduces the boundary layer growth rate from that of the case of no evaporation. However, this interaction is limited by negative feedback since the surface evaporation also acts to increase the boundary layer moisture. Furthermore, reduced surface heating resulting from surface evaporation leads to less turbulence, less downward mixing of dryer air and lower surface wind speed due to weaker downward mixing of momentum. These influences all lead to smaller potential evaporation compared to the case of a dry surface.

In order to speculate on the relative importance of these influences, we now examine the response of boundary layer development to the surface evaporation using the model constructed above. We specify the initial conditions to be the observed atmosphere at 0600 Local Standard Time on Wangara day 33 (Clarke et al., 1971). These are used as arbitrary initial conditions since the lack of moisture flux data preclude actual comparisons with the Wangara data. The model is integrated for a 48-hour period using the net surface radiation reported in Clarke et al. (1971). The vertical resolution is 50m with a vertical domain of 2 km adequate for present purposes. Varying the resolution by a factor of two exerted little influence on the results.

As the specified water availability factor $\beta \equiv E/E_p$ increases from zero (no surface evaporation) to .25 and then .5, the daytime boundary layer growth rate decreases significantly (Figs. 3-4). Further increases of β lead to progressively smaller changes. This nonlinear dependence of boundary layer growth rate on surface moisture availability is due to the reduction of potential evaporation (Fig. 4) discussed above. Of importance is that the difference between the present simple model of boundary layer depth and more sophisticated mixed layer growth models is small compared to the influence of possible variations of the influence of surface evaporation.

Decreasing the atmospheric moisture increases the potential evaporation which in turn reduces the surface heating and boundary layer growth rate. Decreasing the specific humidity by a factor of two exerts only a modest influence on the boundary layer growth rate for the Wangara conditions (Fig. 5).

Using the boundary layer growth rate as an indicator of boundary layer development, Figs. 6-7 show the expected influence of variations of atmospheric stratification and solar radiation. Varying the coefficient C for the gradient correction (11) by a factor of two caused negligible modification of the growth rate.

7. Cloud scheme

The boundary layer model includes a cloud scheme based on the model at the European Center for Medium-range Weather Forecasting (Geleyn, 1980). The fractional boundary layer cloud cover is determined as a function of the excess of the relative humidity over a critical value (here .5) such that

$$CC = \begin{cases} [2\,(RH - .5)]^2 & RH \geq .5 \\ 0 & RH < .5 \end{cases}$$

where CC is the fractional cloud cover and RH is the relative humidity.

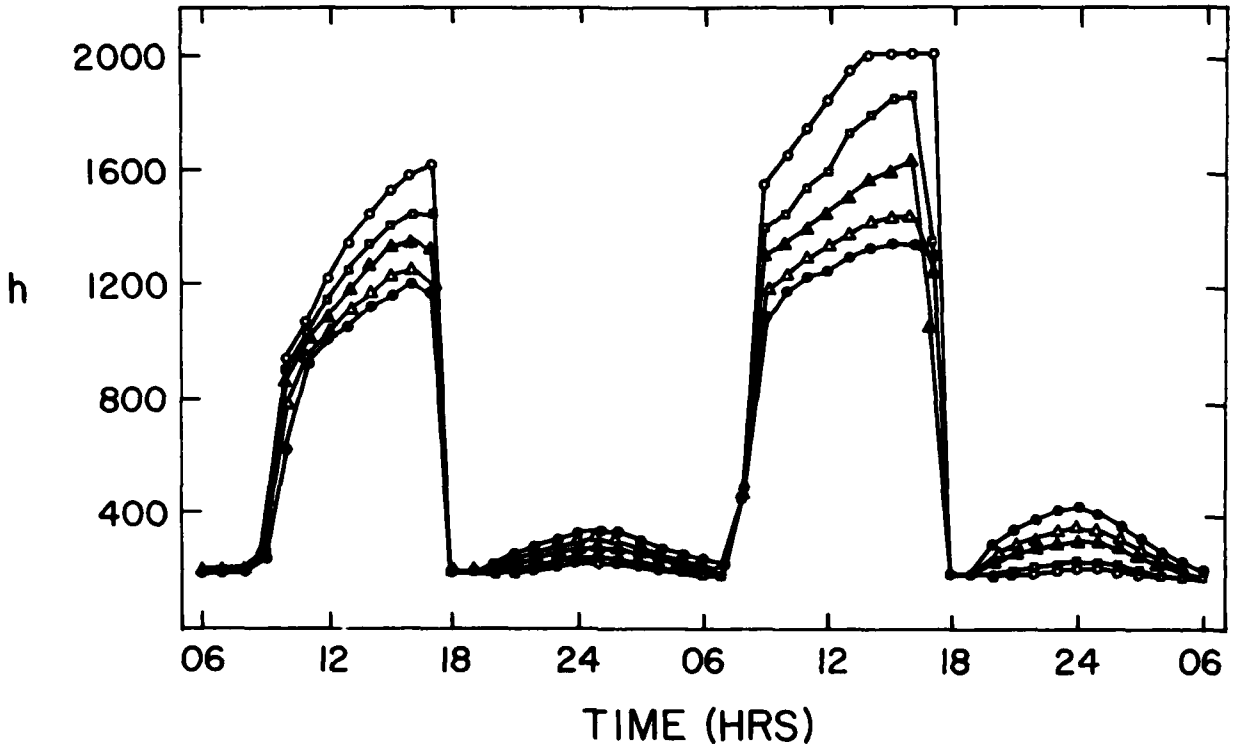

Fig. 3. The boundary layer depth as a function of local standard time for E/E_p=0 (open circles), .25 (open squares), .5 (solid triangles), .75 (open triangles) and 1 (solid circles).

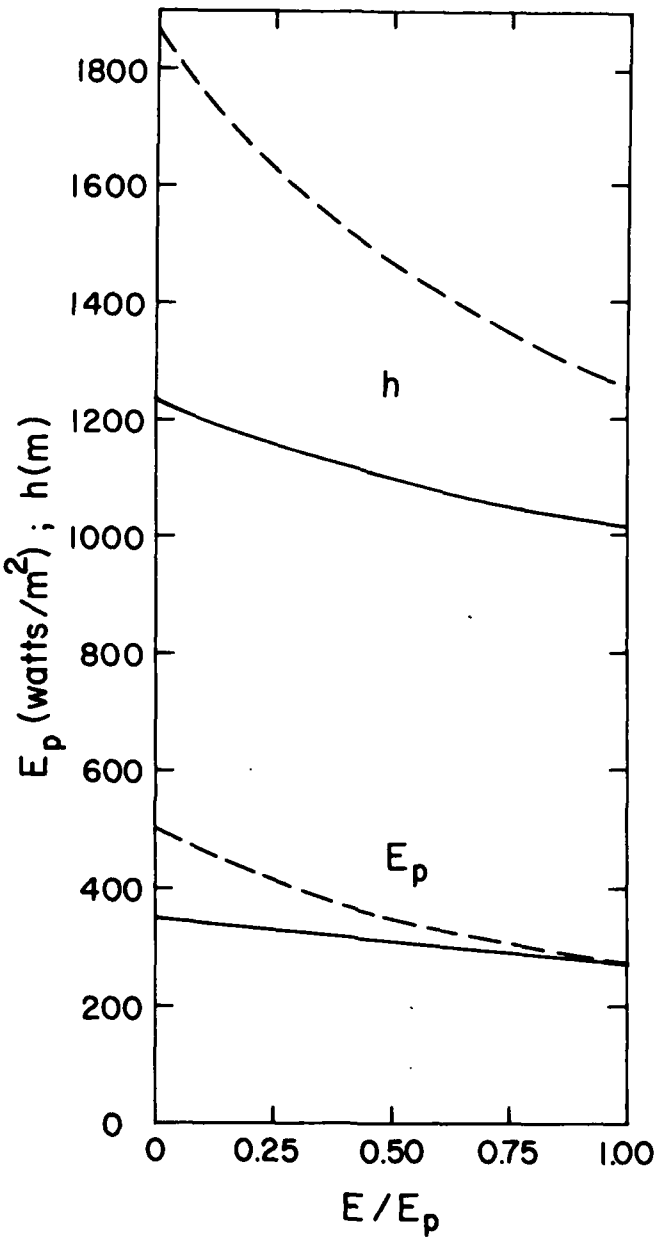

Fig. 4. Boundary layer depth and potential evaporation as a function of specified E/E_p for 1200 local time for day 33 (solid line) and day 34 (dashed line).

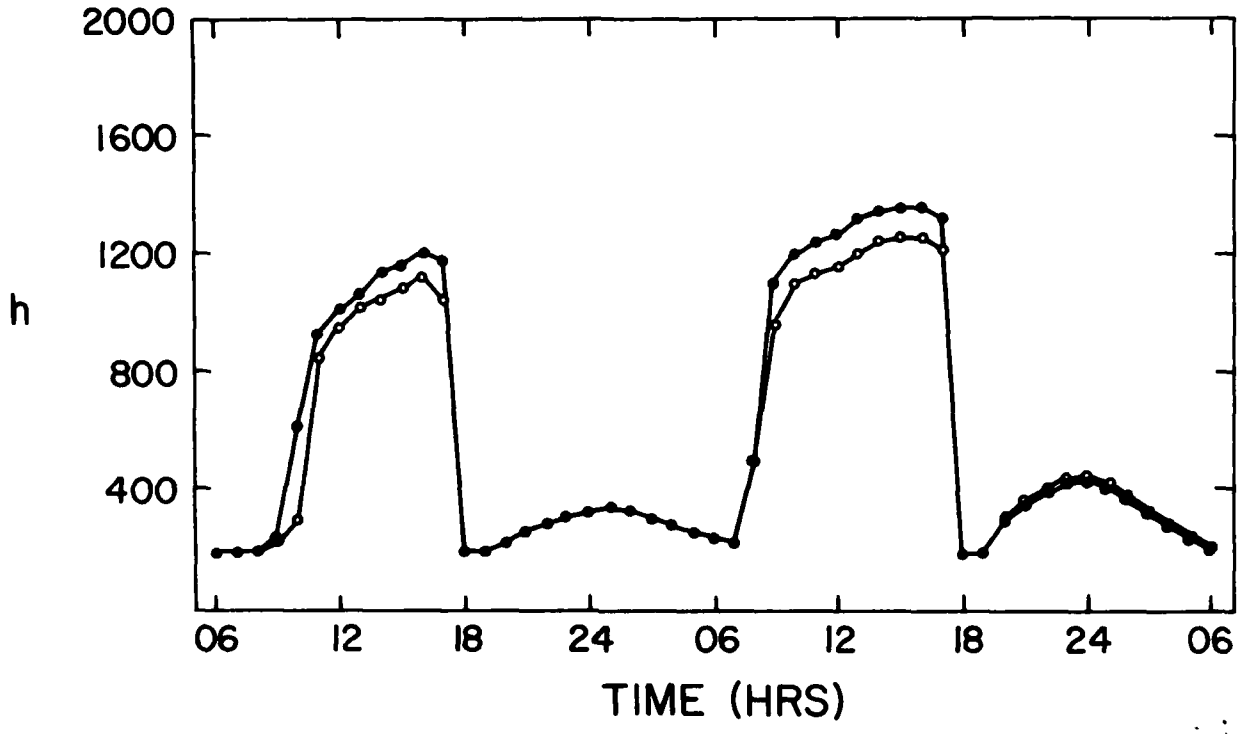

Fig. 5. Boundary layer depth as a function of local time for the Wangara initial conditions (open circles) and for the case with the initial specific humidity decreased by a factor of two (solid circles), $E/E_p=1$.

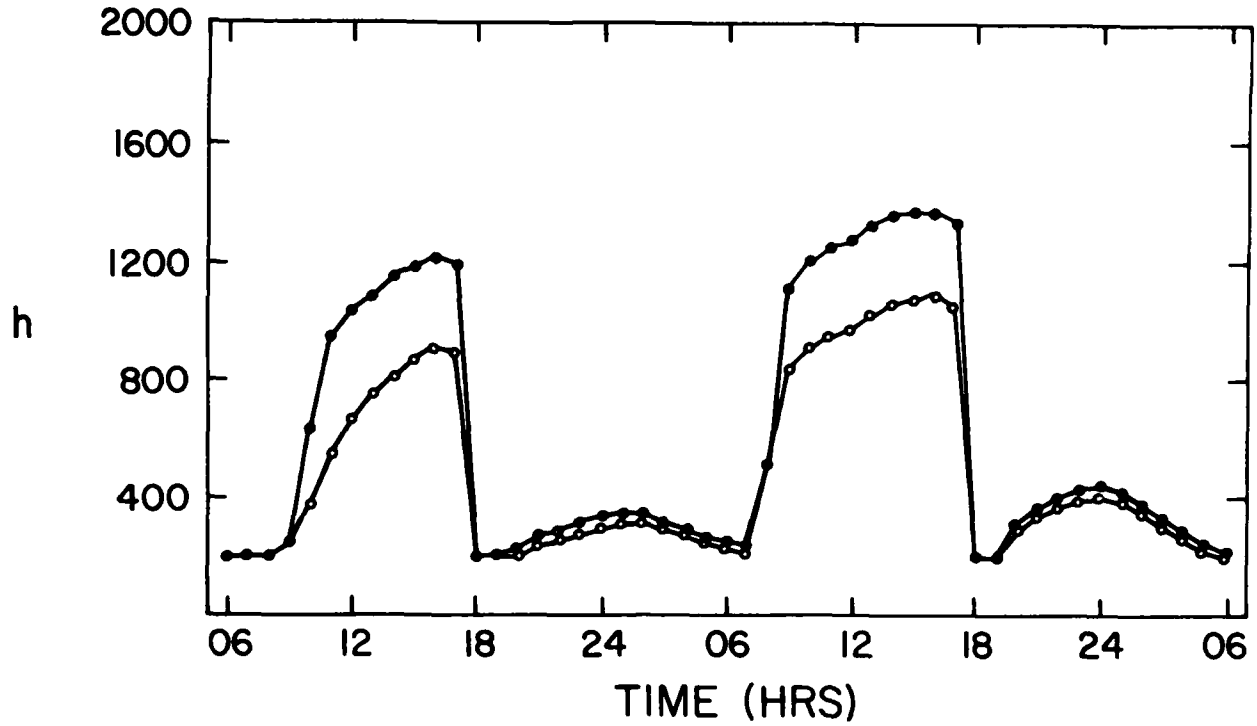

Fig. 6. Boundary layer depth as a function of local time for the prototype experiment (open circles) and for isothermal stratification aloft (solid circles).

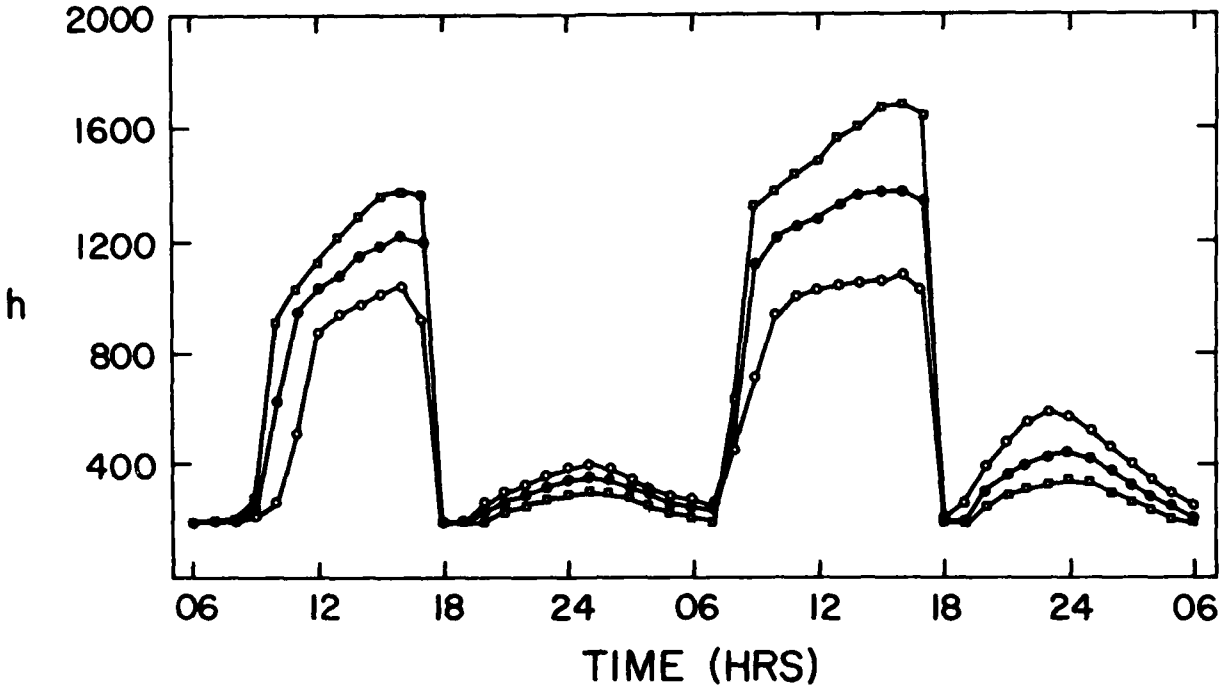

Fig. 7. Boundary layer depth as a function of local time for the prototype experiment (solid circle), solar radiation increased by 50% (open squares) and solar radiation reduced by a factor of two (open circles).

In the present model this expression is evaluated at the second boundary layer level above the surface.

We have not objectively tested this scheme since the general format has already been subject to considerable scrutiny. Our opinion is that this cloud representation can probably be improved considerably, although needed simplicity and truncation errors will limit the degree of potential improvement. The most obvious generalization would be to express the critical relative humidity as a function of basic cloud type.

8. Conclusions

This study develops a numerical model of the atmospheric boundary layer which requires only modest vertical resolution and is sufficiently simple for use in concert with other models. For example, the formulation of the boundary layer depth includes the main features of mixed layer growth but does not lead to special interpolation problems occurring with use of sophisticated mixed layer growth models with low vertical resolution. The simple boundary-layer depth model adopted here includes the influences of mixing generated by both shear and surface heating and allows for a smooth transition to the stable case.

The "counter-gradient correction" to the heat transport by boundary layer scale convective eddies has been generalized to be consistent with surface layer similarity theory and at the same time allows for continuous transition to the mechanically mixed boundary layer.

As an example application, the model is used to study the response of the boundary layer to the surface moisture flux. This flux is formulated as a specified fraction of the potential evaporation. The potential evaporation is

represented by a Penman expression. The daytime growth of the modelled boundary layer is reduced significantly by modest availability of surface moisture. However, additional surface moisture leads to less important changes since the return influence of the boundary layer modifications leads to reduced potential evaporation. These tentative results of the surface-atmosphere coupling suggest that distinction between modest surface moisture deficit and large surface moisture deficit is more important than distinction between a modest moisture deficit and saturated surface conditions. This sensitivity to substantial moisture deficits would be augmented by inclusion of the nonlinear dependence of transpiration on the soil moisture deficit.

Appendix

We assume that the model input from the radiation calculations in the larger scale model includes both short and longwave contributions. The surface energy balance then becomes

$$(1 - \alpha)\, S\downarrow + L\downarrow - \sigma T_o^4 = G + H_o + LE \qquad (A1)$$

where $S\downarrow$ is the downward shortwave radiation, α is the albedo, $L\downarrow$ downward longwave radiation, G the ground heat flux positive when downward, H_o and LE are the sensible and latent heat fluxes respectively, positive when upward.

The latent heating is related to the potential evaporation through the relationship

$$E \equiv \beta\, E_p$$

where E_p is the potential evaporation rate. The coefficient β is related to the soil moisture deficit and plant resistance to transpiration (Monteith, 1981). The present discussion does not explicitly represent the contributions to β. Instead β is arbitrarily varied in order to study the response of the atmospheric boundary layer to the surface moisture flux.

The computation of E_p follows the modified Penman method (of Chapter II) except for one modification motivated by numerical efficiency. The original Penman method requires knowledge of the net radiation and eliminates surface temperature as a parameter. Here, however, we need the surface temperature for radiation and surface heat flux calculations, and we therefore use (A1) to determine T_o in the manner outlined below (A2-A3).

In Chapter II, it was necessary to avoid the use of surface temperature since that development defines potential evaporation for comparison with obser-

vations of evapotranspiration carried out in Chapter IV. In such cases, use of surface temperature over land must be avoided since it cannot be defined in a useful observational framework. Thus the usual combination of the surface energy balance with the bulk aerodynamic relationship was performed in Chapter II in order to eliminate surface temperature.

Once the empirical formulations were completed in Chapter IV, the surface energy balance and surface temperature are reintroduced in the modelling situation of this chapter. It is not inconsistent to use the Penman formulation in concert with the surface energy balance, since the mathematical situation of two unknowns and two equations, is preserved. The usual Penman method is based on a linearization of the saturation vapor pressure in terms of the temperature difference between the lowest atmospheric level and the surface. Linearizing the upward radiation we obtain

$$\sigma T_o^4 \simeq \sigma T_1^4 \left(1 + 4 \left(\frac{T_o - T_1}{T_1}\right)\right) \qquad \text{(A2)}$$

and using the Penman method leads to the following expression for the potential evaporation:

$$E_p = \frac{\rho c_h}{\ell} \left[A(1 + r) + R\Delta\right] (\Delta + 1 + r)^{-1} \qquad \text{(A3)}$$

with

c_h = exchange coefficient for heat

ρ = density

ℓ = L/c_p

L = heat of evaporation for water

c_p = specific heat of air at constant pressure

$$r = \left(\frac{4\sigma R_{gas}}{c_p}\right) \frac{T_1^4}{p \cdot c_h}$$

σ = Stefan-Bolzman constant

p = surface pressure

R_{gas} = gas constant assumed equal to dry-air value

$$\Delta = \left(\frac{L^2 \varepsilon}{R_{gas}\, c_p}\right) q_1^*\ T_1^{-2}$$

ε = ratio of water molecular weight to that of dry air = 0.622

q_1 = specific humidity at atmospheric level

q_1^* = saturation specific humidity at temperature T_1

T_1 = temperature at atmospheric level

$$A = \ell(q^* - q_1)$$

$$R = ((1 - \alpha)S\downarrow + L\downarrow - T_1^4 - G)/(\xi c_p c_h)$$

(A1) is then used to estimate T_o

$$T_o = T_1 + \left[R\left(\frac{1 - \beta}{1 + r} + 1\right) - \beta A\right](\Delta + 1 + r)^{-1} . \qquad (A4)$$

As in previous models, we do not distinguish between the surface air temperature at the level of the roughness elements as used in surface layer similarity theory and the effective surface radiation temperature. Without this assumption, we would need a more detailed formulation of surface conditions than is included in the present development. It should also be noted that model surface temperatures have an uncertain relationship to the actual temperature of the soil surface or plant canopy.

References

André, J.C., G. De Moor, P. Lacerrer, G. Therry, and R. Vachat, 1978: Modelling the 24 hour evolution of the mean and turbulent structures of the planetary boundary layer. J. Atmos. Sci., 35, 1861-1883.

André, J.C., and L. Mahrt, 1982: The nocturnal surface inversion and influence of clear-air radiative cooling. J. Atmos. Sci., 39, 864-878.

Brost, R.A., and J.C. Wyngaard, 1978: A model study of the stably stratified boundary layer. J. Atmos. Sci., 8, 1427-1440.

Busch, N.E., S.W. Chang, and R.A. Anthes, 1976: A multi-level model of the planetary boundary layer suitable for use with mesoscale dynamical models. J. Appl. Meteor., 15, 909-919.

Businger, J.A., J.C. Wyngaard, Y. Izumi, and E.F. Bradley, 1971: Flux-profile relationships in the atmospheric surface layer. J. Atmos. Sci., 28, 181-189.

Chang, S.W., 1979: An efficient parameterization of convective and nonconvective planetary boundary layers for use in numerical models. J. Appl. Meteor., 18, 1205-1215.

_____, 1981: Test of a planetary boundary layer parameterization based on a generalized similarity theory in tropical cyclone models. Mon. Wea. Rev., 109, 843-853.

Clarke, R.H., 1970: Recommended methods for the treatment of the boundary layer in numerical models of the atmosphere. Austr. Meteor. Mag., 18, 51-73.

Clarke, R.H., A.J. Dyer, R.R. Brook, D.G. Reid, and A.J. Troup, 1971: The Wangara Experiment: Boundary layer data. Tech. Paper No. 19, Div. Meteor. Phys., CSIRO, Australia.

Deardorff, J.W., 1966: The counter gradient heat flux in the lower atmosphere and in the laboratory. J. Atmos. Sci., 23, 503-506.

_____, 1972: Parameterization of the planetary boundary layer for use in general circulation models. Mon. Wea. Rev., 100, 93-106.

_____, 1973: The use of subgrid transport equations in a three-dimensional model of atmospheric turbulence. J. Fluids Engr., 95, 429-438.

Geleyn, J.-F., 1980: Some diagnostics of the cloud/radiation interaction in the ECMWF forecasting model. Workshop on Radiation and Cloud-Radiation interaction in Numerical Modelling. European Centre for Medium-range Weather Forecasting, 135-162.

Hojstrup, J., 1982: Velocity spectra in the unstable planetary boundary layer. J. Atmos. Sci., 39, 2239-2248.

Holzworth, G.C., 1964: Estimates of mean maximum mixing depths in the contiguous United States. Mon. Wea. Rev., 92, 235-242.

Louis, J.-F., 1979: A parametric model of vertical eddy fluxes in the atmosphere. Bound.-Layer Meteor., 17, 187-202.

Mahrt, L., 1981a: Modelling the depth of the stable boundayr layer. Bound.-Layer Meteor., 21, 3-19.

Mahrt, L., 1981b: The early evening boundary layer transition. Quart. J. Roy. Meteor. Soc., 107, 329-343.

Mahrt, L., J.C. André, and R.C. Heald, 1982: On the depth of the nocturnal boundary layer. J. Appl. Meteor., 21, 90-92.

Mahrt, L., R.C. Heald, D.H. Lenschow, B.B. Stankov, and I. Troen, 1979: An observational study of the structure of the nocturnal boundary layer. Bound.-Layer Meteor., 17, 247-264.

Mailhôt, J., and R. Benoit, 1982: A finite-element model of the atmospheric boundary layer suitable for use with numerical weather prediction models, J. Atmos. Sci., 39, 2249-2266.

Monteith, J.L., 1981: Presidential address: Evaporation and surface temperature. Quart. J. Roy. Meteor. Soc., 1-24.

Pielke, R.A., and Y. Mahrer, 1975: Technique to represent the heated boundary layer in mesoscale models with coarse vertical resolution. J. Atmos. Sci., 32, 2288-2309.

Priestly, C.H.B., and W.C. Swinbank, 1947: Vertical transport of heat by turbulence in the atmosphere. Proc. Roy. Soc., Ser. A, 189, 543-561.

Smeda, M.S., 1979: A bulk model for the atmospheric planetary boundary layer. Bound.-Layer Meteor., 14, 411-428.

Tennekes, H., 1973: A model for the dynamics of the inversion above a convective boundary layer. J. Atmos. Sci., 30, 558-567.

Troen, I., 1982: Analytical and numerical modeling of flow driven by surface differential heating, Ph.D. thesis, University of Copenhagen, Riso R-452, Riso National Laboratory, Denmark.

Wyngaard, J.C., and R.A. Brost, 1983: Top-down and bottom-up diffusion in the convective boundary layer. Submitted to J. Atmos. Sci.

Wyngaard, T.C., W.T. Pennell, D.H. Lenschow, and M.A. LeMone, 1978: The temperature-humidity covariance budget in the convective boundary layer. J. Atmos. Sci., 35, 47-58.

Yamada, T., and G. Mellor, 1975: A simulation of the Wangara atmospheric boundary layer data. J. Atmos. Sci., 32, 2309-2329.

Yu, T.-W., 1977: A comparative study on parameterization of vertical turbulent exchange processes. Mon. Wea. Rev., 105, 57-66.

Zhang, D., and R.A. Anthes, 1982: A high resolution model of the planetary boundary layer--sensitivity tests and comparisons with SESAME-79 data. J. Appl. Meteor., 21, 1594-1609.

VI. Concluding Remarks

The research described in this report develops a model for stability-dependent potential evaporation (Chapter II), soil hydrology (Chapter III), transpiration and the canopy water budget (Chapter IV) and the atmospheric boundary layer (Chapter V). The construction of these models was partly motivated by the important influences of the surface moisture flux on the diurnal development of the boundary layer, related cloud fields and flow patterns in general. Since existing global circulation models neglect the influence of surface moisture flux over land or incorporate them in a cursory manner, much of the model development in this report is original in nature. The software logistics of the combination of these models is described in the User's Manual corresponding to this report. A rough flow chart is provided in Fig. 1.

The physics of the interaction between models is primarily tied to the hydrological budget. Surface moisture flux from the soil and plant canopy leads to a more moist and cooler boundary layer. The difference between a moist and dry surface can cause major differences in the diurnal evolution of the atmospheric boundary layer over land as was documented with the boundary layer model developed in Chapter V.

The modification of the boundary layer, in turn, influences the surface moisture flux. The atmospheric humidity deficit, wind speed and transmission of shortwave radiation control the "maximum allowed" surface moisture flux. This control is usually formulated through the Penman expression for potential evaporation. Chapter II develops a stability-dependent expression for potential evaporation for use in atmospheric models. Previous models of potential

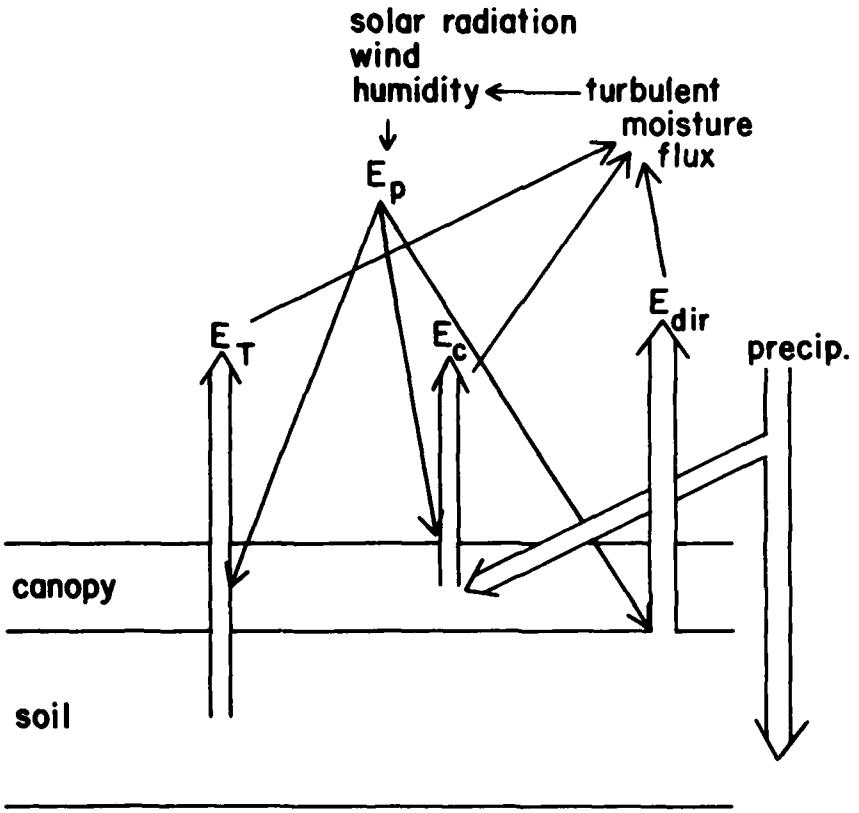

FLOW CHART FOR MOISTURE

Fig. 1a. Diagram of terms in moisture budget (double arrows) and interaction with turbulent boundary layer (thin arrows).

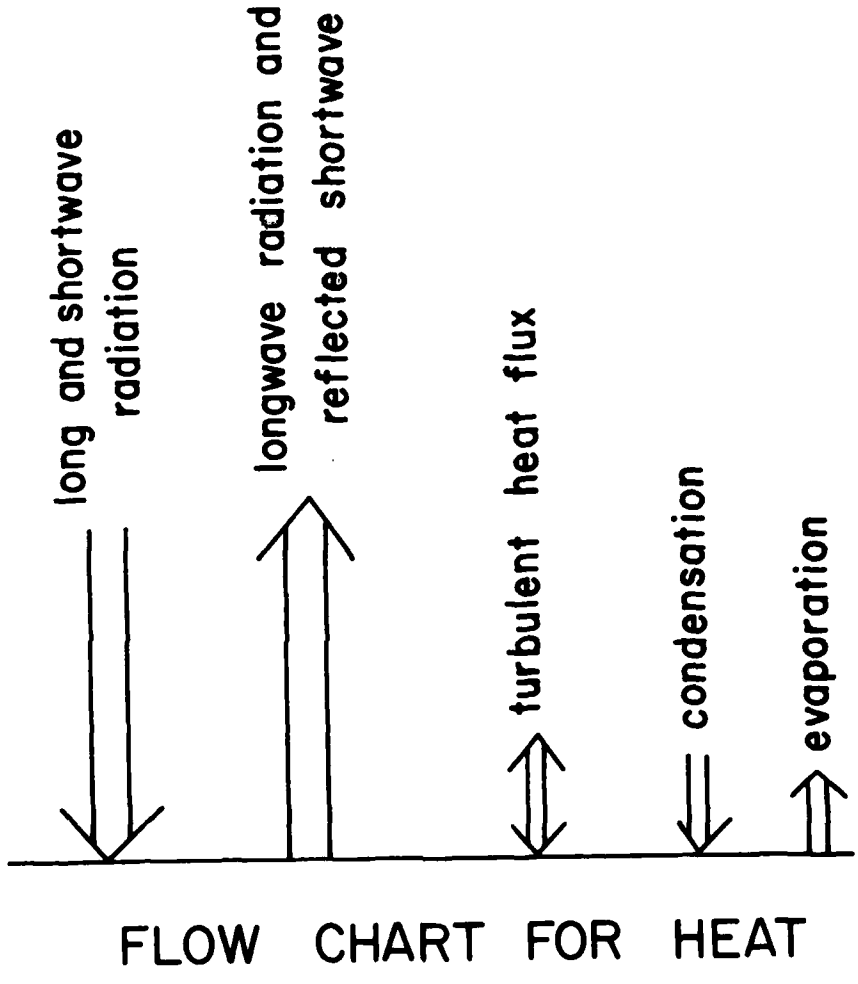

Fig. 1b. Diagram of terms in heat budget.

evaporation are either too complicated for use in general circulation models or have omitted the important influence of stability on potential evaporation.

As noted in Chapter I, the total surface evaporation can be written as

$$E = E_{dir} + E_T + E_c = F\, E_p$$

where E_{dir} is again the direct evaporation from the soil, E_T is the transpiration, E_c is the evaporation of precipitation water intercepted by the canopy, E_p is the potential evaporation and F is a function which relates the various contributions of the surface moisture flux to the potential evaporation.

The function F can be written as

$$F = F_{soil}(1-\sigma_f) + k_v\sigma_f\left[(z_1/z_2)\, g(\theta_1) + \left(\frac{z_2-z_1}{z_2}\right) g(\theta_2)\right]\left[1-(C/S)^n\right] + \sigma_f(C/S)^n$$

$$g(\theta) \equiv \frac{\theta - \theta_{wilt}}{\theta_{ref} - \theta_{wilt}}$$

The function F_{soil} is not formally defined but rather represents the modelled process whereby the direct evaporation from the soil is at the potential rate until the corresponding surface soil moisture decreases below the air-dry value as discussed in Chapter III, Section 4. At this point, the soil evaporation rate becomes less than the potential rate and becomes controlled by the soil moisture profile and surface air-dry value. The relevant soil moisture profile is determined by the soil moisture in a thin upper layer of the soil of depth z_1. Transpiration is more dominated by the soil moisture in a deeper layer of depth z_2-z_1.

The contributions to the surface moisture flux for the total grid area are modulated by the fractional coverage of vegetation, σ_f, which reduces direct evaporation from the soil and leads to non-zero transpiration or evaporation of precipitation intercepted by the canopy. The intercepted water, C, in turn, reduces the transpiration according to the amount of canopy water with respect to the total water capacity of the canopy, S.

The transpiration is controlled by the stomatal resistance of the vegetation represented by the plant coefficient, k_v, and controlled by the soil moisture deficit represented by the function $g(\theta)$. Transpiration becomes monotonically reduced after the soil volumetric water content, θ, decreases below the reference value, θ_{ref}. Transpiration vanishes altogether when the soil water content is depleted to the wilting value, θ_{wilt}. Again, transpiration is controlled mainly by the water content of the deep lower layer, θ_2, while direct evaporation from the soil is dictated by the soil water content of the thin upper layer, θ_1.

Numerical experiments were performed where the soil, canopy and atmospheric boundary layer models were run in concert. These sensitivity tests are not reported here. Significant meaning could not be attached to the results except that the total model appeared to behave in a reasonable manner. Attempts to compare the model with classical soil moisture data from the USDA laboratory in Phoenix led to identification of severe inconsistencies in the corresponding atmospheric data needed to evaluate the model. Comparisons with data from the O'Niell field program were also conducted; however, data gaps and the limited availability of the soil moisture data became sufficiently important to render

comparisons inconclusive. Recent data from the KMNI facility near de Bilt, Netherlands may provide more meaningful comparisons although this data represents a rather narrow range of soil moisture conditions.

Certainly considerable effort is required to further examine the interaction between the various model components for a variety of atmospheric conditions.

Reports and Articles (prepared under this contract)

1. The influence of the diurnal variation of stability on potential evaporation (Michael B. Ek). Master of Science thesis, Department of Atmospheric Sciences, Oregon State University, Corvallis, Oregon 97331.

2. The influence of atmospheric stability on potential evaporation (L. Mahrt and M. Ek): to appear in J. Climate Appl. Meteor.

3. A two-layer model of soil hydrology (L. Mahrt and H. Pan): to appear in Bound.-Layer Meteor..

4. A boundary layer formulation for atmospheric models (Ib Troen and L. Mahrt): submitted to Quart. J. Roy. Met. Soc.

5. Remotely sensed satellite data as an input into the moisture component of a global climatic model (Anthony Lewis). Special report to the Atmospheric Prediction Branch (AFGL).

6. A boundary layer parameterization for a general circulation model (L. Mahrt, H. Pan, James Paumier and Ib Troen). A final report to the Atmospheric Prediction Branch, AFGL (AFGL-TR-84-0063).

The Influence of the Diurnal Variation of Stability on Potential Evaporation

by

Michael Bryan Ek

A THESIS

Submitted to

Oregon State University

in partial fulfillment of
the requirements for the
degree of

Master of Science

Completed December 10, 1982

Commencement June 1983

AN ABSTRACT OF THE THESIS OF

Michael Bryan Ek for the degree of Master of Science in Atmospheric Sciences presented on December 10, 1982. Title: The Influence of the Diurnal Variation of Stability on Potential Evaporation.

Abstract approved: _____

Larry J. Mahrt

A method of calculating surface evapotranspiration by separately including the effects of vegetation and atmospheric evaporative demand under the condition of nonlimiting soil moisture is presented. A literature survey is conducted to determine the effects of plants on evapotranspiration.

To represent the atmospheric evaporative demand, the original potential evaporation equation of Penman (1948) is utilized and then modified to include the effect of atmospheric stability using turbulent exchange coefficients formulated by Louis et al. (1982). The original and modified Penman expressions are compared for different asymptotic cases. Using boundary layer data from the Wangara experiment (Clarke et al., 1971), the diurnal variations of the original and modified Penman equations are compared. The daily total potential evaporation using linearized and integrated forms of the original and modified expressions are also compared. Finally, the nonlinear effects of averaging both the original and modified expressions are examined. It is found that including the diurnal variations of stability in the modified expression causes large hourly differences with the original expression under non-neutral conditions, while daily averages of the two compared fairly well. The diurnal variation of the surface moisture flux appears to be much larger than predicted by the original Penman expression. However, the original Penman expression remains a reasonable estimate of the 24-hour total potential evaporation.

THE INFLUENCE OF ATMOSPHERIC STABILITY ON POTENTIAL EVAPORATION

L. Mahrt

Michael Ek

Department of Atmospheric Sciences
Oregon State University
Corvallis, OR 97331

15 November 1983

Abstract

The Penman relationship for potential evaporation is modified to simply include the influence of atmospheric stability on turbulent transport of water vapor. Explicit expressions for the stability-dependent, surface exchange coefficient developed by Louis are used. The diurnal variation of potential evaporation is computed for the stability-dependent and original Penman relationship using Wangara data.

The influence of afternoon instability increases the aerodynamic term of the modified Penman relationship by 50% or more on days with moderate instability. However, the unmodified Penman relationship predicts values of daily potential evaporation close to that of the stability-dependent relationship. This agreement is partly due to compensating overestimation during nighttime hours. Errors due to use of daily-averaged variables are examined in detail by evaluating the nonlinear interactions between the diurnal variation of the variables in the Penman relationship.

A simpler method for estimating the exchange coefficient is constructed from an empirical relationship between the radiation Richardson number and the Obukhov length. This method is less accurate, but allows estimation of the stability-dependent exchange coefficient using only parameters already required for evaluation of the Penman relationship. Finally, the diurnal variation of the atmospheric resistance coefficient appearing in the Penman-Monteith relationship is presented.

A Two-layer Model of Soil Hydrology

L. Mahrt and H. Pan

Department of Atmospheric Sciences
Oregon State University
Corvallis, Oregon 97331
USA

15 January 1984

Abstract

A two-layer model of soil hydrology is developed for applications where only limited computer time and complexity are allowed. Volumetric soil water is computed in a thin upper layer for use in calculation of surface evaporation. Storage of water is computed for an underlying deeper layer.

In an effort to identify the influence of significant asymmetric truncation errors in the two-layer model, this model is compared with the 100-level model of Boersma et al. (1983). Comparisons are made for modelled soils with clay, loam and sand properties for various time dependencies of potential evaporation and precipitation. Truncation errors in the resulting two-layer model appear to be modest at least compared to errors associated with difficulty in estimation of the hydraulic diffusivity and its strong dependence on soil water content.

Minimization of the influence of truncation errors requires: 1) choosing the upper layer to be sufficiently thin, 2) allowing the soil water gradient to directly control surface evaporation and 3) using suitable numerical implementation of the evaluation of internal soil water flux.

A BOUNDARY LAYER FORMULATION FOR ATMOSPHERIC MODELS

Ib Troen[1] and L. Mahrt

Department of Atmospheric Sciences
Oregon State University
Corvallis, Oregon 97331
USA

January 15, 1983

[1]On leave from the Riso National Laboratory, 4000 Roskilde, Denmark

ABSTRACT

A simple model for the atmospheric boundary layer is proposed for use in operational global weather prediction models and other models where simplicity is required. Surface fluxes are represented in terms of similarity theory while turbulent diffusivities above the surface layer are formulated in terms of bulk similarity considerations and matching conditions at the top of the surface layer. The boundary layer depth is represented in terms of a modified bulk Richardson number. Attention is devoted to the interrelationship between predicted boundary layer growth, the turbulent diffusivity profile, "counter-gradient" heat flux and truncation errors. The model is especially suited for use in models where some resolution is possible within the boundary layer, but where the resolution is still insufficient for resolving the detailed boundary layer structure.

As an example application, the model is used to study the influence of surface moisture flux on the boundary layer development.

Remotely Sensed Satellite Data as an Input into the Moisture Component of a Global Climatic Model

prepared by

Anthony Lewis

Environmental Remote Sensing Laboratory

Oregon State University
Corvallis, OR 97331 USA

Contract F 19628-81-K0046
(L. Mahrt, Principal Investigator)

Atmospheric Prediction Branch
Air Force Geophysics Laboratory
Cambridge, MA

21 August 1983

END
9-84